DELFT UNIVERSITY OF TECHNOLOGY

Costs competitive large-scale green hydrogen production in North-Africa in 2030.



Author:
Rogier Doodeman (4380649)

Thesis supervisor:
Prof. dr. A.J.M. van Wijk

Thesis committee:
Prof. dr. A.J.M. van Wijk
Prof.dr.ir. Z. (Zofia) Lukszo
Dr. Arno H.M. Smets
Frank Wouters

TU Delft

March 16, 2022

Abstract

The European Green Deal states that it wants to develop 40 GW of electrolyzer capacity by 2030 in North Africa to combat climate change. Using PV power as the primary energy source, a system is designed that can produce green hydrogen and ammonia to investigate how the location and the capacity of the components can be optimized to produce at the lowest possible levelized costs. This way the competitiveness of green hydrogen and ammonia can be examined against hydrogen and ammonia produced using fossil fuels. Incorporating batteries for electricity storage, a salt cavern for hydrogen storage and cryogenic tanks for nitrogen storage, the system is designed to work as flexible as possible to cope with the variations in PV output.

Scaled to an industrial scale output of 200.000 ton-NH_3 per year, the resulting LCOH in 2030 will be 1.63 €/kg-H_2, and the LCOA will be 0.394 €/kg-NH_3. The competitiveness with fossil fuel-based production is dependent on the price of natural gas, which in this case will need to be higher than 3.16 $/MBTu or 12.25 €/MWh (converted using a USD/EUR rate of 0.88 and a conversion factor of 0.29308 MWh/MBTU, and taking into account a carbon price of 100 €/ton-CO_{2-eq}) for green hydrogen to be competitive. For green ammonia to be cheaper, the gas price must be greater than 4.49 $/MBTu or 17.41 €/MWh.

A sensitivity analysis shows that if the CAPEX and OPEX cost of the five most contributing components to the levelized cost would be 50% higher, the LCOH (2.4770 €/kg-H_2) and LCOA (0.5817 €/kg-NH_3) would still compare favourably to blue hydrogen and ammonia with a natural gas price of 7.71 $/MBTu (29.89 €/MWh) and 9.04 $/MBTu (35.05 €/MWh). By analyzing the operations of the salt cavern, it is discovered that 6.4% of the salt cavern is used from the available capacity of 3300 ton-H_2. Even when the necessary yearly output of ammonia is raised 2 or 4 times, the salt cavern uses only 12.7% and 16.8% of the available capacity. Overall this research shows that green hydrogen and ammonia can compete with hydrogen and ammonia produced from fossil fuels in 2030 and that the possibilities of salt cavern storage for hydrogen are greater than expected because a capacity of 250 ton-H_2 is enough for a yearly production of 200.000 ton NH_3.

Preface

First and foremost, I would like to thank Prof. Ad van Wijk for providing a clear vision of the objectives of my thesis. Even though we have never spoken to each other in person, the online meetings enabled me to keep a good sense of direction.

Next to Prof.Ad van Wijk I would like to thank Prof. Zofia Lukszo for providing a clear framework for the optimization by asking thought-provoking questions about what I wanted to achieve in my research. As well as looking out for my well being during isolated times in this pandemic by introducing me to fellow students who work on relatable hydrogen research.

Special thanks to Peter Horvath from the company Deep Kbb who supplied me with information on salt caverns in Morocco and knowledge to calculate the capacity limits.

Lastly, I would like to thank the captains of industry Hans Verhoeven, Paul Bogers and Frank Wouters, for discussing their vision of a hydrogen and ammonia economy with me.

Contents

Abstract i

Preface ii

1 Introduction 5
1.1 Background . . . 5
1.1.1 Current levelized cost . . . 5
1.1.2 Carbon Price . . . 6
1.1.3 Effect of Natural Gas price . . . 8
1.2 Problem Statement . . . 11
1.3 Research Gap . . . 11
1.4 Research Question . . . 13
1.5 Research Objective . . . 14
1.6 Research Scope . . . 14
1.7 Research Method . . . 15
1.8 Report Outline . . . 15

2 System Design 16
2.1 System Layout . . . 16
2.1.1 Wind Power . . . 17
2.2 Corresponding Parameters . . . 19

3 Production Processes 21
3.1 Photovolataic panels . . . 21
3.2 Battery . . . 23
3.3 Electrolyzer type . . . 23
3.4 Hydrogen Production . . . 24
3.5 Salt Cavern . . . 24
3.6 Air Separation Unit . . . 25
3.7 Nitrogen Tank . . . 26
3.8 Ammonia Production . . . 26
3.9 Feed Water . . . 26
3.10 Compressor . . . 27
3.11 Balance of System . . . 27

4 Model description 28
4.1 Optimization model . . . 28
4.2 Working principle of the model . . . 29
4.3 Modeling PV load . . . 31
4.4 Modelling Buffers . . . 31
4.4.1 Assumptions Initial capacity . . . 32
4.5 Operational Constraints . . . 33
4.6 Initial Condition, Load Range and Ramping Constraints . . . 34
4.7 Problem-Based approach to Mixed Integer Linear Problem . . . 34

5 Location Determination **36**
5.1 Renewable Energy Resources . . . 36
5.1.1 Solar Irradiance . . . 36
5.2 Geological storage opportunity . . . 37
5.2.1 Salt Cavern locations . . . 38
5.2.2 Hydrogen storage capacity . . . 39

6 Results **42**
6.1 Optimal Capacity of Components . . . 42
6.2 Allocation Energy Carriers in Integrated System . . . 44
6.3 Levelised costs . . . 47
6.3.1 Levelized Cost of Energy . . . 47
6.3.2 LCOH and LCOA . . . 48
6.4 Sensitivity Analysis . . . 50
6.4.1 Sensitivity to the components . . . 50
6.4.2 Sensitivity to the WACC . . . 51
6.4.3 Sensitivity of the Model . . . 52

7 Conclusion **54**

8 Discussion **55**

9 Recommendations **57**

A Appendix **65**
A.1 Determined location of the project . . . 65
A.2 Temperature influence on PV panels . . . 66
A.3 Map of the terrain on the proposed location . . . 67
A.4 Installed and planned electrolyzer capacity . . . 68
A.5 Component load distribution . . . 69
A.6 PV distribution . . . 71
A.7 Wind Capacity Factors . . . 72
A.8 Model Description . . . 76

Nomenclature

Acronyms

ASU Air Seperation Unit

CAPEX Capital expenditures

CH_4 Methane

CO Carbon monoxide

CO_2 Carbon Dioxide

CRF Capital Rate Factor

DC Direct Current

DHI Diffuse Horizontal Irradiance

DNI Direct Normal Irradiance

e^- Electron

GHI Global Horizontal Irradiance

H_2 Hydrogen

H_2O Water

HPC High Computing Cluster

KOH potassium Hydroxide

Lat. Latitude

LCOA Levelized cost of ammonia

LCOE Levelized cost of energy

LCOH Levelized cost of hydrogen

Lon. Longitude

MILP Mixed Integer Linear Programming

MPP Maximum Power Point

N_2 Nitrogen

NH_3 Ammonia

O_2 Oxygen

OH^- Hydroxide ions

OPEX operating expenses

PEM Proton Exchange Membrane

PV Photovoltiac

SMR Steam Methane Reforming

SOC State of Charge

SOEC Solid Oxide Electrolyzer Cell

WACC Weighted Average Cost of Capital

Symbols

δH	Difference in enthalpy	[kJ/mol]
$\dot{m}$	Mass flow rate	[(kg $\cdot mol$)/s]
η	Isentropic efficiency	[-]
ρ	Density	[kg/m^3]
g	Gravitational acceleration	[m/s^2]
k	Ratio of specific heats	[-]
M	Molar mass	[kg/mol]
m	Mass	[kg]
ns	Number of stages	[-]
P	Pressure	[kPa]
R	Universal Gas constant	[J/(K $\cdot mol$)]
V	Volume	[m^3]
Z	Compressibility factor	[-]
T_{am}	Ambient Temperature	[K]

List of Figures

1.1 Price for emitting one ton of CO_2 equivalent greenhouse gasses. Modified from (Carbon Price Viewer 2022) to show the three predicted scenario's. 7
1.2 The price of natural gas of the previous 5 years. Showing both the American price traded on the Nymex market and the Dutch price traded on the ICE-ENDEX TTF. To compare the two the Dutch national gas price is converted using USD/EUR rate of 0.88 and a conversion factor of 0.29308 MWh/MBTU. 8
1.3 LCOH produced from fossil fuels. Created with data from table 1.3. On the x-axis the price of natural gas and CO_2 ranges from the minimum to the maximum. 9
1.4 LCOA produced from fossil fuels. Created with data from table 1.3. On the x-axis the price of natural gas, electricity and CO_2 ranges from the minimum to the maximum. 10
1.5 Modified from (Hieminga and Tillier 2021) to show natural gas price in $/MBTu as well. Converted using a USD/EUR rate of 0.88 and a conversion factor of 0.29308 MWh/MBTU. 11
2.1 Schematic of the system modeled in this research. Scaled to the ammonia output of 200.000 ton per year. 17
2.2 Average capacity factor of wind and solar power per hour. 18
2.3 Average weekly capacity factor of solar and wind power. 19
3.1 The photovoltaic effect illustrated. Retrieved from (Kavaz et al. 2014) 21
3.2 The learning rates of various studies collected in the comprehensive study of (Atkins 2020) 22
3.3 Schematic layout of alkaline electrolysis. Modified from (Mulder and Geerlings 2020) 25
4.1 Constraints implemented in the model that determine the capacity of different components with a brief description. 30
4.2 Constraints that simulate a realistic working of the buffers implemented in the system. 31
4.3 Set of constraints that allocate the energy carriers. 33
4.4 Set of constraints that create a more realistic model by imposing load ranges, ramping constraints and the initial SOC of the battery and the salt cavern. 34
5.1 Difference between PV output in Rotterdam and Essaouira. Created in Matlab using Sandia's National Libraries PV_LIB Toolbox (Stein et al. 2016) and meteorological data from the website Solcast (Solcast 2021) 37
5.2 Salt tectonic map of Morocco. Showing multiple basins including Essaouira and Souss basin retrieved from (Tari et al. 2017) 38
5.3 2D image of subsurface Essaouira basin including the Tidsi diapir, retrieved from (Tari et al. 2017). 39
5.4 Lithologic summary of the Tamergat well. Drilled in 1982. Approximate location Latitude: 31.41, Longtitude: -9.55. Cropped from (Tari et al. 2017) to cut off deeper layers. 41
6.1 Schematic of system with the optimized capacity size of the components included as well as information on the electric system and the pressure required in some components. 42
6.2 Sankey diagram of the allocation of energy carriers. H_2, N_2 and NH_3 values are converted to GWh using energy densities of 39.4 kwh/kg (Harrison et al. 2010), 712 kJ/kg (Rizvi et al. 2021) and 22.5 MJ/kg (Valera-Medina et al. 2018), respectively. 45

6.3 In subfigure 1, the electricity output in kWh on an hourly basis of the PV farm is shown. In subfigure 2, the state of charge of the battery is plotted. In the last subfigure, the state of charge of the salt cavern is shown. The clear cut at 20% and 95% in subfigure 2 results from the assumed load range of 20% and 95%. For the salt cavern, the load range is already implemented in the capacity limit calculated in chapter 5.2.2. 46
6.4 The load distributin of the electrolyzer and Haber-Bosch plant during a simulation period of nine months. 47
6.5 The orange numbers are the LCOE of PV power for different variables in this paper and the black numbers represent the lowest bids in solar auctions across the world. Portugal bid (Bellini 2020), Abu Dhabi bid (Global Solar Atlas 2021). . 48
6.6 The components of the LCOH and LCOA are arranged from their contributions to the levelized cost, with the PV and electrolyzer having the biggest impact on both the LCOH and LCOA. The grey area represents the levelized cost from the method using SMR discussed in chapter 1.1.3. The price of carbon is assumed to be 100 €/ton-CO_2, and the electricity price is 100 $/MWh 50
6.7 Sensitivity analysis of the most contributing components in the production of hydrogen and ammonia. Created by running the model with 50% higher and lower CAPEX and OPEX costs for each component. 51
6.8 Sensitivity analysis of the LCOH and LCOA with a varying WACC. 52
6.9 Sensitivity of the model to the simulation time. The circles represent the levelized cost corresponding to a certain simulation time. 53
A.1 The location of the proposed project is represented by the pin. One of the conclusions from this research is that the levelized cost could be lower when a smaller salt cavern can be used to find a location with more solar irradiance. Picture taken from (Solargis 2013). 65
A.2 Comparison between ambient and module temperature during daytime. Created in Matlab using Sandia's National Libraries PV_LIB Toolbox (Stein et al. 2016) and meteorological data from the website Solcast (Solcast 2021) 66
A.3 The area defined by the yellow line represent the PV farm. It is located just South of the Tamergat well discussed in chapter 5.4. (Google Earth 2021) was used to create the image. 67
A.4 Installed and planned electrolyzer capacity according to the (IEA 2020) database. The size of the bubbles represents the average electrolyzer capacity, while the vertical axis corresponds to the total sum of installed or planned capacity. The capacity will increase tremendously in the coming years. 68
A.5 The load distribution of the PV farm, Battery Electrolyzer and Salt Mine. The load is shown in percentages of certain components to show that they are bounded to a specific load range stated in table 2.2. 69
A.6 The load distribution of the PV farm, Battery Electrolyzer and Salt Mine. The load is shown in percentages of certain components to show that they are bounded to a specific load range stated in table 2.2. 70
A.7 The total electricity distribution of the PV farm for the entire simulation period of 9 months. 71
A.8 Retrieved from wind atlas Created with data from (Solcast 2021) 72
A.9 Created with data from (Solcast 2021) 73
A.10 Created with data from (Solcast 2021) 73
A.11 The log output of the simulation. Run on the HPC cluster for a period of nine months. 75

List of Tables

1.1 Levelized costs of hydrogen and ammonia taken from (Birol 2019) and converted to euro's using the exchange rate at the moment of publication of (Macrotrends LLC 2021), 1.1237 EURO-USD. 6
1.2 The effect of the carbon price for different production methods is related to the emission factor. Emission factors obtained from the (Birol 2019). 8
1.3 Values converted from (Birol 2019) using a USD/EUR rate of 0.8898 from the day of publication. (IEAGHG 2017) used for the CAPEX, gas consumption and emission factor of hydrogen. 10
2.2 Parameters for all system components in 2030 20
6.1 The results for an increase in ammonia output. For a value 4 times the initial output the salt cavern reaches only 16.7% of the possible capacity. 43
6.2 The components are listed from left to right according to their contributions to the levelized cost of hydrogen and ammonia. 49

1 Introduction

The interest in hydrogen to transform our fossil fuel-based economy to a carbon-zero based economy has reached an all-time high, with countries like Germany and France announcing to invest respectively 9 billion and 7 billion in hydrogen technologies (Crampes and Ambec 2021). Additionally, the European Green Deal plans to build 40 GW of electrolyzer capacity in Europe and 40 GW in North Africa. Meanwhile, only 200 MW of electrolyzer capacity has yet been installed (IRENA 2021). Leaving the question of how these ambitious plans can be realized.

This research aims to determine how the planned large-scale green hydrogen production can be cost-competitive with fossil-fuel produced hydrogen in 2030. However, instead of only producing hydrogen, the designed system makes the sequential step to produce ammonia. This is done because 55% of the hydrogen produced in the world today is already solely produced for ammonia production; therefore, this is a logical step so that a broader comparison of both energy carriers can be made (Brown. Trevor 2017). Additionally, in the announced plans for the two biggest electrolyzers that will be built with a capacity of 2 GW and 3 GW, this step is also included (Burgess 2021), (Gupta 2021). Gaining an understanding of the cost-competitiveness of green hydrogen and ammonia is essential in attracting future investments and determining what amount of subsidies will be necessary to reach the goal of 40 GW capacity in North Africa by 2030.

1.1 Background

The European Green deal was presented on 11 December 2019. Four years after the Paris agreement in which 195 governments agreed to combat the effects of climate change by lowering greenhouse gas emissions. The European Green deal presents a roadmap on how the goals set by the Paris Agreement can be accomplished. In the report, the importance of hydrogen is emphasized. Especially for heavy industries like steel production, hydrogen is the only green alternative. Resulting, for example, in a recent announcement made by Tata Steel that their steel plant in IJmuiden, the Netherlands, will switch to hydrogen instead of coal as a fuel for their blast furnaces. Similar announcements will result in a rapidly increasing demand for hydrogen in the near future. To meet this increasing demand, the Green Deal proposes to build 80 GW of electrolyzer capacity before 2030. The production would be split between Europe and North Africa to reach this amount. To make use of the abundant solar resources in countries like Tunisia and Morocco. Additionally, the production in North Africa would also contribute to the employment opportunities in the region and reduce the migration of labour migrants.

1.1.1 Current levelized cost

Currently, more than 95% of hydrogen is still produced with a method called steam methane reforming (SMR) equation 1. In this process, methane is deprived of its carbon atoms by reacting with steam at a temperature of around 900 °C and pressures between 3-25 bar (US Department of Energy 2021). The deprived methane atom binds with an oxygen atom to form carbon monoxide. However, it also creates hydrogen molecules.

$$CH_4(g) + H_2O(g) \xrightarrow[\text{Pressure}]{\text{Heat}} CO(g) + 3H_2(g) \tag{1}$$

The hydrogen created with SMR has a LCOH between 1.0-3.0 \$/kg-H_2. If ammonia would then be created from the hydrogen according to the Haber-Bosch reaction, it would have a LCOA between 0.15 \$/kg-NH_3 and 0.50 \$/kg-NH_3 (Birol 2019). According to the same report, the levelized cost of hydrogen and ammonia produced from renewable energy in 2019 is between 2.5 - 6 \$/kg-H_2 and 0.48-0.70 \$/kg-NH_3 respectively. To bridge this gap and allow green hydrogen and ammonia to compete with grey hydrogen and ammonia without subsidies, innovations and economy of scale effects will have to decrease the levelized cost. However, since 2005 the European Union has also employed a different method to stimulate renewable energy. Forcing companies to buy emission certificates that allow them to produce carbon dioxide or any other greenhouse gas expressed in the equivalent of carbon dioxide. The price of emitting greenhouse gasses can be controlled. This will be explained further in chapter 1.1.2. If this price would reach 100 €/ton-CO_2 it would translate to a LCOH between 1.42 - 3.56 €/kg-H_2 and a LCOA between 0.27 - 0.67 €/kg-NH_3 (Birol 2019). Converted to dollars using the exchange rate at the moment of publication (1.1237 EURO-USD (Macrotrends LLC 2021)) this translates to a carbon price of 112.37 \$/ton-CO_2 and a LCOH between 1.6-4 \$/kg-H_2 and a LCOA between 0.30-0.75 \$/kg-NH_3.

Levelized costs in Dollars			
	2019 renewables	2019 fossil fuels (25 \$/ton-CO_{2-eq})	2030 fossil fuels (112.37 \$/ton-CO_{2-eq})
LCOH \$/kg-H_2	2.5 - 6.0	1.0 - 3.0	1.6 - 4.0
LCOA \$/kg-NH_3	0.48 - 0.70	0.15 - 0.50	0.30 - 0.75
Levelized costs in Euro's			
	2019 renewables	2019 fossil fuels (22.24 €/ton-CO_{2-eq})	2030 fossil fuels (100 €/ton-CO_{2-eq})
LCOH €/kg-H_2	2.2 - 5.3	0.89 - 2.67	1.42 - 3.56
LCOA €/kg-NH_3	0.43 - 0.62	0.13 - 0.45	0.27 - 0.67

Table 1.1: Levelized costs of hydrogen and ammonia taken from (Birol 2019) and converted to euro's using the exchange rate at the moment of publication of (Macrotrends LLC 2021), 1.1237 EURO-USD.

1.1.2 Carbon Price

In 2005 the European emission trading system (EU ETS) was launched to help combat greenhouse gas emissions in the EU to meet the Kyoto protocol's goals. Emissions certificates were allocated to companies, allowing them to emit a certain amount of greenhouse gasses. If more greenhouses gasses were emitted, additional certificates could be bought using the EU ETS. The purpose of this system was to gradually make fossil-fuels based products more expensive by decreasing the number of certificates that were being allocated. This would incentivize investing in renewable alternatives to produce fewer greenhouse gasses. However, the number of certificates in circulation remained too high, resulting in a constant price per ton of carbon dioxide equivalent of around €5. In 2018 this changed when it was announced that reforms meant that more certificates would be taken out of circulation. Since 2018, the annual supply of certificates has been significantly reduced. In figure 1.1 the resulting price increase can be seen.

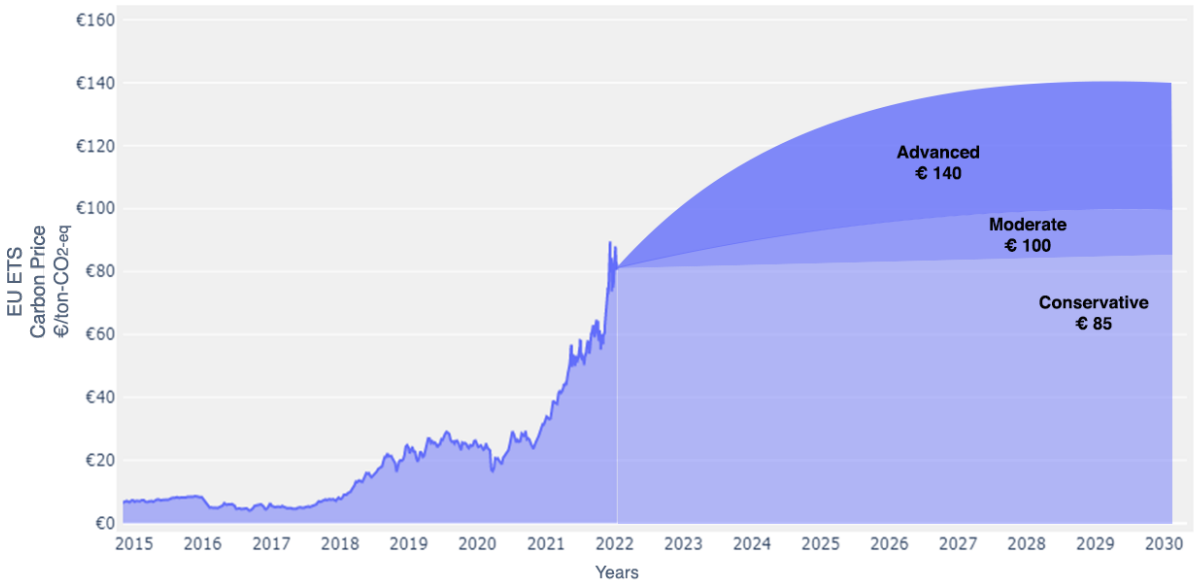


Figure 1.1: Price for emitting one ton of CO_2 equivalent greenhouse gasses. Modified from (Carbon Price Viewer 2022) to show the three predicted scenario's.

On December the 8th, the highest price ever recorded of 89.37 €/ton-CO_{2-eq} was reached. This is already more than the European Commission impact assessment projects group predicted. They stated that the price would be somewhere between 50 and 85 €/ton-CO_{2-eq} in 2030 (European Commission 2021). This corresponds with the conservative scenario in figure 1.1. Other analysts predict that the carbon price will be higher in the future. These predictions are represented in figure 1.1 with the moderate and advanced scenarios with corresponding prices of 100 and 140 €/ton-CO_{2-eq} in 2030 (Birol 2019), (Dumas and Saleheen 2021).

This research assumes that the recent rally on carbon certificates will slow down once the energy prices are stable again. The energy price has a significant effect on the carbon price because a higher energy price will make it more profitable for coal plants to produce electricity and because coal is the most polluting fossil fuel, the demand for emission allowances increases. In (Dumas and Saleheen 2021) it is even elucidated that the energy price explains one-third of the variations in the carbon price. Recent price spikes can also be contributed by the strategy of the European Commission to gradually reduce the supply of emission allowances. This strategy is well known, and because the EU Emission Trading System is an open market, the future reductions are already priced in. To make a relevant comparison between green and grey hydrogen and ammonia production. The influence of the carbon price on the levelized cost is constructed using the moderate scenario.

The direct effect of the carbon price on the levelized cost is very significant when the emission factor is high. In table 1.2 it shows that for coal without carbon capture, a carbon price of 100 €/ton-CO_{2-eq} will result in an added cost of 2.02 €/kg-H_2. This would double the price of hydrogen. The future of hydrogen report (Birol 2019) proposes that the cheapest production method to produce hydrogen and ammonia from fossil fuels in 2030 will be natural gas reforming with carbon capture. This is because of the lower emission factor due to the capturing of carbon before it is released into the atmosphere. Therefore, natural gas with carbon capture will be the main competitor of electrolysis-based hydrogen and ammonia production.

	Emission Factor [kg-CO_2/kg-(H_2 or NH_3]		Costs per kg with 100 €/ton-CO_{2-eq}	
	H_2	NH_3	H_2	NH_3
Natural Gas	8.9	2.14	€0.89	€0.214
Natural gas with carbon capture	1.0	0.11	€0.1	€0.011
Coal	20.2	3.9	€2.02	€0.39
Coal with carbon capture	2.1	0.2	€0.21	€0.02

Table 1.2: The effect of the carbon price for different production methods is related to the emission factor. Emission factors obtained from the (Birol 2019).

1.1.3 Effect of Natural Gas price

If natural gas with carbon capture storage is going to be the main competitor, the price of natural gas will play a decisive role. To separate hydrogen from methane, using steam methane reforming, large amounts of natural gas are required. Therefore the cost of hydrogen and ammonia produced from fossil fuels is heavily influenced by the price of natural gas. At a natural gas price of 18.41 €/MWh, it would contribute to 50% of the LCOA of 0.44 \$/kg-NH_3 when using a carbon price of 100 €/ton-CO_{2-eq}. In table 1.1 the bandwidth of the levelized cost is also the result of variations in the price of natural gas.

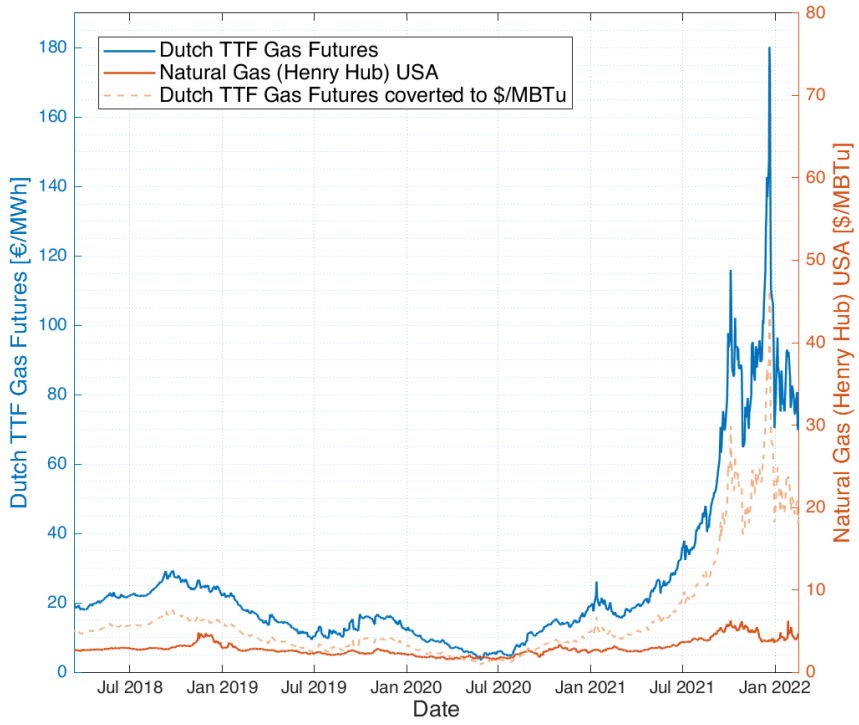


Figure 1.2: The price of natural gas of the previous 5 years. Showing both the American price traded on the Nymex market and the Dutch price traded on the ICE-ENDEX TTF. To compare the two the Dutch national gas price is converted using USD/EUR rate of 0.88 and a conversion factor of 0.29308 MWh/MBTU.

Natural gas is traded throughout the world on different markets. The price on these markets varies as well as the units used. The American gas price serves as a worldwide benchmark and is traded using the unit \$/ MBTu (million British Thermal units). The amount of gas traded in the Dutch market is given in MWh using a conversion factor of 0.2931 Mwh/MBTu. The prices from the past five years are shown in figure 1.2. The price of natural gas traded on the Dutch market is also converted to \$/MBTu to make it easier to compare with the gas traded on the American market. Due to hydraulic fracking being deployed on a large scale and large natural gas reserves, the price of natural gas has been lower on the US market. In the past half-year, the price in Europe has dramatically increased due to the tensions between Russia and Ukraine. The uncertainty about the situation combined with the already low natural gas supplies has caused the recent rapid increase. These factors had little impact on the price of American gas, as can be seen from the relative stable line in figure 1.2.

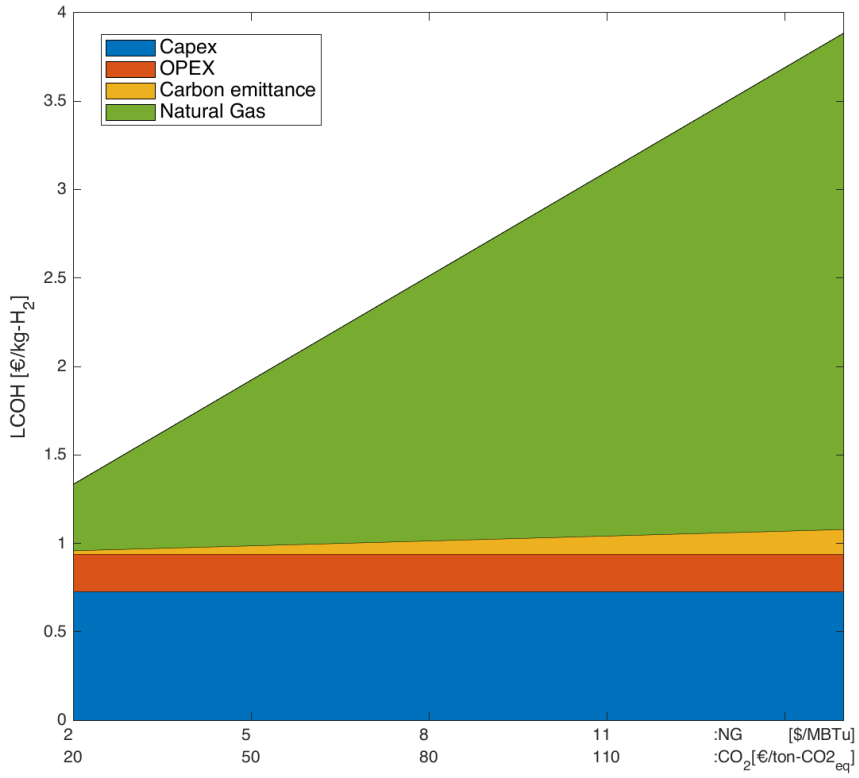


Figure 1.3: LCOH produced from fossil fuels. Created with data from table 1.3. On the x-axis the price of natural gas and CO_2 ranges from the minimum to the maximum.

The large impact of the price of natural gas on the levelized cost of hydrogen and ammonia has already been mentioned in the first paragraph of this chapter. Additionally, it is also visualized in the figures 1.3 and 1.4. The levelized cost has been calculated using equation 11 and the values presented in table 1.3. The values have been converted to €/kg for the CAPEX cost. To compare them with values from literature is difficult as most papers use different units ($\$/\text{kw}_e$, $\$/\text{kw}_H 2 - LHV$, $\$/\text{kw}_H HV$). To understand the difference between these capacity indications, the LHV and HHV must be understood. In literature, most papers use the LHV of (33.3 kWh/kg-H−2 in calculations. However, this is often a mistake as the LHV does not consider that the heat of the vaporized water is recovered after combustion by simply determining the amount of heat released during combustion with a starting temperature of 25°Celsius and a final temperature of 150°Celsius after cooling down. The LHV can be used in calculations in

which hydrogen is burned. However, in this research, it is transformed to ammonia; therefore, the HHV is preferred over the LHV. Because it represents the thermal energy released of all reaction products during hydrogen combustion, the HHV and LHV can also be described as the gross calorific value or the gross energy and the net calorific value.

	H_2	NH_3
CAPEX	8.48 €/kg-H_2	1.42 €/kg-NH_3
OPEX	2.5 % of CAPEX	2.5 % of CAPEX
Gas Consumption	173.72 MJ/kg-H_2	38.3 MJ/kg-NH_3
Electricity Consumption	-	1.3 MJ/kg-NH_3
Emission factor	1 kg-CO_2/kg-H_2	0.11 kg-CO_2/kg-NH_3

Table 1.3: Values converted from (Birol 2019) using a USD/EUR rate of 0.8898 from the day of publication. (IEAGHG 2017) used for the CAPEX, gas consumption and emission factor of hydrogen.

By observing the significant contribution of the natural gas price to the levelized cost of hydrogen and ammonia, it can be concluded that the competitiveness of green hydrogen and ammonia is primarily dependent on the natural gas price. A NG price of 7.81 $/MBTu would already lead to a LCOH of 2.5 €/kg-H_2 and a LCOA of 0.5311 €/kg-NH_3. In section 6.3 the levelized cost results of this research will be discussed, after which it is possible to determine the price that natural gas would have to reach to make the green alternative competitive.

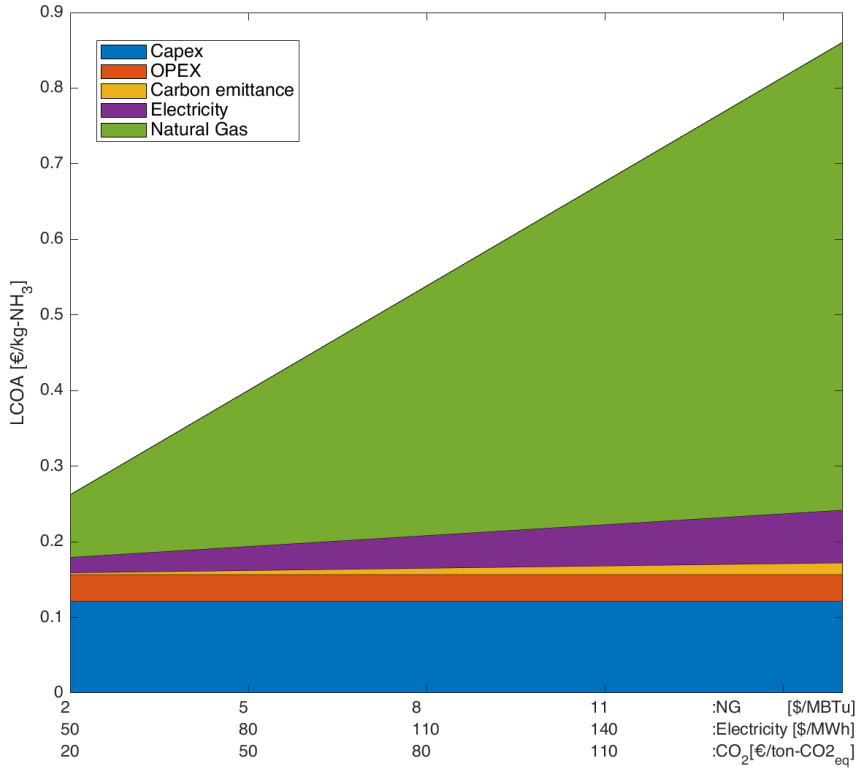


Figure 1.4: LCOA produced from fossil fuels. Created with data from table 1.3. On the x-axis the price of natural gas, electricity and CO_2 ranges from the minimum to the maximum.

The rapid increase in levelized cost due to the price of natural gas seems almost inconceivable. Nonetheless, comparing the increase of LCOH at the hands of the price of natural gas

with a study from the dutch bank ING (Hieminga and Tillier 2021), a similar increase can be observed using their results depicted in figure 1.5. Although the LCOH in the figure represents the prices in October 2020, the cost will not differ that much since the effect of an increase in CO2 price will probably compensate for a slight decrease in CAPEX. Therefore, it is assumed that the values used in table 1.3 are correct and give an accurate impression of the cost of hydrogen and ammonia produced with natural gas.

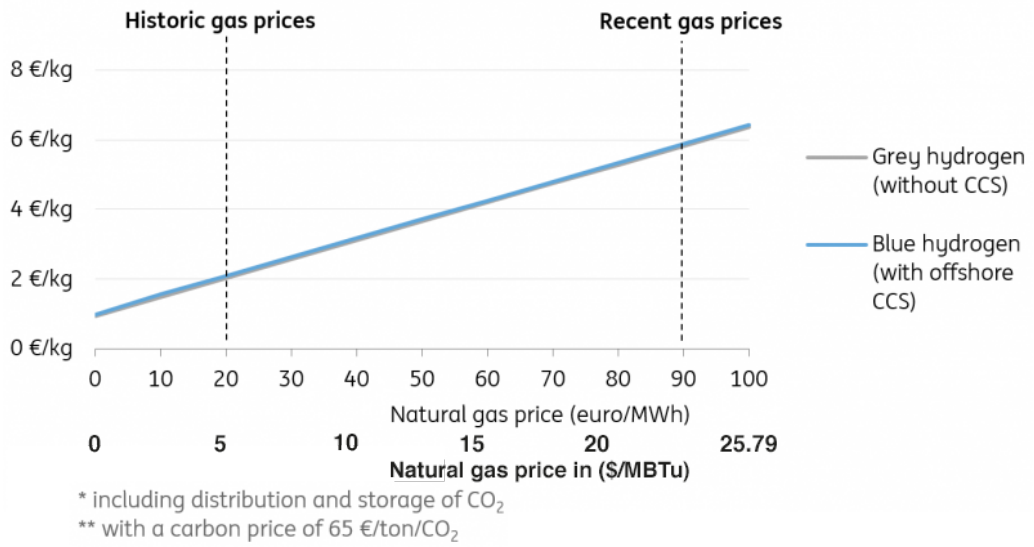


Figure 1.5: Modified from (Hieminga and Tillier 2021) to show natural gas price in $/MBTu as well. Converted using a USD/EUR rate of 0.88 and a conversion factor of 0.29308 MWh/MBTU.

1.2 Problem Statement

Determining the minimum levelized cost of future green hydrogen projects is essential in attracting more investments. This works in two ways as companies will have more certainty about their predicted revenue and, therefore, borrow money more efficiently, decreasing the WACC. Secondly, governments will better understand the measures required to bridge the gap between fossil fuel-based projects. However, there are not yet many large-scale green hydrogen or ammonia projects operating in the world today. Figure A.4 shows the current and planned capacity of electrolyzers around the world. This means that predictions of future projects rely primarily on simulation models instead of information gained from previous projects. In literature, the current solar to ammonia systems can be modelled more flexibly by using more independent components, such as separating the production from ammonia by inserting a cryogenic tank for nitrogen storage between the ASU and Haber-Bosch plant. These simulation models need to be as reliable as possible to draw a sensible conclusion about future green hydrogen and ammonia projects.

1.3 Research Gap

Numerous papers were thoroughly examined to determine how this paper could expand on the existing knowledge of solar power to ammonia systems. The differences between system designs, optimization models, proposed year of operation and whether it would produce hydrogen or ammonia as well have all been examined. Subsequently, four categories were defined to determine the knowledge gap. Separating papers that determine today's levelized costs and

those that determine the cost of future projects. Further distinguished by the production of ammonia and hydrogen or only hydrogen.

Starting with papers focused on systems designed to minimize the LCOH at the present time. (Grimm et al. 2020), (Gutiérrez-Martín et al. 2020) give a detailed look at the production of hydrogen with electricity generated from PV panels. The latter also integrates battery storage in the systems to deliver a more constant supply of electricity to the electrolyzer, thereby reducing the size of the electrolyzer. In (Grimm et al. 2020) a continuous optimization method is used to find the optimal scaling between the PV models and the electrolyzer, while in (Gutiérrez-Martín et al. 2020) a discrete, brute-force approach is used.

Extending on the PV to electrolyzer systems, the following studies take it one step further by adding an ASU and Haber-Bosch plant to produce ammonia from renewable energy sources. In (Fúnez Guerra et al. 2020), (Morgan et al. 2014) the Net Present Value of all components are minimized, while in (Cheema and Krewer 2018) the efficiency of the production process is optimised using a brute-force approach. (Morgan et al. 2014) is the only study that uses storage of hydrogen as well as nitrogen using cryogenic tanks. The study gives beneficial information on the specific processes in the components necessary for the production of ammonia using wind power on an island in the state of Maine in the USA. However, scaling the ammonia output to the load profile of a specific case that uses wind power instead of solar makes it difficult to compare the costs, especially when the levelized cost is not calculated but only the Net Present Value. In (Armijo and Philibert 2020) the levelised cost of both hydrogen and ammonia are both calculated by using a brute-force approach, and the lowest value is taken. Both batteries and nitrogen storage are left out of the designs in these systems. This has a negative impact on the flexibility of the system.

The studies that focus on the production of hydrogen in the future are (Gallardo et al. 2021) and (Mallapragada et al. 2020). In (Gallardo et al. 2021) the LCOH for 2018 as well as 2025 is calculated with a brute force approach in Matlab/Simulink. While the system does not contain batteries to reduce the size of the system, it is an extensive study similar to (Mallapragada et al. 2020) which calculates the minimal LCOH for 2030. In the latter, more components were optimized using mixed-integer linear programming.

In the last category of techno-economic articles about green hydrogen and ammonia production, the following studies all calculate the minimal cost of ammonia in 2030. In the extensive research of (Ikäheimo et al. 2018) the optimal operation was modelled for the complete energy production of certain regions in the North of Europe. In (Nayak-Luke et al. 2018) and (Nayak-Luke and Bañares-Alcántara 2020) an optimization of the component size is done to minimize the cost of LCOA. In the first paper, the system is explained, using hydrogen storage as the only buffer in the system. While in the second paper, the competitiveness with grey ammonia is comprehensively explained by calculating the LCOA for 534 different locations with the model delineated in (Nayak-Luke et al. 2018).

To summarise, not one paper uses the same system as the other papers. This makes it difficult to compare the influence of the individual components. Secondly, in the papers modelling ammonia production, hydrogen storage in salt caverns have not been included in any model. Instead, more expensive hydrogen storage tanks were used. Thirdly, most papers have primarily neglected the effect of the price for emitting CO_2, which will play a big part in the competitiveness with grey hydrogen and ammonia. Therefore, this paper focuses on a com-

prehensive system combining all of the components mentioned in the aforementioned papers while using a salt cavern to store hydrogen and elaborates on the price for emitting carbon dioxide.

1.4 Research Question

This research can be formulated in one main question and five sub-questions. The sub-questions are there to divide the main question into smaller parts, leading to a better understanding of the required knowledge necessary to answer the main question. At the time of writing, the main question is very relevant to the energy transitions. Based on well-founded research, decisions are made to invest in similar projects or opt for alternative renewable energy technologies. That is why it is essential to state that the answer to the main question presented in this paper is not the only possible answer.

Main Question:
How can a system that produces green hydrogen and ammonia be optimized to minimize the levelized cost and will this system be able to compete with fossil fuel based production in 2030?

As explained in the chapter 1.1 the current green hydrogen and ammonia projects are still around twice as expensive as hydrogen and ammonia produced using fossil fuels. Therefore, the date of 2030 has been chosen to investigate if this could be the turning point. An accurate answer will be constructed by simulating the production process of hydrogen and ammonia. The answer to sub-question one will provide a detailed schematic of the required system.

Sub-Question 1:
What components should be included in the design of a system that is able to produce green hydrogen and ammonia for the lowest LCOH and LCOA?

To find the minimum LCOH and LCOA, the components need to be scaled in perfect correlation with each other. The model also needs to allocate the energy carriers to meet all the constraints for the entire simulation period. How this can be achieved is the focus of sub-question 2 and 3.

Sub-Question 2:
How can the capacity of the components in the system be optimised to produce the lowest possible levelized cost per kg of H_2 or NH_3?

Sub-Question 3:
What kind of optimization problem is this and which program should be used to model it?

Once the system is designed, the optimization should produce the lowest possible LCOH and LCOA. Specific economic values must be defined to calculate the levelized cost. Sub-Question 4 also applies to the technical parameters necessary to formulate realistic constraints, for example, the load range of specific components.

Sub-Question 4:
What financial and technical data should be used in the model to optimize the capacity of the components and the allocation of the energy carriers?

As described in section 1.3 most of the current research in green hydrogen and ammonia has overlooked the potential of simulating hydrogen storage in salt caverns. That is why extra time is spent on the exact determination of the location in this research.

Sub-Question 5:
What is the best location for the system taking into account the solar irradiance and the possibility of storing hydrogen in a salt cavern?

With the aforementioned sub-questions, it will be possible to create a realistic simulation of hydrogen and ammonia production and optimize this to obtain the lowest possible levelized costs.

1.5 Research Objective

The main objective of this research is to create a realistic model that can minimize the levelized cost of the production of hydrogen and ammonia. When this is achieved, the levelized costs can be compared to the levelized cost of the alternative production method using fossil fuels. A conclusion will be drawn from this comparison to determine if green hydrogen and ammonia can compete with hydrogen and ammonia produced from fossil fuels in 2030. The production process simulation also gives a chance to analyze the functioning of the various components. By calculating the energy consumption, state of charge and capabilities of the components, conclusions will be drawn about the optimal design of the system.

1.6 Research Scope

Before defining the research scope, it must be noted that the reference date for the proposed project is set in 2030. This means that small changes in the applied technologies are inevitable, and therefore, this research will not dive into great technical detail of some of the production processes. It is assumed that this has no added value when answering the research questions. For the system design, the scope is limited to components that can be scaled to minimize the total levelized cost. As a result, the operations of the feed water production plant or the hydrogen compressor, necessary in the salt cavern, are not separately modelled but combined with the existing cost of running the electrolyzer and salt cavern, respectively. The electrical system is also not further examined after examining the electronic feasibility of the connections between the components. Because the rated voltage and current of the components will also change over time.

Furthermore, this research is limited to the production of hydrogen and ammonia. The academic value lies in the optimization model to calculate the minimal levelized cost of hydrogen and ammonia thereby, excluding research into the cost of transportation of the energy carriers to different parts of the world.

A specific location has also been selected instead of researching multiple locations. Extensive research has already been done in (Mallapragada et al. 2020) and (Nayak-Luke and Bañares-Alcántara 2020) to determine the best solar irradiance profile to reach the lowest levelized cost possible. This research will take that knowledge into account and examine the production on a specific location more intensively. This choice is also made as the aforementioned papers describe that their models spend days running on either a high performance computing cluster at the Massachusetts Institute of Technology (Mallapragada et al. 2020) or a network of

40 computers linked together (Nayak-Luke and Bañares-Alcántara 2020).

The scope of the model will have some limitations as well. Firstly, the energy efficiency of the components is assumed to be constant. In (Mallapragada et al. 2020) it is shown that the difference in electrolyzer efficiency between a minimum power loading and the maximum is 5%. This will have a minor impact on the produced levelized cost and will therefore not be modelled.

1.7 Research Method

The research method is composed of the following parts to provide well-founded answers to the research questions. First, a design of a system able to produce hydrogen and ammonia is constructed by combining the system designs of (Morgan et al. 2014) and (Mallapragada et al. 2020). Next, the corresponding CAPEX and OPEX costs plus the technical parameters of the components in the final system design are extracted from different research papers online. These numbers are verified by different industry leaders, including; Prof. Ad van Wijk, Frank Wouters, Hans Vrijenhoef and the company Deep.Kbb, for the salt cavern properties.

An optimization will be performed on the capacity sizes of the components to find the lowest levelized cost possible. For this optimization, Matlab's Optimization Toolbox is used in combination with the commercial program Gurobi to run the optimization as efficiently as possible. Using a problem-based approach to the mixed-integer linear programming problem instead of a solver-based approach allows for a more convenient notation of the many constraints present in the model. This is because all components are formulated following an object-orientated paradigm.

As input for the PV power, the capacity factor of the solar irradiance is calculated using Sandia's National Libraries PV_LIB Toolbox in Matlab (Stein et al. 2016) taking into account the temperature effects as well with data obtained from (Solcast 2021). The capacity factor is verified by calculating the total irradiance output and matching this against the data provided on the website *www.globalsolaratlas.info* for the same region. The obtained solar data is in time-steps of one hour, the smallest time-step possible to create a realistic simulation. However, this leads to a very long-running time and a large amount of memory usage, making it necessary to run the model on a high performance computing cluster of the TU Delft.

1.8 Report Outline

This report is structured as follows. In chapter 2 the layout of the designed system to produce hydrogen and ammonia is described together with the corresponding parameters of the components. Next, the production process is extensively discussed based on the various components in chapter 3. Chapter 4 elaborates on how these processes are modelled to calculate the minimum levelized cost. The determination of the location of this system is elaborated in chapter 5. The results of simulating the system are discussed in chapter 6, followed by a brief conclusion that summarizes the results in chapter 7. The relevance of the results are discussed in chapter 8 and to stimulate further research in this field, recommendations are given in chapter 9.

2 System Design

This chapter will elaborate on the system design necessary for hydrogen and ammonia production from solar energy for the lowest possible levelized costs. In chapter 2.1 the layout of the system is explained. Followed by an overview of all the parameters used for the different components of the system in chapter 2.2.

2.1 System Layout

After careful examination of the recent literature on the production of green hydrogen and ammonia (Mallapragada et al. 2020), (Gutiérrez-Martín et al. 2020), (Fúnez Guerra et al. 2020), (Gallardo et al. 2021), (Armijo and Philibert 2020) and (Ikäheimo et al. 2018) the system pictured in figure 2.1 was composed. The schematic of the system can be read from left to right. Starting with the PV block functioning as the primary source of energy. As described in chapter 3.1 the photovoltaic panels generate electricity from the incident irradiance using the photovoltaic effect. This electricity is distributed to the battery, electrolyzer, ASU and Haber-Bosch plant. The amount of electricity distributed is scaled to reach a yearly output of 200.000-ton ammonia. This amount has been chosen as it is commonly used in the industry. However, systems of this size can not rely on the electricity grid as a backup source because the amount of power required in the components is too high. Therefore, the electricity stored in the battery and consumed in the electrolyzer, ASU and Haber-Bosch plant is all provided by the PV panels. This, however, leads to great dependence on the incident solar irradiance. To combat the consequences of periods of lower irradiance due to cloud coverage. Three buffers are implemented in the system.

The largest of the three buffers (in terms of energy storage) is the salt cavern, depicted in figure 2.1 after the electrolyzer. This is because the Haber-Bosch plant is the most expensive component in the system, and the capacity will therefore be minimized. In order to minimize the capacity, a stable supply of hydrogen is essential because of the load limits defined in table 2.2. Load limits also apply to the electrolyzer; however, the CAPEX of the electrolyzer is much smaller than that of the Haber-Bosch plant, and the load limit is 1% - 110% as explained in chapter 3.4. This is a more extensive range than the load limit of the Haber-Bosch plant, namely 20%-100%. The resulting capacity of the battery will therefore be smaller than the capacity of the salt cavern. Finally, the last buffer in the system is the nitrogen storage tank. Further discussed in chapter 3.7 it ensures that the system operates as flexible as possible by allowing the ASU to produce more than the required amount of nitrogen in times of abundant solar irradiance.

The last two components in the system are pictured in figure 2.1 without a rectangle around them because they are not operated in island mode like the other components. In table 2.2 they are written under the column operational costs. They include the feedwater for the electrolyzer and the electricity use of the compressor. They are not operated in island mode because their power use is small compared to the power required by the other components. Therefore, they can retrieve electricity from the grid, which is assumed to be widely available as 99.6% of the Moroccan population had access to electricity in 2019 (World Bank Global Electrification Database 2019). Additionally, being independent of the electricity provided by the solar panels also creates a more flexible system, resulting in a lower levelized cost.

Finally, the smaller components in the system are taken into account under the name; bal-

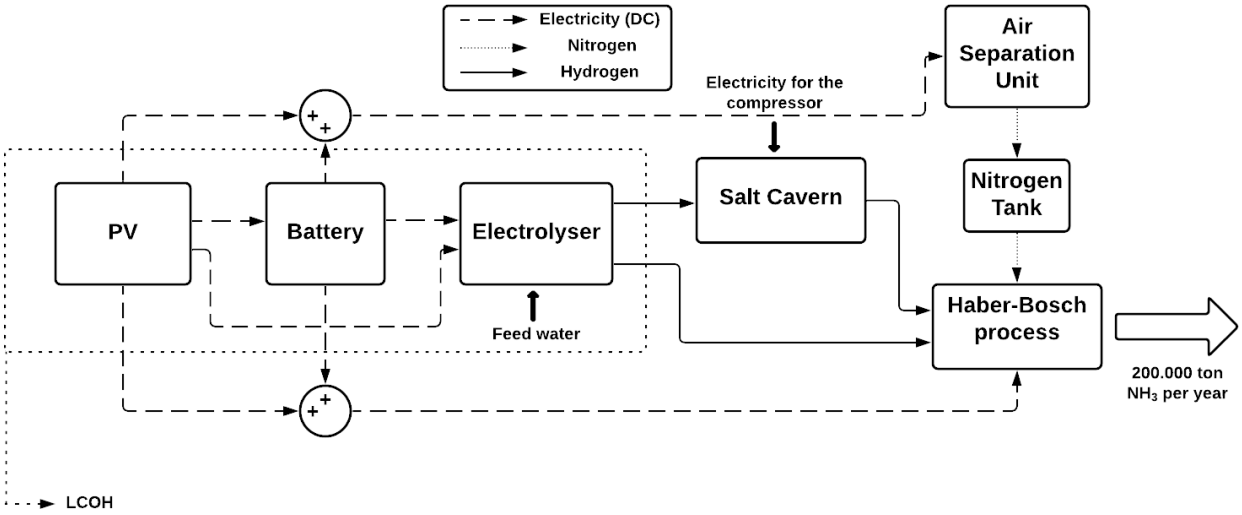


Figure 2.1: Schematic of the system modeled in this research. Scaled to the ammonia output of 200.000 ton per year.

ance of system costs. This is a conventional way of collecting the costs for the electric cables, converters, mounting frames, etcetera. 10% of the total levelized cost is taken to represent these costs. A more detailed approach has not been taken because the costs for these smaller components in 2030 are out of the scope of this research as they will have little influence on the total levelized cost and cannot be separately scaled. Therefore, it will not be taken into account in the optimization model but instead be added to the final outcome.

2.1.1 Wind Power

The electricity necessary to produce green hydrogen and ammonia can either be produced with wind or solar power or a combination of both. As figure 2.1 shows, this research only uses solar power; however, the possibility of using wind power has also been examined.

Figure 2.2 shows the average daily capacity factors of wind and solar, and even though the spike in wind power at the end of the day, when solar power is rapidly declining, looks very promising, the model does not allocate any capacity to the wind farm. This is mainly contributed to two reasons. One is the fluctuations of wind speeds throughout the year. This creates a somewhat unreliable source of electricity, as can be seen from the average weekly capacity factors shown in figure 2.3. To construct the capacity factor, the wind speed data has been taken from (Solcast 2021). The wind speed data is given at a height of 10 meters above the ground; however, the wind speed increases at higher altitudes. Equation 2 is used to calculate the wind speed at a hub height of 121 meters. The variation in the wind speed is pictured in a Weibull distribution shown in figure A.10. The probability density distribution shows that the most common wind speed is between 4 and 7 [m/s].

$$v = v_0 \frac{\ln\left(\frac{h}{z_0}\right)}{\ln\left(\frac{10}{z_0}\right)} \tag{2}$$

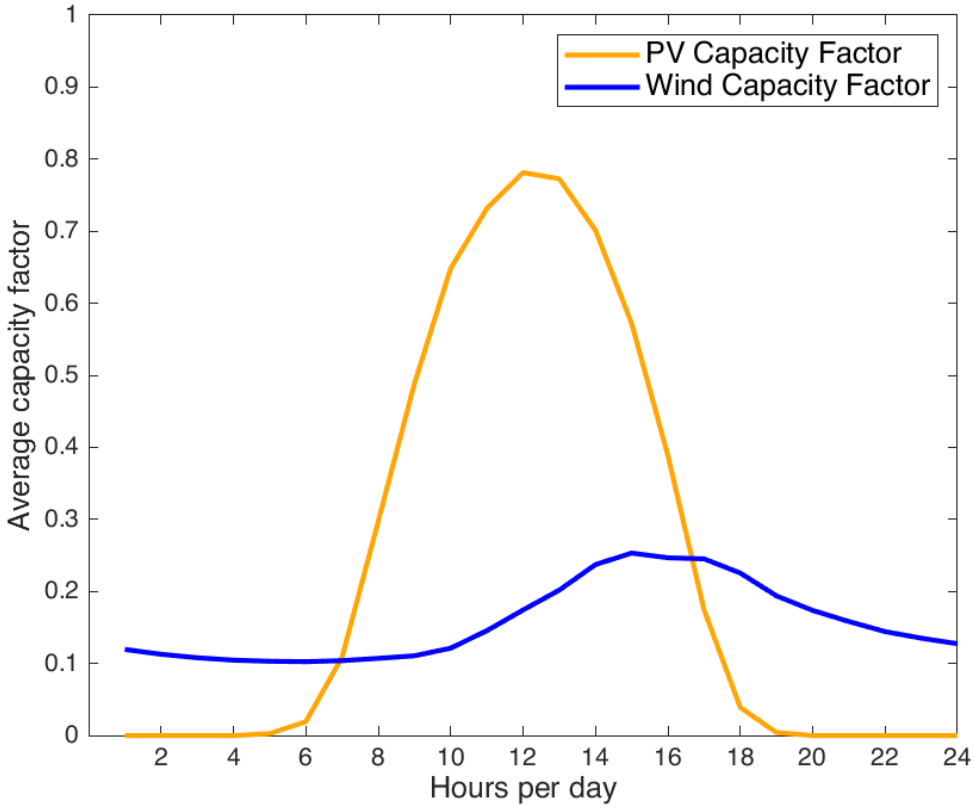


Figure 2.2: Average capacity factor of wind and solar power per hour.

The second reason the model does not allocate any capacity to the wind farm is that the capacity factors are relatively low. The average daily peak observed in figure 2.2 has a capacity factor of 0.25, while the average peak of solar power seen in the same figure has a capacity factor of 0.78. The average capacity factor for the entire year of solar is also much higher than for wind, 0.24 compared with 0.16. With an assumed cost for a land-based wind farm in 2030 of 630 €/kW (CAPEX) (National Renewable Energy Laboratory 2019), the model calculates that it is cheaper to install more batteries and store the abundant solar energy than to install wind turbines.

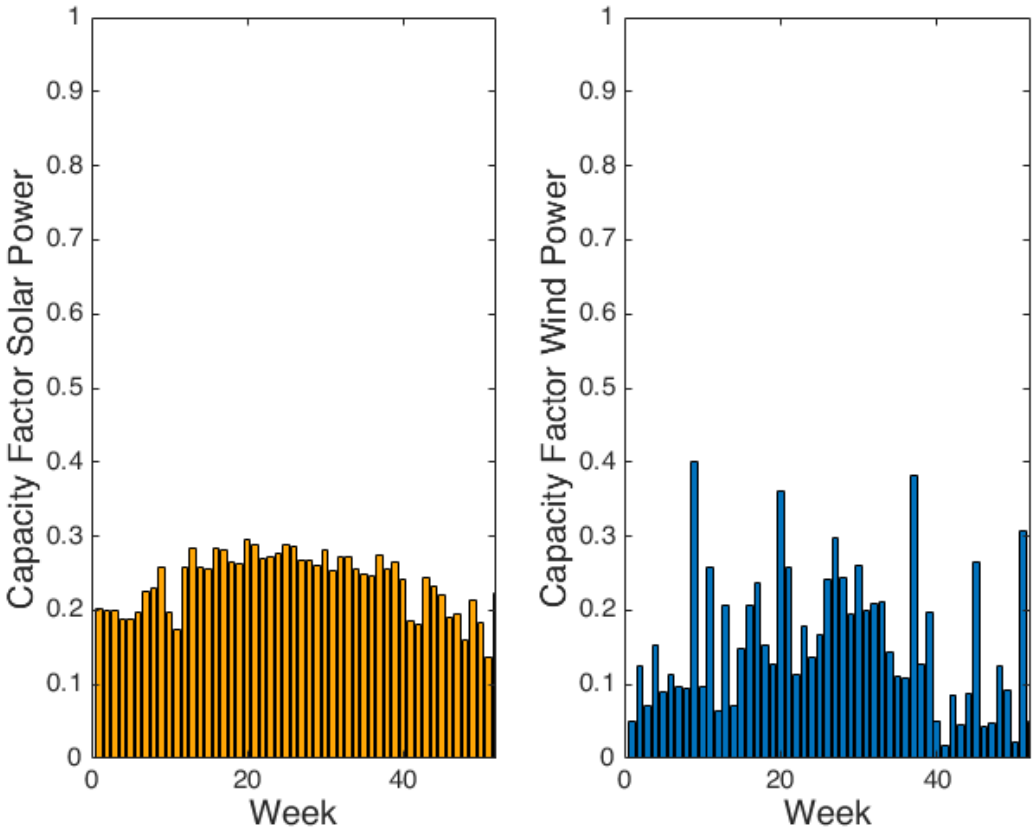


Figure 2.3: Average weekly capacity factor of solar and wind power.

2.2 Corresponding Parameters

From all of the components depicted in figure 2.1 the technical and financial data is necessary to create a realistic model. This data is collected in table 2.2. The components are separated into components that have a capital cost contribution and an operational cost contribution and the ones that only have an operational cost contribution. Furthermore, the last category contains the balance of system costs.

Cost assumptions 2030 of optimized components				
Component	CAPEX	OPEX (% capex)	Lifetime years	Additional Information
PV [a]	400 €/kw-DC [38,49]	1% [50,55]	30 [55]	Efficiency: 25% [55]. Irradiance data retrieved from [68].
Battery Power Capacity [a]	400 €/kW [55]	1% [55]	-	Self-discharge rate is expected to be 0.05% per day in 2030 [37].
Battery Energy Capacity [a]	70 €/kWh [55]	-	20,000 cycles [37]	Round-trip efficiency: 98% [37]. Self-discharge rate is expected to be 0.05% per day in 2030 [37].
Alkaline Electrolyzer [a]	180 €/kW [65]	1% [65]	100,000h stacks [5]	HHV of hydrogen: 39.4 kWh/kg. [30] Efficiency: 83% [65]. Load range stack: 10% - 110% relative to nominal load [6]
Salt Cavern Storage	16 €/kg [75] (0.4 €/kWh)	2% [25]	∞	Compressor cost included [75]. Not included electricity consumption of 1.42 kwh/kg-H_2 [61].
Haber-Bosch synthesis [b]	3000 €/kg-NH_3/h [35] (480 €/kw)	2% [35]	20 [35]	Electricity consumption is 0.532 MWh/ton-NH_3 [35]. Load range: 20% - 100% [57]. For a production of 20.000 ton ammonia 3600 ton hydrogen is required [78].
Air Separation Unit [c]	1450 €/kg-N_2/h [35] (7330 €/kWh)	2% [35]	20 [35]	Electricity consumption is 0.108 MWh/ton-N_2 [35].
Nitrogen Tank [d]	2.5 €/kg-N_2/h (12.50 €/kwh)	2%	30	Industrial scale cryogenic tanks 500-1500 m^3.

Operational costs, also optimized			
Component	Consumption	Cost	Application
Hydrogen compressor	1.42 kwh-AC/kg H2	0.07 €/kwh-AC	To compress hydrogen before entering the salt cavern.
Feed water	10 L/kg-H_2 [6]	0.42 €/m^3-H_2O [20]	The feed water used in the electrolyzer. Added to electrolyzer cost so it will be otpimized

Additional cost, not optimized			
Component	Consumption	Cost	Application
Balance of System	-	10% off levelized cost	To account for DC-cabling, converters and mounting installations of the system.

Table 2.2: Parameters for all system components in 2030

[a] Prices have been converted to euro's using the average exchange rate in the year of publication [47].
[b] Initial value was 3000 €/kg NH_3 per hour but has been converted using the energy density of Ammonia of 22.5 MJ/kg [74], resulting in 6.25 kwh/kg.
[c] Initial value was 1450 €/kg N_2 per hour but has been converted using the energy density of liquid Nitrogen of 712 kJ/kg [64], resulting in 0.19 kwh/kg .
[d] Consulted Frank Wouters and Linde Inc. for the costs of cryogenic storage tanks for liquid nitrogen. With a density of 500-600 kg/m^3.

3 Production Processes

This chapter gives a detailed description of every step in the production process. For the components most effected by the surge in renewable energy investments the chosen costs and learning rates will also be explained. This includes the PV panels, battery, electrolyzer and salt cavern. Starting with a detailed description of the workings principle of a solar cell in chapter 3.1. Following the flow of energy as presented in figure 2.1 the implementation of the battery is discussed in more detail in chapter 3.2. In chapter 3.3 the chosen technology for the electrolyzer is discussed followed by a detailed description of the electrolysis process in chapter 3.4. The implementation of a salt cavern in the system for storing hydrogen is discussed in chapter 3.5. The supply of nitrogen for ammonia production is discussed in chapter 3.6 and chapter 3.7. The last component in the production process of ammonia is the Haber-Bosch plant. The production process in this plant is described in chapter 3.8. Furthermore, the remaining components that receive electricity from the grid instead of the PV panels are elaborated on in the chapter 3.9 and 3.10.

3.1 Photovolataic panels

Electricity is generated in the PV panels due to the photovoltaic effect. A phenomenon already discovered in 1839 by Edmond Becquerel (Lincot 2017). When sunlight hits a semiconductor material like silicon, the photons in light cause the electrons and holes to split. These are positively and negatively charged particles that want to recombine. However, when a junction is created between these particles, the only option to recombine is if the electrons move through the metal contacts connecting the front and back of the cell. This flow of electrons is the electric current produced by the PV panels. In the designed system, the current generated will be used to power the electrolyzer, ASU or Haber-Bosch plant or charge the batteries.

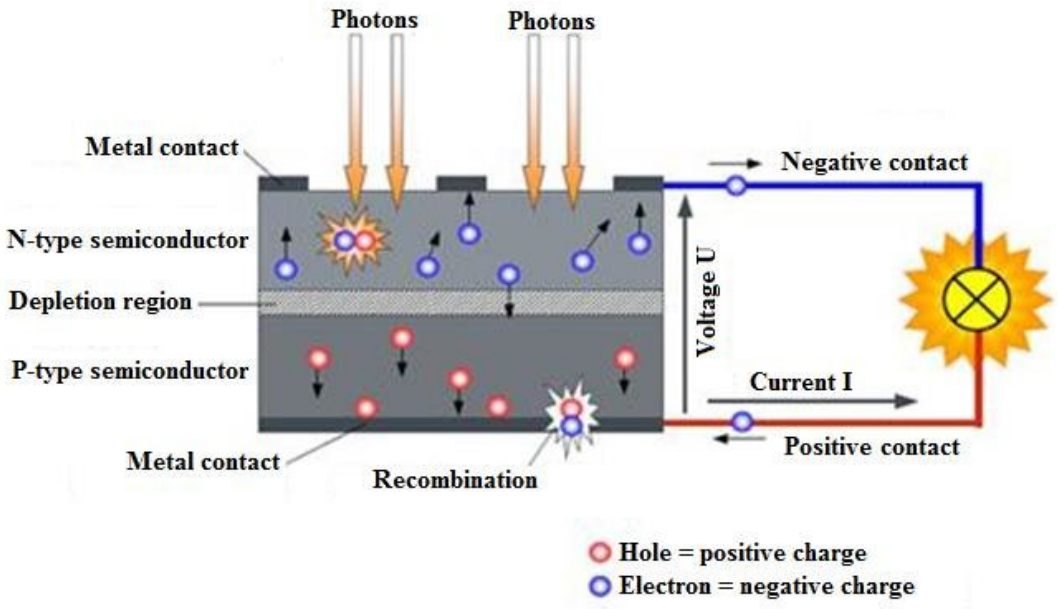


Figure 3.1: The photovoltaic effect illustrated. Retrieved from (Kavaz et al. 2014)

An average PV panel of 245 watts has an open circuit voltage of 37.5 volts and a short

circuit current of 8.68 amperes. The maximum power point (MPP) tracking software tries to maximize the efficiency by keeping the voltage close to its V_{mpp} and I_{mpp} values of 30.2 volts and 8.13 amperes (International Finance Corporation 2015). However, every type of PV panel has different technical specifications, and over the years, these specifications will develop as well. Therefore, this research leaves these electric specifications out of the scope as this will not affect the final outcome since it is already proven that PV farms of this size can be built and operated effectively.

To discover the values written in table 2.2 for the cost and efficiency in the year 2030, the learning rates presented in literature together with the estimated price of the CAPEX and OPEX have been used. The 25% efficiency used for the solar panels is a result of a historical average increase in efficiency of 0.5% per year extrapolated to the year 2030 **??**. For the CAPEX cost the values in literature vary considerably, in (IRENA 2019) a price between 340 and 834 $/kW (300 - 735 €/kW, converted with 1.1350 USD/EUR the average rate in month of publication) is suggested. While (Atkins 2020) has performed a comprehensive study to the learning rates described in various studies. Pictured in figure 3.2 shows the variation in price in 2030 between 320 €/kW and 800 €/kW. In this research a CAPEX cost of 400 €/kW was assumed corresponding to the fast scenario of (Vartiainen et al. 2020) which uses compound annual growth rate of 20%.

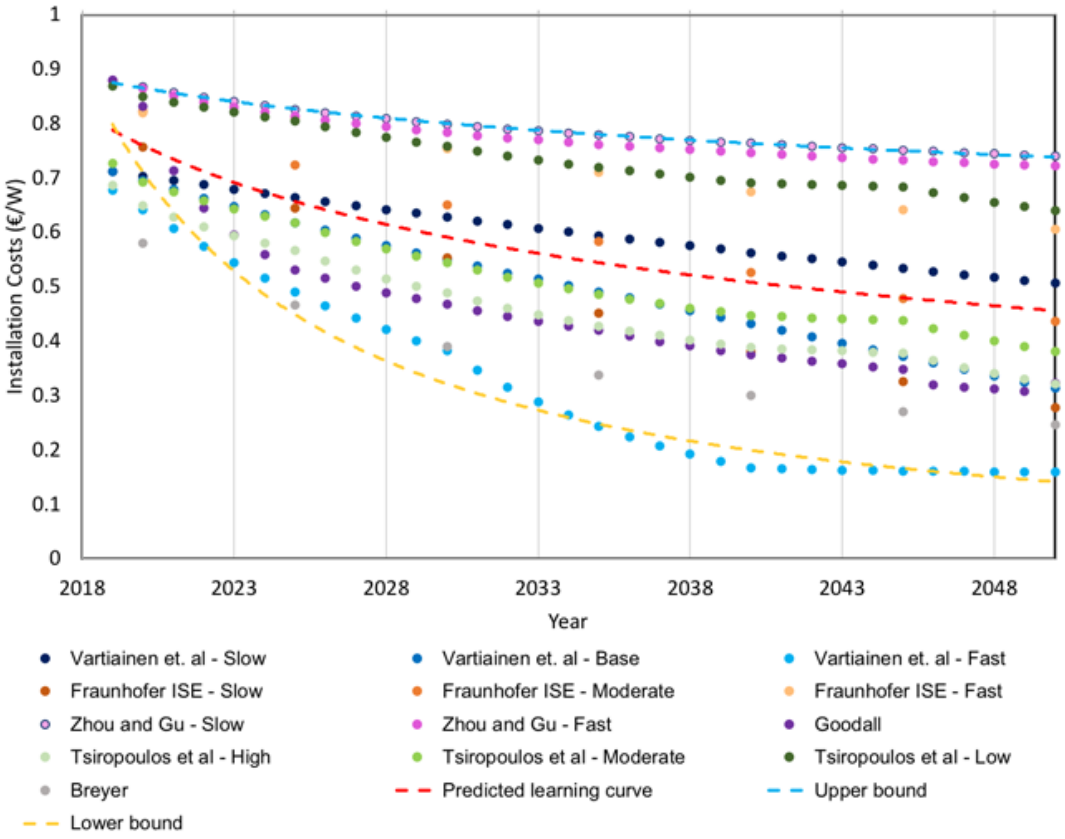


Figure 3.2: The learning rates of various studies collected in the comprehensive study of (Atkins 2020)

3.2 Battery

The battery is implemented in the system to store electricity during the day and release the electricity at night to keep the production of hydrogen, nitrogen and ammonia running. It is also used to control the flow of electricity more stably so that the ramping up limits of 20% are not exceeded. However, the solar irradiance gradually increases or decreases in most cases because not many clouds hover above the PV panels. Resulting in a battery capacity that only has to keep the production operations of hydrogen, nitrogen and ammonia going at a minimum.

The prediction is that lithium-ion batteries will be the cheapest technology according to the (National Renewable Energy Laboratory 2019), with degradation of 0.05% a day and no need to convert the electricity back to AC. Lithium-ion batteries are an efficient way of storing electricity. The working principle of lithium-ion batteries is similar to the PV panels, but instead of silicon, lithium is used as a semiconductor material. During discharge, the lithium ions in the anode spilt from the electrons and travel through the electrolyte to the cathode. The electrons, eager to recombine with the lithium ions, move through the external circuit to the cathode creating an electric current. When charging the batteries, the process is reversed, and the electrons and lithium ions move in opposite directions. The nominal voltage of the batteries often matches the nominal voltage of the PV panels. As a result, the number of batteries connected in series is the same as the number of PV panels connected in series. For this research, the electricity plan does not affect the desired results, and therefore it does not dive deeper into the electronic connections.

The CAPEX cost of the battery is divided into the power and storage capacity. The power capacity is the amount of power that can be released at a particular moment in kW, while the energy capacity represents the amount of energy that can be stored, measured in kWh. Both of these components are separately modelled to find their optimal value. The ratio between the two is used to determine the storage duration of the battery. In literature, the cost of batteries in future scenarios is often given for a storage duration of four hours. Meaning that the energy stored is four times as high as the power capacity. In (NREL Annual Baseline Technology Report 2021) the cost for the two capacities combined in 2030 is $ 566/kW. This number has been derived by taking a learning rate of 7.7% from 2020 to 2025 and a learning rate of 6.5% for the remaining five years. The assumption of taking the most commonly used storage duration value of 4 hours will be evaluated by investigating the capacity results in chapter 6.1.

3.3 Electrolyzer type

Similar to the photovoltaic effect described in chapter 3.1, the electrolysis of water resulting in the production of Hydrogen and Oxygen is already centuries old. Performed first in 1789 by Adriaan Paets van Troostwijk and Jan Rudolph Deiman (Mulder and Geerlings 2020). Nowadays, there are three main types of electrolyzers.

- **Alkaline**: Is the oldest and most commonly used technique in large-scale electrolysis. Pictured in Figure 3.3 the system requires the least amount of maintenance. However, they take up 0.095 (m^2/kWe) around twice as much space as PEM electrolyzers, 0.048 (m^2/kWe)(Birol 2019).
- **Proton Exchange Membrane (PEM)**; PEM electrolyzers are more flexible than alkaline electrolyzers, although they work with similar pressure and temperature. However, the

electrode materials (platinum, iridium) are scarcer than the nickel used in alkaline electrolysis, resulting in higher installation costs.

- **Solid Oxide Electrolyzer Cell (SOEC)**: This technology has much potential but is currently not yet commercially available. Working at a temperature of around 800 °Celsius the components degrade faster. The advantages are a higher efficiency, and it can also be operated as a fuel cell, producing electricity from hydrogen.

The combination of a desolate location providing enough space and the scale of the project results that alkaline electrolysis is the preferred technology in this research. Similar studies show that alkaline electrolysis produces the lowest LCOH as well (Gallardo et al. 2021).

3.4 Hydrogen Production

In Alkaline production, two electrodes are placed next to each other with a permeable membrane in between to prevent oxygen and hydrogen from mixing. The membrane does allow hydroxide ions and the electrolyte to pass through, keeping the solution in balance. In order to retain sufficient ionic transfer, 25%-30% potassium hydroxide (KOH) is often added to the electrolyte. The chemical reactions that occur when a current runs through the electrodes are:

$$Cathode : 2H_2O(l) + 2e^- \implies H_2(g) + 2OH^-(aq) \tag{3a}$$

$$Anode : 2OH^-(aq) \implies \frac{1}{2}O_2(g) + H_2O(l) + 2e^- \tag{3b}$$

$$\boldsymbol{Overall\ Reaction : 2H_2O(l) \implies 2H_2(g) + O_2(g)} \tag{3c}$$

According to (Birol 2019) the load range of an individual stack is 10%-110% to prevent a dangerous mixture of oxygen and hydrogen from forming. To improve the load range of the whole electrolyzer the stacks can be placed in parallel. If the load would then reduce to less than 10%, multiple series of stacks could be shut down while keeping a few running. This way, if ten rows of stacks are placed in parallel, the minimum load range would reduce to 1%. The operating limits for the individual stacks are 120A and between 37V and 41V (Ursúa et al. 2016). Therefore, to connect ten rows parallel, the electrolyzer must be connected to 1200A.

The cost as formulated in table 2.2 for the electrolyzer have come about by combining the costs in literature with the prediction of Prof. Ad van Wijk. This value is lower than most values is literature that seem to have a minimum of 300 $/kW (Mallapragada et al. 2020). This is done because the predictions in literature for such an extremely fast developing technology often lag behind the development that has already been done during the time between the research and publishing the article. To determine the required learning rate that is necessary for the CAPEX to reach 180 €/kW in 2030, a CAPEX of 685 €/kW in 2020 is taken (converted from (Mallapragada et al. 2020) using EUR/USD on day of publication). This results in a learning rate of 7.3% per year and a total decrease by 73.7%.

3.5 Salt Cavern

To provide a stable source of hydrogen for ammonia production. Hydrogen will be stored in a salt cavern. The Capex costs of this method vary from 2.69 €/kg-H_2 (Penev et al. 2019) to 33 €/kg-H_2 (Ahluwalia et al. 2019), (Mallapragada et al. 2020) depending on the cost that are included. In this research 16 €/kg-H_2 of (Van Wijk and Wouters 2019) is used, which includes

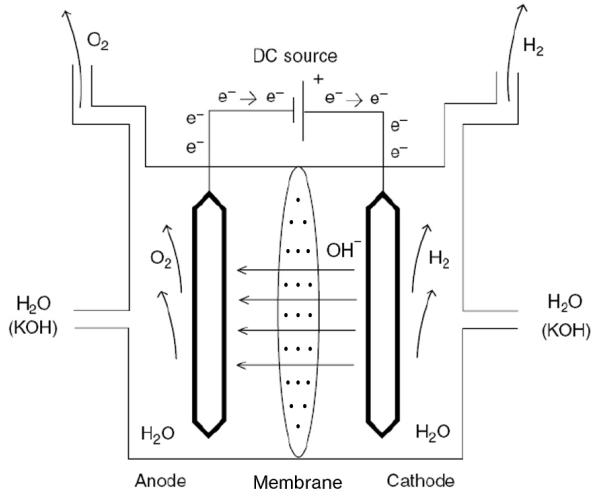


Figure 3.3: Schematic layout of alkaline electrolysis. Modified from (Mulder and Geerlings 2020)

the installation cost of the compressor. The cost of the cushion gas, which accounts for about 30% of the salt cavern's capacity (Lord et al. 2014) is also taken into account. The cost can be calculated by multiplying the production costs of hydrogen with the amount of cushion gas and adding the opportunity costs over this investment. Lastly, the cushion gas can be extracted once the project is finished. Selling the remaining cushion gas creates revenue which can be subtracted from the cushion gas cost (Quintela De Saldanha 2021).

$$\begin{aligned}\text{Cushion Gas Cost} = \text{Cavern Capacity} \cdot 0.3 \cdot H_{2\ Production\ price} \\ \cdot (1 + WACC)^{Lifetime} - \text{Cavern Capacity} \cdot 0.3 \cdot H_{2\ Price}\end{aligned} \tag{4}$$

The method for adding the opportunity costs to the overall cost of the cushion gas is similar to the composition of the salt cavern initial costs discussed in chapter 4.4. The total cushion gas cost calculated with equation 4 is added to the overall cost of the salt mine. The final costs can be found in chapter 6.3.1, but they remain minor compared to the other costs. This was also concluded by (Quintela De Saldanha 2021).

3.6 Air Separation Unit

The ASU is responsible for retrieving nitrogen from the air to react with hydrogen to form ammonia. The first step in retrieving nitrogen from the air is to remove the dust and pollen using an air filter. Carbon dioxide and hydrocarbons are also removed by compression in a purification unit to prevent ice and dry ice from forming water vapour. Finally, the temperature is brought down to -173 °C, and nitrogen is separated by fractional distillation in a distillation column. Nitrogen is liquefied at -196 °C under standard pressure of 1 bar, while Oxygen (-183 °C) and Argon (-186 °C) are liquefied at different temperatures. This process is widely used worldwide as liquid nitrogen is commonly used as a refrigerant. Gaseous nitrogen is also extensively used for various purposes like food packaging, steel production and crude oil extractions.

3.7 Nitrogen Tank

Once the nitrogen is separated from the air under -173 °C temperatures, it is directly transported through pipelines to a cryogenic tank. This tank remains below the boiling temperature of nitrogen so that the gas stays in its liquid form. According to (Linde AG 2021) and an employee of Linde AG contacted through e-mail, the pressure in the tank is 18 bar. Similar to the pressure in the ASU. The resulting density is between 500 - 600 kg/m^3. For industrial-scale storage, the volume of cryogenic tanks are in the range of 500-1500 m^3 (information supplied by Frank Wouters, Worley). Therefore, the maximum mass of liquid nitrogen that can be stored is 750.000 kg. This is taken into account in the model.

The liquid nitrogen coming from the ASU is forced to enter the cryogenic tank before moving to the Haber-Bosch plant. This design has been chosen because of the extremely low temperatures and the relatively small amounts of nitrogen, making it harder to keep the nitrogen liquefied. After the salt cavern, the nitrogen tank is also the cheapest component in the system, making it less of a priority to find its absolute minimum capacity.

3.8 Ammonia Production

Once the liquid nitrogen leaves the cryogenic tanks, it enters the last stage of the production process of ammonia from solar energy. In the Haber-Bosch plant, the nitrogen is recombined with hydrogen at around 400 to 500 °C and 7 to 30 bar of pressure. The two gasses are pushed through an iron catalyst that creates an endothermic reaction written in equation 5. This process is energy-intensive because of the high temperatures. It consumes 0.532 MWh of electricity per ton ammonia (Ikäheimo et al. 2018). Potassium hydroxide is often added to the iron for higher efficiencies.

$$N_2(g) + 3H_2(g) \Longleftrightarrow 2NH_3(g) \quad \delta H = -93[kJ/mol] \tag{5}$$

3.9 Feed Water

In the production of hydrogen, written in equation 3c, water together with electricity is the only necessary inputs. The supply of electricity is already extensively discussed in the aforementioned chapters. However, the feedwater supply has not yet been elaborated on until now. This is because the feedwater supply chain can be set up independently of the system discussed in this report. Depending on the capacity of the local water distribution system, the project is either able to directly deionize the water creating the necessary demi water from the available freshwater sources. Alternatively, seawater will need to be transported through pipelines to a desalination plant to extract the salt. The sequential step of deionizing the water can take place. Rather than simulating this process, a price of 0.42 €/m$_3$ has been taken for the feed water cost (Franz 2017). This simplification is justified based on the calculation of the total feed water cost and the minimal impact that this cost has on the total levelized cost.

$$\text{Feed Water Cost} = 200,000\,_{ton\ NH_3} \cdot \frac{1}{\text{Ratio_NH}_3\text{_H}_2} \cdot \text{Ratio_Water_H}_2 \cdot \text{Feed_Water_price} \tag{6}$$

When using the highest number found in the literature for the conversion of water to hydrogen, 30.2 kg-H_2O/kg-H_2 (Lampert et al. 2016). The corresponding feed water cost per year is 0.55 million euro, when using a Ratio_NH_3_H_2 of 5.56 [kg-NH_3/kg-H_2]. Although this is a vast number, in figure 6.6 it can be seen that the contribution to the levelized cost is minimal and therefore simplified using a constant price of 0.42 €/m_3.

3.10 Compressor

The hydrogen in the salt cavern can be stored between 60 and 200 bar, as calculated in chapter 5.2.2. However, the hydrogen leaves the electrolyzer with a pressure of 30 bar. A compressor is used to make up for the pressure difference. An electric consumption of 1.42 kWh-AC/kg-H2 is taken from (Penev and Hunter 2019). The total amount of electricity consumed is relatively small, and as a result, the compressor can be connected to the electricity grid and does not have to rely on the PV panels. This benefits the installation cost of the compressor because there is no need for an inverter anymore.

In reality, the consumption of electricity by the compressor would vary according to the pressure difference that needs to be overcome. A higher electricity consumption is expected if the pressure gap is larger. However, in (Quintela De Saldanha 2021), the author calculates that the electricity consumption given by the Max energy intensity is 0.52 kWh/kg for the compression of hydrogen from 32 to 84 bar. Meanwhile, the compression of 55 to 180 bar would require 0.50 kWh/kg using the equations 7 and 8. The contradictory result is explained by the effect of the inlet temperature of the hydrogen.

$$\text{Power} = Z \cdot \dot{m} \cdot R \cdot T \cdot ns \cdot \frac{1}{\eta} \cdot \frac{k}{k-1} \cdot \left[\frac{P_{\text{outlet}}}{P_{\text{inlet}}}^{\frac{k-1}{n \cdot k}} - 1 \right] \quad [kW] \tag{7}$$

$$\text{Max Energy Intensity} = \frac{\text{Power}_{Compressor}}{\text{Max Peak Capacity}} \quad \left[kWh \cdot kg^{-1} \right] \tag{8}$$

The results for the differences in consumption of electricity in (Quintela De Saldanha 2021) show that the difference is small compared to the difference in pressure. For this reason, combined with the small contribution of the compressor to the total levelized cost, described in chapter 6.3.1. The electricity consumption is assumed constant with a value of 1.42 kWh-AC/kg-H2 (Penev and Hunter 2019). After consulting Prof. Ad van Wijk, it is also assumed that the hydrogen lost in the compression is negligible, and an efficiency of 100% is therefore used in the model.

3.11 Balance of System

To encompass all costs related to installing and maintaining a solar to ammonia system, the BOS cost is included to represent everything besides the main components. This includes; the wiring with DC-cabling to transport the electricity, the pipelines necessary to transport hydrogen, nitrogen and ammonia, converters that change the voltage of electricity, thyristors to control the flow of electricity, a mounting system for the PV panels and many smaller components. Assuming a 40% decline in the BOS cost the (National Renewable Energy Laboratory 2019) a value of 10% is used for the BOS costs of the entire system.

4 Model description

The model responsible for implementing the technologies discussed in the previous chapter is elaborated in this chapter. A general description of the optimization model is given in chapter 4.1. Followed by an in-detail description of the exact working principles of the algorithms behind the optimization model in chapter 4.7. The starting point for the optimization model is the capacity factor of the PV farm. The necessary steps to model the capacity factor are described in chapter 4.3. To create a complete picture of the model, an explanation of the most difficult to model components, the buffers, is given in chapter 4.4.

4.1 Optimization model

To calculate the optimal amount of capacity for the different components in the system in order to minimize the LCOA. MATLAB's Problem-Based approach was used in combination with Gurobi. This presented a challenge because the time step should be as small as possible to create a realistic model. Otherwise, the intermittency of renewable energy would not be considered. Using meteorological data of Solcast available in 1 hour time steps, the array size in MATLAB gets too large to run on a standard laptop for periods longer than four months. An HPC cluster of the TU Delft was used to combat this problem and run the model for a period of nine months. A simulation for an entire year was preferred. However, the time it takes for the model to run increases exponentially when extending the simulation period. A simulation period of nine months already took two days to run on the HPC cluster, using 230 GB. A simulation of 10 months already extended the maximum run time of seven days.

$$\underline{\textbf{Objective Function}} = Minimize\Big(Lev.\ cost\ PV + Lev.\ cost\ Battery\ Energy + Lev.\ cost\ Battery\ Power + Lev.\ cost\ Electrolyzer + Feed\ Water\ cost + Lev.\ cost\ Salt\ Cavern\ capacity + Salt\ Cavern\ opportunity\ cost + Compressor\ electricty\ cost + Lev.\ cost\ ASU + Lev.\ cost\ Nitrogen\ Tank + Lev.\ cost\ Haber{-}Bosch\ plant \Big) \tag{9}$$

In the objective function of the model written in equation 9 the abbreviation of *Lev.* stands for levelized, referring to the levelized cost of the components. Adding these individual levelized costs together with the feed water cost used in the electrolyzer and the electricity used by the compressor in the salt cavern, the total levelized cost is calculated. With the corresponding degrees of freedom, constraints and model parameter enclosed in the appendix, the model can be solved using MATLAB's problem-based solver for Mixed Integer Linear Programming. This program automatically selects the *intlinprog* function to find a suitable ratio between the capacity sizes of the components in order to minimize the objective function. Formulas 10 and 11 were used to calculate the levelized cost.

$$CRF = WACC \cdot \frac{1}{1 - \frac{1}{(1+WACC)^t}} \tag{10}$$

$$Levelized\ Cost = \frac{CRF \cdot CAPEX + OPEX}{Amount\ produced} \tag{11}$$

The risk of the proposed project for the investors was assumed to be relatively low, based on the fact that Morocco already has much experience with the successful construction of renewable energy projects. Last decade Morocco invested 5.3$ billion in renewable energy projects, resulting in a 20% share of renewable electricity in the total demand (Kasraoui 2021). Therefore, a Weighted Average Cost of Capital (WACC) of 7% has been used. Combined with the costs of the components written in table 2.2 as well as additional parameters, the model was constructed.

4.2 Working principle of the model

In essence, the model finds the cheapest levelized cost to produce 200,000 ton-NH_3 per year. The levelized cost is dependent on every component written in table 2.2 as shown in equation 11. An increase in the capacity of a component will mean an increase in the levelized cost; therefore, the model tries to keep the capacity of all components to a minimum. However, because some components are more expensive than others, like the Haber-Bosch plant, the effort to minimize the capacity of those components will be prioritized.

The constraints in figure 4.1 are used to determine the capacity. Using MILP, further discussed in chapter 4.7 the model will carry out iterations in which the capacity of a single component is changed. If this decreases the levelized cost, it will continue down this path. All while keeping the other constraints, like state of charge and ramping limits, satisfied. All constraints are written in chapter A.8 of the appendix. Divided into four sections, the capacity determining constraints also pictured in figure 4.1 affect the levelized cost directly. The other three groups of constraints are there to create a realistic model. The operational constraints, for example, ensure that the energy balances in the system are correct. In the first constraint, the output of the PV farm and the battery is equal to the battery's input, ASU, Haber-Bosch plant and electrolyzer. This corresponds to all the DC-electricity lines in figure 2.1.

Capacity Determining Constraints

1. $PV_{Out,t} = CF_{PV} * Cap_PV$
2. $SOC_Bat_t = SOC_Bat_{(t-1)} + \frac{vBat_{in,t} * \eta_{Bat,Charge} - \frac{vBat_{Out,t}}{\eta_{Bat,Discharge}}}{Cap_Bat_Ene}$
3. $\mid vBat_{in,t} + \frac{vBat_{Out,t}}{\eta_{Bat,Discharge}} \mid \leq Cap_Bat_Pow$
4. $1\% \leq \left(\frac{vElec_In_t}{Cap_Ele}\right) * 100 \leq 110\%$
5. $SOC_Sal_t = SOC_Sal_{(t-1)} + \frac{vSalt_{In,t} - vSal_{out,t}}{Cap_Sal}$
6. $SOC_Sal_{(t=1)} = Cap_Salt_Cavern_Initial$
7. $\frac{vASU_Elec_t}{\text{Ratio_Elec_N}_2} \leq Cap_ASU$
8. $0\% \leq \left(\frac{N_2_Tank_Mut_t + N_2_Tank_Mut_{(t-1)}}{Cap_Nitrogen_Tank}\right) * 100 \leq 100\%$
9. $20\% \leq \left(\frac{(vSal_{out,t} + Ele_H_B_t) * \text{Ratio_NH}_3\text{_H}_2}{Cap_H_B}\right) * 100 \leq 100\%$
10. $vElec_Com_used = \text{Com_Ene_H}_2 * vSalt_{In,t}$
11. $H_2O_used = \text{Ratio_Water_H}_2 * vEle_In_t * \text{HHV_H}_2$

1. The primary energy produced is determined by multiplying the PV capacity times the capacity factor.
2. The battery's capacity is determined by the cumulative difference between electricity going in and electricity going out.
3. The battery power is the amount of electricity that can be charged or discharged at a particular moment
4. The capacity of the electrolyzer is set so that the electricity going in will never breach the limits of 1% and 110%.
5. Similar to the battery, the capacity of the salt cavern is determined by the cumulative difference of hydrogen going in and out.
6. The initial amount of hydrogen in the salt cavern is also calculated and present in the objective function.
7. The capacity of the ASU is given in kg-N2/h; therefore, the electricity going in is divided by the electricity consumption to produce nitrogen.
8. The maximum build-up of nitrogen sets the dimension for the capacity of the cryogenic tanks.
9. The capacity of the Haber-Bosch plant is defined in kg-NH3; therefore, the two hydrogen feed streams are multiplied with Ratio_NH3_H2.
10. The electricity consumed by the compressor is calculated by multiplying the electricity consumption times the hydrogen going in.
11. Calculates the demineralized water used in the electrolyzer.

Figure 4.1: Constraints implemented in the model that determine the capacity of different components with a brief description.

4.3 Modeling PV load

The system starts with the output of the PV farm. However, the PV capacity is not yet known because the optimization model, explained in chapter 4.1, still needs to calculate all the capacities of the components to find the minimal levelized cost. Therefore, this paper uses a capacity factor with an hourly time step that is multiplied by the variable PV capacity to simulate the primary energy of the system.

The capacity factor is calculated using meteorological data from the website (Solcast 2021). This data distinguishes three types of solar irradiance; Direct Normal Irradiance (DNI), Global Horizontal Irradiance (GHI) and Diffuse Horizontal Irradiance (DHI). Using Sandia's National Libraries PV_LIB Toolbox (Stein et al. 2016) these three types can be combined to calculate the total incident irradiance on the PV panels. The resulting values are given for every possible tilt angle from 0°to 90°and every azimuth angle between 0°and 360°. However, in this research, we use a fixed setup as described in chapter 5.1.1, so the combination of both angles that deliver the highest total incident irradiance is calculated. The last step in creating the capacity factor is to deduct the temperature losses, calculated with the provided wind speed and the ambient temperature in the data of (Solcast 2021).

4.4 Modelling Buffers

The three buffers bring flexibility to the system by storing energy during surpluses and releasing energy when needed in either the electrolyzer or Haber-Bosch plant. However, the choice to store energy or release energy at any given moment is very complex due to many related constraints. They must contain enough energy to support the operations of the ASU, electrolyzer and Haber-Bosch plant to run on minimal capacity; however, the boundaries of the state of charge must be respected, all while considering future weather changes. The model chooses the decision that produces the lowest levelized cost by considering all possible outcomes for the current situation and its effects in the future.

Buffer Constraints

Battery

$$vSalt_{In,t} \leq M * vZ_X$$
$$vSalt_{Out,t} \geq M * vZ_Y$$
$$vZ_X + vZ_Y \leq 1$$

Salt Cavern

$$vBat_{In,t} \leq M * vS_X$$
$$vBat_{Out,t} \geq M * vS_Y$$
$$vS_X + vS_Y \leq 1$$

Nitrogen Tank

1. $N_2_Tank_Out_t = \left(vElec_In_t * HHV_H_2 * \eta_{Ele} + vSalt_{Out,t} - vSalt_{In,t}\right) * \text{Ratio_N}_2\text{_H}_2$
2. $\frac{vASU_Elec_t}{\text{Ratio_Elec_N}_2} - N_2_Tank_Out_t = N_2_Tank_Mut_t$
3. $0\% \leq \left(\frac{N_2_Tank_Mut_t + N_2_Tank_Mut_{(t-1)}}{Cap_Nitrogen_Tank}\right) * 100 \leq 100\%$

Figure 4.2: Constraints that simulate a realistic working of the buffers implemented in the system.

The difference between the working principle of the battery and salt cavern compared with the nitrogen tank is evident from figure 4.2. Instead of using the binary variables vZ_X defined in equation 13 the possible output of the nitrogen tank is calculated with the first constraint. This describes the volume of nitrogen necessary to combine with the volume of hydrogen that is delivered at that moment to the Haber-Bosch plant. In the second constraint, the nitrogen input coming directly from the ASU is deducted by this nitrogen tank output to calculate the mutation in the level of nitrogen in the cryogenic tanks. This is then kept between the limits of 0% to 100% with constraint. The assumption that the nitrogen can simultaneously flow in and out of the nitrogen tank is made because this avoids integers, leading to a longer solving time. Due to the extremely cold temperatures required to keep nitrogen in its liquid form, it is also assumed that the ASU cannot distribute the nitrogen to the cryogenic tanks directly. Surpassing the cryogenic tanks would mean more pipelines that need to be cooled to extremely cold temperatures, which would mean more energy losses. Both assumptions can be made because of the small scale of the nitrogen supply chain compared to the rest.

The constraints for the battery and salt cavern pictured in figure 4.2 are used to prevent the buffers from simultaneously charging and discharging. This might look overly complicated. However, it is necessary as Matlab does not allow variables to be multiplied with other variables using a problem-based approach. This would create a non-linear problem that it can not solve, resulting in an error. The letter M is introduced to work around this problem. It represents an extensively large number that will always be higher than the highest value for the in or output of the buffers. Next, it is important to note that the value of the output range from [- ∞, 0]. Therefore, vZ_Y or vS_Y cannot be higher than the right side of the equation. Only equal when both sides are zero. The input, on the other hand, is always smaller or equal and therefore, in combination with the last constraint, which ensures that vZ_X and vZ_Y are not both zero or one, the buffers will not simultaneously charge and discharge.

4.4.1 Assumptions Initial capacity

It is assumed that some energy is present in the buffers to create a realistic scenario. If the system would run for multiple years, this would also be the case. However, nitrogen storage is assumed to start empty because it is assumed to be a relatively small component. To establish continuous operations over the years, the batteries and salt cavern have to end with the same state of charge, depicted in the second and last constraint of the operational constraints in figure in chapter A.8 of the appendix. The energy assumed in the battery at the beginning of operating the whole system is 30% of the total capacity. While the initial amount of hydrogen stored in the salt cavern is determined by the model using the sixth constraint in figure 4.1.

$$Salt\ Cavern\ opportunity\ cost = (\textbf{\textit{Cap_Salt_Cavern_Initial}} \cdot Benchmark_LCOH) \cdot 1.07^{Lifetime} \tag{12}$$

The most optimal amount is determined instead of taking 30% or 0% of the total capacity for the salt cavern's initial value. This is done by calculating the opportunity costs of the hydrogen that will form the initial capacity. Equation 12 calculates the opportunity cost by multiplying the initial capacity of the salt cavern with the benchmark LCOH to create the missed revenue from not selling the hydrogen stored underground in the salt cavern. The opportunity cost is

present in the objective function to ensure it is considered when determining the minimal levelized cost. To determine the initial capacity using this method results in a substantially longer running time for the model, making it impractical for the battery and nitrogen tank. However, the alternative method for the salt cavern is used because of the size and, therefore, the impact on the system.

The initial capacity of the salt cavern is assumed to be zero, and while it would have been more consistent to make this 30%, like the initial capacity of the battery, this was not achievable as it caused a longer running time. A longer running time would be created because the storage value at the end of the simulation would need to match the initial capacity. However, when setting the initial capacity to zero, this extra constraint can be left out as every value will be higher than zero or equal, and therefore, it makes continuous operations over the years possible.

4.5 Operational Constraints

Opertational Costraints

1. $vPV_Load_t + \frac{vBat_{Out,t}}{\eta_{Bat,Discharge}} = vBat_{In,t} * \eta_{Bat,Charge} + vElec_In_t + vH_B_Elec_t + vASU_Elec_t$
2. $SOC_Bat_{(t=1)} = SOC_Bat_{(t=end)}$
3. $vH_B_Elec_t = \text{Ratio_Elec_NH}_3 * \eta_{H_B} * \text{Ratio_NH}_3\text{_H}_2 * \left(vElec_In_t * HHV_H_2 * \eta_{Ele} + vSalt_{Out,t} - vSalt_{In,t}\right)$
4. $Amm_{out,t} = \text{Ratio_NH}_3\text{_H}_2 * \eta_{H_B} * \left(vElec_In_t * HHV_H_2 * \eta_{Ele} + vSalt_{Out,t} - vSalt_{In,t}\right)$
5. $N_2_Tank_Out_t = \left(vElec_In_t * HHV_H_2 * \eta_{Ele} + vSalt_{Out,t} - vSalt_{In,t}\right) * \text{Ratio_N}_2\text{_H}_2$
6. $\frac{vASU_Elec_t}{\text{Ratio_Elec_N}_2} - N_2_Tank_Out_t = N_2_Tank_Mut_t$
7. $SOC_Sal_{t=1} = SOC_Sal_{t=end}$

Output Constraint

8. $\sum_{t=1}^{8760}\left(vAmm_{out,t}\right) = 200{,}000\ [\text{ton-NH}_3]$

1. Energy balance of the DC-currents in the system.
2. The initial SOC of the battery must be the same as in the end to ensure continuous operations.
3. Electricity consumed by the Haber-Bosch plant is calculated by converting the hydrogen input to ammonia and multiplying this with the electricity consumption per ton NH3.
4. The final output of the system is calculated by converting the hydrogen input in the H-B plant to NH3 and multiplying it with the efficiency of the H-B plant.
5. The required output of the nitrogen tank scaled to the matching input of hydrogen in the H_B plant.
6. The input minus the output of the nitrogen tank is equal to the mutations in the tank.
7. Just as in constraint 2, the initial SOC of the salt cavern must be the same as in the end.
8. The system is scaled to a final output of 200,000 ton NH3

Figure 4.3: Set of constraints that allocate the energy carriers.

The operational constraints shown in figure 4.3 ensure that the components in the system receive the necessary energy in the form of electricity, hydrogen or nitrogen required to produce 200,000 tons of NH_3 per year. Using conversion ratios written in the model description in the appendix, the amount of hydrogen, nitrogen, and electricity required simultaneously to produce a certain amount of ammonia is calculated per hour. This is achieved by implementing constraints 3 and 5. Furthermore, it can be concluded from looking at the constraints in figure

4.3 that the energy carriers all influence each other. A slight variation in the output of the PV load will result in less energy available for the Haber Bosch plant, resulting in a smaller hydrogen and nitrogen feed stream in the electrolyzer. All these connections require the model to make many considerations before deciding on the optimal value for the energy carriers and the required capacity of the components.

4.6 Initial Condition, Load Range and Ramping Constraints

Before the whole system is completely running, it is conventional to fill the buffers to a certain amount to ensure that the system will operate smoothly. Therefore, initial condition constraint 1 in figure 4.4 is set. Besides the load ranges in constraints 2 to 6, the system also applies ramping constraints. The usefulness of ramping constraints when using hourly data can be debated as the intention is to limit the spontaneous increase or decrease of power. However, when using hourly data, the ramping is already not spontaneous anymore since it can be spread out over the period of an hour. Nonetheless, they do not restrict the running time of the model, and since similar research also applies (Nayak-Luke and Bañares-Alcántara 2020) ramping constraint on hourly time scales, this research implements constraints 7 and 8.

Initial Condition & Load Range & Ramping Costraints

1. $SOC_Bat_{(t=1)} * 100 = 30\%$
2. $20\% \leq SOC_Bat_t * 100 \leq 95\%$
3. $1\% \leq \left(\frac{vElec_In_t}{Cap_Ele}\right) * 100 \leq 110\%$
4. $0\% \leq SOC_Sal_t * 100 \leq 100\%$
5. $20\% \leq \left(\frac{vSal_{out,t} + Ele_H_B_t}{Cap_H_B}\right) * 100 \leq 100\%$
6. $0\% \leq \left(\frac{N_2_Tank_Mut_t + N_2_Tank_Mut_{(t-1)}}{Cap_Nitrogen_Tank}\right) * 100 \leq 100\%$
7. $| vElec_In_t - vElec_In_{(t-1)} | \leq 20\%$
8. $| \text{Ratio_NH}_3\text{_H}_2 * \left(\left(vElec_In_t * HHV_H_2 * \eta_{Ele} + vSalt_{Out,t} - vSalt_{In,t} \right) - \left(vElec_In_{(t-1)} * HHV_H_2 * \eta_{Ele} + vSalt_{Out,(t-1)} - vSalt_{In,(t-1)} \right) \right) | \leq 20\%$

1. Initial SOC of the battery is 30%.
2. Battery SOC must stay within 20% to 95%.
3. The electrolyzer can not run outside its load range of 1% and 110%.
4. The SOC of the salt cavern is limited to 0% and 100%.
5. Imposes the load range of 20% to 100% of the Haber-Bosch plant.
6. Calculates the SOC of the nitrogen tank and limits it to 0% and 100%.
7. The electrolyzer can not ramp up more than 20% per hour.
8. The Haber-Bosch plant can not ramp up with more than 20% per hour.

Figure 4.4: Set of constraints that create a more realistic model by imposing load ranges, ramping constraints and the initial SOC of the battery and the salt cavern.

4.7 Problem-Based approach to Mixed Integer Linear Problem

In the previous chapter, it is briefly mentioned that a problem-based approach is used to solve the MILP problem by automatically selecting the *intlinprog* function. This chapter will elabo-

rate on the algorithms encoded in the function that allows the model to calculate the lowest objective function value while satisfying all constraints, but first, a brief description of a MILP problem is given.

The optimization problem in this research can be distinguished as a MILP problem because it does not contain quadratic expressions and is therefore linear. Secondly, there are some continuous variables and some discrete, making it mixed-integer. These integers are used for the decision to send electricity to the buffers or not. They are used as binary variables and are formulated in the model like equation 13.

$$\text{Z_X = optimvar('Z_X',T,'Type','integer','LowerBound',0,'UpperBound',1);} \tag{13}$$

In this case, the resulting value of Z_X means to charge (1) or discharge (0) the batteries. Integer variables create a non-convex problem; this makes it more challenging to solve. Because with convex problems, there is only one solution, the global optimum. With a non-convex problem, there might be many feasible, local optimums, but every combination must be tested to find the global optimum.

A linear programming problem will typically be solved using a non-deterministic concurrent algorithm, which means that the result will not necessarily be the same for each run and that depending on the number of cores available different solvers will run simultaneously. This speeds up the reaction as the first outcome is chosen as a final solution. In Gurobi's interface, the non-deterministic concurrent algorithm is denoted with method three. Unfortunately, it is impossible to set the algorithm option to choose method three or any other method when using Gurobi on Matlab (Gurobi Optimization 2020). As a result, the MILP problem is first solved using a barrier algorithm. This is discarded in line 151 of the log output shown in figure A.11 in the appendix. The program then switches to the dual simplex algorithm to solve the problem in this simulation. This algorithm can process much more iterations in the same amount of time. Ultimately leading to a solution after 155,139.22 seconds.

The correlation between the primal problem and the dual problem needs to be understood to understand the dual simplex algorithm. In this research, the primal problem's objective function is given by equation 9. The dual problem is sort of the inverse of the primal problem. The number of constraints equal the number of variables in the objective function of the primal problem and vice versa. This leads to interesting properties as the solution to the dual problem is equal to the shadow prices of the primal problem. The shadow price represents the difference in the sum of the objective function if a value of the constraint is changed with one unit. The dual simplex algorithm uses this information to determine which variable can be changed to affect the objective function positively. Each iteration calculates the solution of the dual problem for different constraints. If this gives a negative value, the shadow price of the primal problem is also negative. That means that the sum of the objective function will be lower. In equation 14 that is not desirable, but the objective function in equation 9 is supposed to be minimized. The result of changing the variable is therefore positive. The following iterations will continue to change this variable until it no longer shows a positive effect. At that time, another variable will be changed, and in that way, the optimal combination of the capacities of the components in the system will be calculated.

$$
\begin{array}{lcl}
\underline{\text{Primal Problem}} & & \underline{\text{Dual Problem}} \\
\text{Max } J(x) = 5x_1 - 2x_2 & & \text{Min } F(\boldsymbol{\mu}) = 9\mu_1 + 2\mu_2 + 3\mu_3 \\
2x_1 + x_2 \leq 9 & & 2\mu_1 + \mu_2 - 3\mu_3 \geq 5 \\
x_1 - 2x_2 \leq 2 & \Longleftrightarrow & \mu_1 - 2\mu_2 + 2\mu_3 \geq -2 \\
-3x_1 + 2x_2 \leq 3 & & \\
x_1, x_2 \geq 0 & & \mu_1, \mu_2, \mu_3 \geq 0
\end{array}
\tag{14}
$$

5 Location Determination

In the production process of hydrogen from renewable energy sources, the production plant's location is vital, relying on wind or solar energy for the electricity necessary to produce hydrogen using electrolysis. These sources must be in abundance and with the lowest variations possible to compete with grey hydrogen. This chapter delineates the required geographical circumstances for a suitable location to produce green hydrogen and ammonia for the lowest possible levelized costs by first illustrating the solar resources on the chosen location in chapter 5.1.1. Followed by a description of the geological hydrogen storage opportunities to determine the exact location of the system in chapter 5.2

5.1 Renewable Energy Resources

In this research, the combination of wind energy with a rectifier to produce direct current for the electrolyzer is neglected because, as explained in chapter 4.1 the previously stated combination is more expensive per kWh than a combination of PV panels and batteries. This chapter shows that Morocco has sufficient irradiance levels when hydrogen production solely relies on solar energy as a primary energy source.

5.1.1 Solar Irradiance

Being located close to the Sahara desert and the equator, Morocco constantly receives high solar irradiance levels throughout the year. When compared to the Maasvlakte in Rotterdam, the Netherlands, a place often mentioned as a possible location to produce hydrogen for the adjacent heavy industry, Figure A.2 shows not only higher levels of PV output per kWh/m^2-DC, but also a smaller seasonal fluctuation. Less variation in the PV output affects the size of the buffers as ramping limits of the electrolyzer, Haber-Bosch unit, and Air Separation Unit (ASU) limit the system's flexibility.

Using Sandia's National Libraries PV_LIB Toolbox (Stein et al. 2016) in Matlab, the yearly PV output has been calculated for the coordinates given in 5.2.2. This resulted in a PV output of 534.53 kWh/m^2 for a fixed PV panel configuration. Compared to the Maasvlakte (307.481 kWh/m^2) this is 74% more. If the PV panels were installed on a single rotating axis from east to west, the difference between Essaouira (661.568 kWh/m^2) and the Maasvlakte (364.235

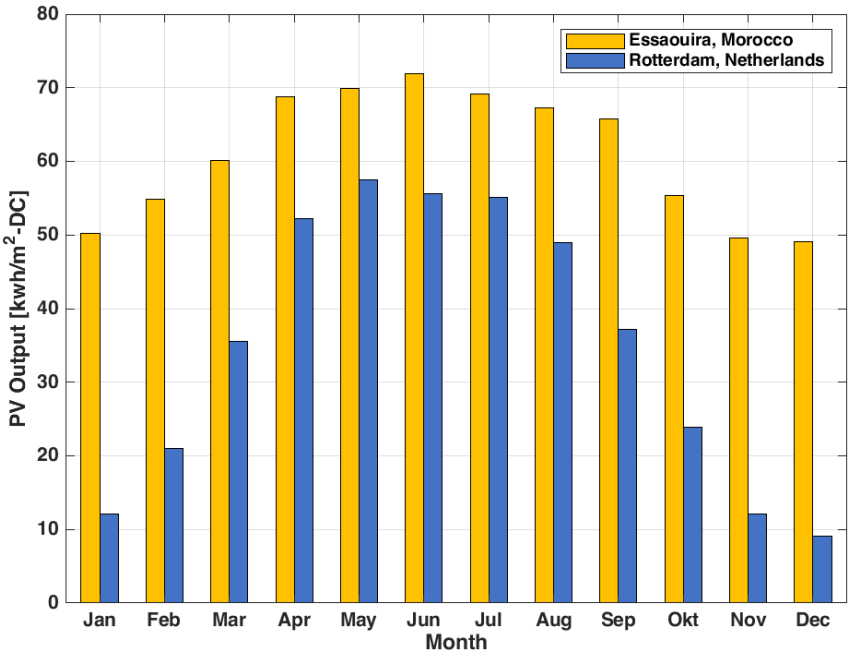


Figure 5.1: Difference between PV output in Rotterdam and Essaouira. Created in Matlab using Sandia's National Libraries PV_LIB Toolbox (Stein et al. 2016) and meteorological data from the website Solcast (Solcast 2021)

kWh/m^2) would be even more, namely 82%. This means that installing a single-axis rotating system instead of a fixed configuration would improve the output by 24%, in line with (Bolinger et al. 2019). This improvement outweighs the extra cost. Therefore, nearly 70% of new PV farms are built with single-axis tracking from east to west.

However, being close to the Sahara desert also brings difficulties with it. Due to the sandy environment, small sand particles will probably cause abrasive wear in the rotating, mechanical parts. This will lead to much maintenance and higher OPEX costs, influencing the credibility of the results obtained in this research. The PV panels are therefore modelled in a fixed configuration. Still generating enough electricity to keep the levelized costs of energy on a competitive level.

5.2 Geological storage opportunity

Another geographical factor important for hydrogen production is the ability to store the hydrogen. As hydrogen is the smallest element in the periodic table, this can be difficult and expensive. The cheapest medium of storing hydrogen is in salt caverns. Currently, there are five facilities in the world using salt caverns for large-scale hydrogen storage (Mallapragada et al. 2020). The oldest of these facilities is already successfully in use since 1972 in Teesside, UK (Crotogino 2016). Showing that this is a reliable option for the storage of hydrogen. Research into the subsurface of Morocco has been published since 1960 (Tortochaux 1968) for the purpose of hydrocarbon excavations. These geological screenings can be recycled to determine the available capacity of salt caverns for hydrogen storage. This chapter will elaborate on the suitable locations for large-scale hydrogen storage in section 5.2.1 and explain the methods used to determine the capacity of an appropriate salt cavern in chapter 5.2.2.

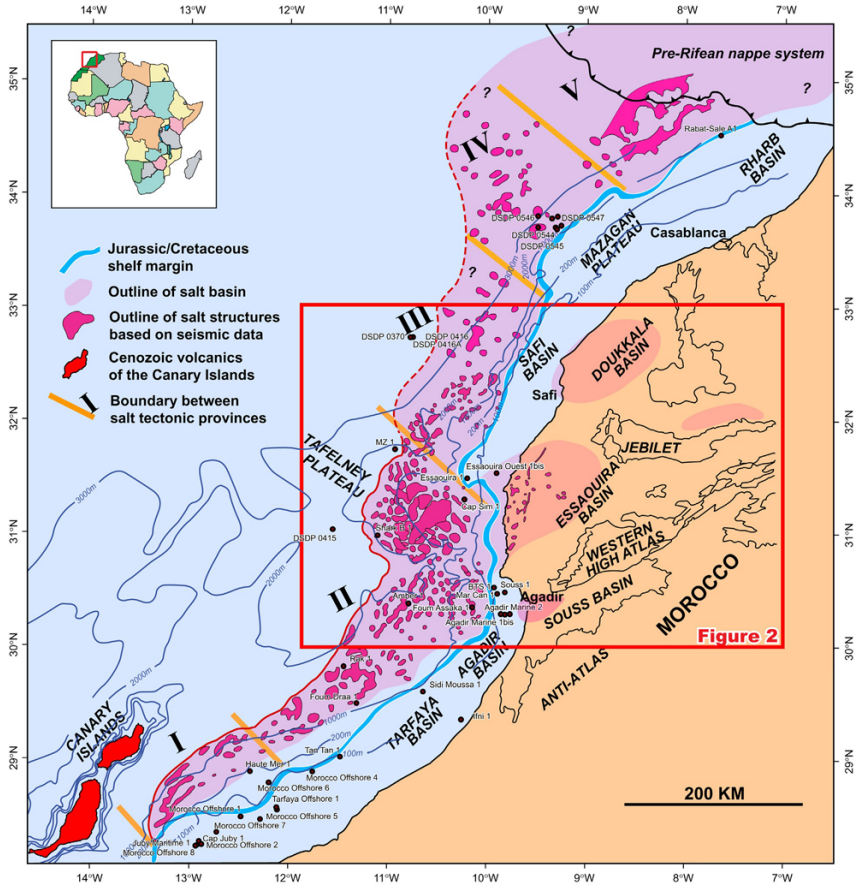


Figure 5.2: Salt tectonic map of Morocco. Showing multiple basins including Essaouira and Souss basin retrieved from (Tari et al. 2017)

5.2.1 Salt Cavern locations

The opportunity of hydrogen storage in a salt cavern, instead of in tanks, has such a positive impact on the business case (Mallapragada et al. 2020) that the required location of the proposed project is dependent on suitable caverns. Specific geological properties are essential to determine the amount of hydrogen that can be stored in a salt cavern: the cavern height, cavity volume, depth and spatial structure all influence the hydrogen storage potential. There are several onshore salt basins of which these properties are known. This research does not include the offshore basin stretching for 100km as this would not co-function well with the onshore solar farm.

The Souss-Massa basin (stated in figure 5.2 only as the Souss basin) and the Essaouira basin are the two most southerly located basins. Combined with higher solar irradiation towards the south, these two are the most promising locations and are therefore examined closer in this research to find a possible location for the system.

Beginning with the Souss-Massa, basin salt layers have been discovered at different heights near the surface. Varying between depths of 185-200 m, 315-415 m and 425-545 m. This is relatively close to the surface. Combined with the discovered maximum thickness of the salt layers here of around 120 m, this does not create the best conditions for large-scale hydrogen storage. Although it would be possible to store hydrogen, the volumes of the salt caverns would likely

be smaller than 20.000 m^3 (Hssaisoune et al. 2017). Due to the shallow depth, large pressures can not be achieved, making the Souss-Massa basin not ideal for large-scale hydrogen storage.

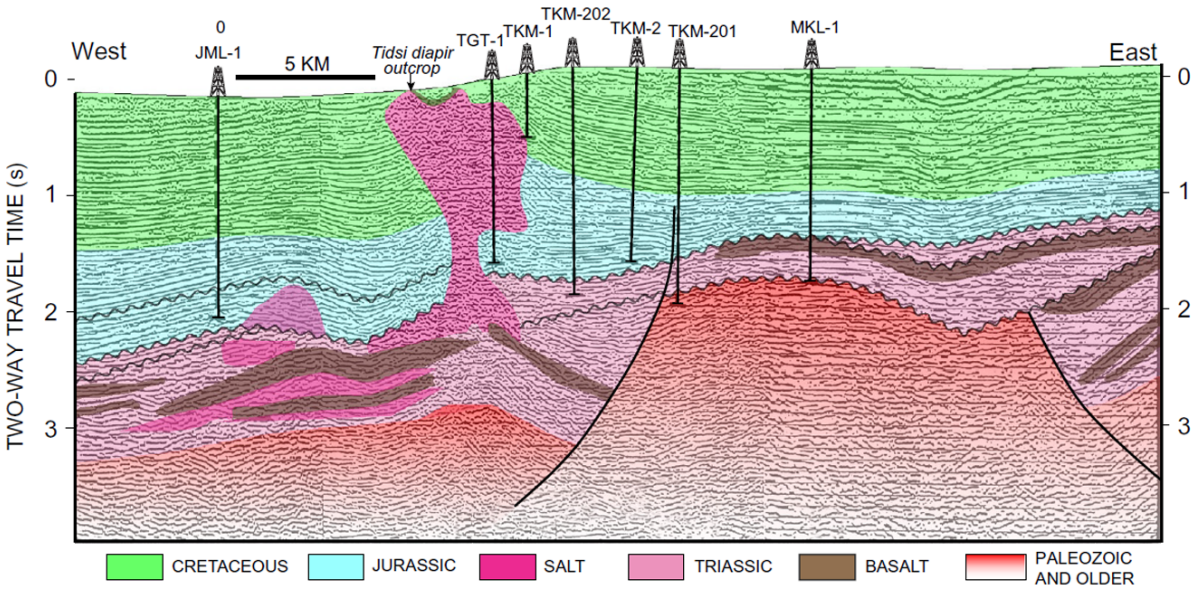


Figure 5.3: 2D image of subsurface Essaouira basin including the Tidsi diapir, retrieved from (Tari et al. 2017).

On the other hand, the Essaouira basin has very promising geological properties. One of the salt caverns called the Tidsi diapir, pictured in figure 5.3 has a minimum cavity volume of 200.000m^3 according to internal information received from Deep-KKB. The composition of the subsurface can be seen in a lithologic summary of the Tamergat-1 (TGT-1) well. This well on the east side of the Tidsi diapir was drilled in 1982 for hydrocarbon exploration after oil was found in the nearby reservoirs called Sidi Rhalem and Toukmit (Tari et al. 2017). At a depth of 550 m, salt structures were encountered until a depth of 1800 m, after which salt layers started to alternate with layers of limestone and anhydrite. In combination with the depth of 1800 m, this would make a suitable location for large-scale hydrogen storage.

5.2.2 Hydrogen storage capacity

The equations provided in (Caglayan et al. 2020) are used to calculate the weight of hydrogen in kilogram that can be stored in this cavern. The appropriate geological values of the ambient temperature, depth, cavern height, and rock density are required to perform the calculations correctly. In the previous chapter 5.2.1 the values for the depth and cavern height are already stated; however, it was advised by one of the authors of the paper (Caglayan et al. 2020) to use 1700 m for the depth as higher values are very uncommon. The cavern height is a dimension dependent on the spatial structure of the salt cavern. In this case, 300 m is used corresponding with a domal salt cavern structure, instead of 120 m used with bedded structures. The advised rock density was 2100 kg/m^3. Lastly, the ambient temperature was available in the data of (Solcast 2021), previously used to calculate the solar irradiance. All other values used in the equations 15 till 18 are specific properties of hydrogen.

$$\mathbf{T}_{average} = T_{am} + 0.025 \cdot (depth - \frac{cavernHeight}{2}) \tag{15}$$

$$\mathbf{P}_{overburden} = \rho_{rock} \cdot g \cdot (depth - cavernHeight) \tag{16}$$

$$\rho_{H_2} = \frac{P \cdot M}{Z \cdot R \cdot T_{average}} \tag{17}$$

$$m_{workingGas} = (\rho_{H_2,maximum} - \rho_{H_2,minimum}) \cdot V_{cavern} \cdot \theta_{safety} \tag{18}$$

After calculating the overburden pressure using equation 16 the maximum and minimum pressure can be calculated by taking 80% and respectively 24% of the overburden pressure calculated by equation 16. Using a gravitational acceleration of 9.81 m/s^2 this gives a maximum value of 197.6 bar and a minimum of 59.3 bar. This influences the density, as can be seen by equation 17. Whereby, the molar mass [M] is given by 2.016^{-3} kg/mol, the compressibility factor [Z] of hydrogen is 1.15 (Makridis 2016), the universal gas constant [R] is 8.134 $JK^{-1}mol^{-1}$ and the temperature 321,75 K calculated with equation 15. The total mass of hydrogen that can be stored in the salt cavern is eventually calculated by taking the difference between the highest and lowest density and multiplying this with a safety factor [θ_{safety}] of 70% and a cavity volume of 500.000 m^3.

This is an estimated guess for the cavity volume as it is known that the minimum value for this cavern is 200.000 m^3 and that the largest caverns can reach up to 1.000.000 m^3 (Michalski et al. 2017), (Bünger et al. 2016). This results in a capacity of 3300-ton hydrogen for the Tidsi diapir at the exact location; Lat: 31.41, Lon: -9.55.

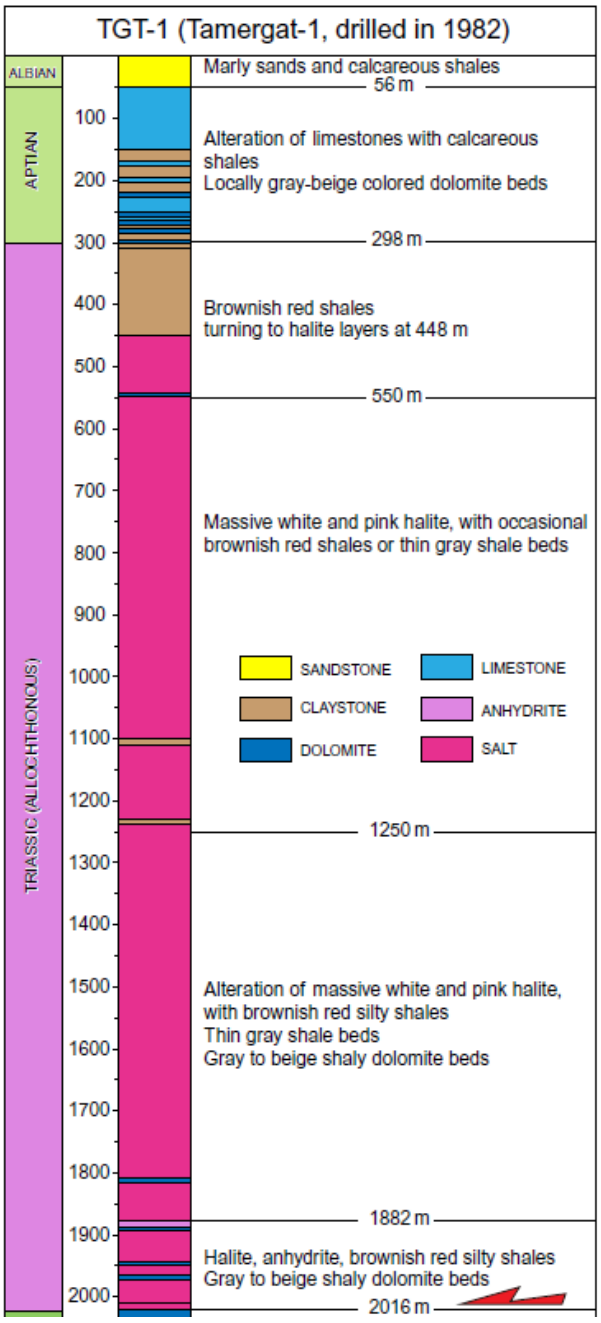


Figure 5.4: Lithologic summary of the Tamergat well. Drilled in 1982. Approximate location Latitude: 31.41, Longtitude: -9.55. Cropped from (Tari et al. 2017) to cut off deeper layers.

6 Results

This chapter aims to present all the results obtained from the model in a clear manner. Starting with the optimal sizing of the components to achieve the lowest levelized cost in chapter 6.1. The allocation of the energy carriers is described in chapter 6.2 to discover how the model operates. In chapter 6.3 essential information about the obtained levelized cost is presented, followed by a sensitivity analysis of the obtained levelized costs in chapter 6.4.

6.1 Optimal Capacity of Components

As described in chapter 4 the capacity of the components is used in the calculation of the levelized cost by multiplying it with the CAPEX and OPEX cost in table 2.2. The values written in bold numbers in figure 6.1 are the result of running the model for a simulation time of nine months. As expected, the primary energy source, photovoltaic power, has the highest capacity. Furthermore, the effect of hydrogen and nitrogen buffers is evident when comparing the capacity of the Haber-Bosch plant to the electrolyzer. The two can be compared by converting 25.8 ton NH_3/h to megawatt, using a value of 22.5 MJ/kg (Valera-Medina et al. 2018) for the energy density. This results in a capacity of 180 MW for the Haber-Bosch plant, which means the electrolyzer has 3.8 times more capacity. If the electrolyzer and Haber-Bosch plant were directly coupled, this scaling factor would be 1.2. Not 1.0, because it is assumed the efficiency of the electrolyzer is 83%.

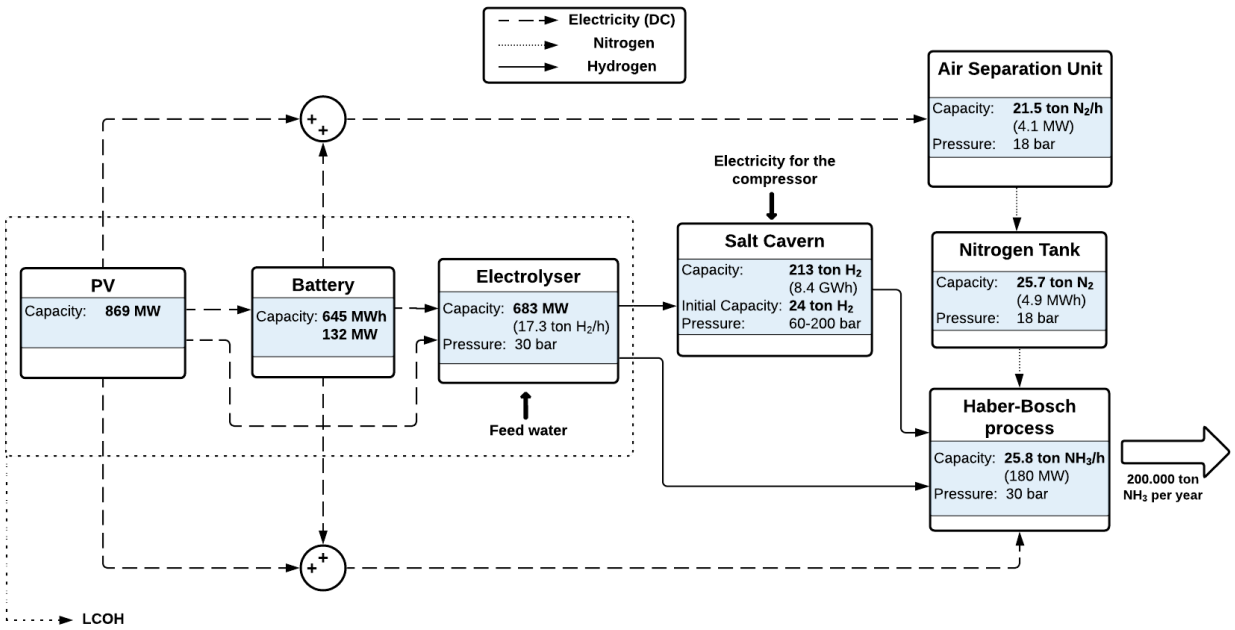


Figure 6.1: Schematic of system with the optimized capacity size of the components included as well as information on the electric system and the pressure required in some components.

The determined capacity of the salt cavern, 213 ton-H_2, is only 6.4% of its maximum potential calculated in 5.2.2. This amount could be compared to the amount of hydrogen produced by the electrolyzer if it were to run for 15 hours on 100% capacity. To discover if this relatively low storage capacity depends solely on the amount of hydrogen produced or if a mistake was

present in the model. The optimization is also performed with different desired outputs of 400.000 and 800.000 ton NH_3 per year instead of 200.000 ton NH_3. With these values that are two and four times as high, the capacity of the salt cavern increases with 97.6% and 160.4%, to 12.7% and 16.8% of the initially assumed capacity of 3,300 ton-H_2 table 6.1. To put these numbers into perspective, the largest planned green ammonia project with 3 GW of PV capacity and 0.5 GW of wind power capacity will produce 900.000 ton-NH_3 per year (Gupta 2021). This shows that the size and geological properties of the salt cavern elaborated in chapter 5.2 has more than enough capacity to store hydrogen for the largest projects that are yet to be built.

If only a small part of the total storage capacity of the salt cavern will be used, as can be seen in column 3 of 6.1. The maximum pressure in the cavern will not reach its limit of 297.6 bar as calculated in chapter 5.2.2. It would differ with a small amount from the minimum pressure of 59.3 bar. Reaching a maximum pressure of 68.4 bar for the proposed output of 200,000 ton NH_3 per year. Consequently, the assumption of taking a constant value for the electricity consumption by the compressor instead of using a variable consumption affected by the difference in pressure is justified. As discussed in chapter 3.10 the difference was already minimal if the pressure went from 55 to 180 bar or from 32 to 84 bar. A difference of 9.1 bar would, therefore, definitely be negligible.

Yearly NH_3 output [ton-NH_3]	Capacity [ton-H_2]	Percentage of 3300 ton-H_2 [%]	Pressure range [bar]	PV capacity [GW]	Electrolyzer capacity [GW]
200,000 ton-NH_3	213	6.4%	59.3 - 68.4	0.87	0.68
400,000 ton-NH_3	420	12.7%	59.3 - 77.2	1.76	1.38
800,000 ton-NH_3	554	16.8%	59.3 - 82.9	3.58	3.03

Table 6.1: The results for an increase in ammonia output. For a value 4 times the initial output the salt cavern reaches only 16.7% of the possible capacity.

The capacity results show that the designed system is feasible as all components and their corresponding capacity have been constructed before except for the alkaline electrolyzer with a capacity of 683 MW. The largest electrolyzer in use today has a capacity of 10 MW (Radowitz 2021). However, the stacks in the alkaline electrolyzers are modular, just like the PV panels, making it possible to increase the capacity exponentially in a short period. Consulting the electrolyzer projects database of (IEA 2020) also shows that the average electrolyzer capacity will be much higher in 2030, figure A.4.

In chapter 3.2 it was assumed that the battery required a storage duration of 4 hours, which corresponds to the chosen CAPEX costs. When dividing the energy capacity result by the power capacity result, the answer is 4.89. Therefore, the assumption was correct since the other available CAPEX costs are given in 2, 6, or 10-hour storage durations. However, a combination of 4 and 6-hour storage duration batteries will give the most accurate value for the CAPEX cost.

PV Area

To calculate the area required for a PV farm with a capacity of 869 MW, one must consider that the area will be more than only the surface area of the PV panels. Access roads, service buildings, substations and other infrastructure must be present on the location. Furthermore, the PV panels need to be placed at a distance from each other as the panels' shadows will otherwise cast over each other. In (Ong et al. 2013) the average weighted-capacity land use is calculated with data consisting of PV farms with an accumulated capacity of 744 MW_{AC}. The

result is that the direct land use for a fixed configuration of the PV panels is 43 MW_{AC}/km^2. A conversion factor of 0.85 MW_{AC}/MW_{DC} was used. Using this information, the area required for the PV farm in this research would be 17.2 km^2. Considering a higher efficiency for the PV panels in this research than the PV panels examined in (Ong et al. 2013) will result in a smaller area. The average efficiency in (Ong et al. 2013) is 11%, while this research assumes 25%. The resulting decrease in PV panel surface will therefore be 127%. The PV panel surface can be calculated with the equation 19. Resulting in an area of 3.39 km^2, if an efficiency of 25% is used. The term max(fixed_Output_Solar_DC stands for the peak output of the PV panels in W/m^2, which is 225 [W/m^2]. Considering the higher efficiency, the area reserved for the PV farm would decrease from 17.2 km^2 to 12.87 km^2. This translates to 3.66 acres per megawatt, which is in line with the proposed 4 acres per MW, for an efficiency of 18%, in (Narasimhan 2014).

$$\text{PV Panel surface} = \frac{\boldsymbol{Cap_PV}}{max(fixed_Output_Solar_DC} \tag{19}$$

6.2 Allocation Energy Carriers in Integrated System

To better understand the capacity size of the components and how the model operates. The allocation of the energy carriers is discussed in this chapter. In figure 6.2 it is visualized using a Sankey diagram, scaled to the sizes of the energy output calculated in GWh for the whole simulation period. The first bar represents the PV energy output. It shows that only 0.5% of the produced electricity is allocated to the ASU. The ASU also receives electricity from the battery, and although the proportion of electricity from the battery to the ASU is higher, the amount is still only 2.1%. This results in the ASU and nitrogen tank having the smallest capacity when scaled to GWh. Furthermore, the dominant role of the salt cavern as a buffer in the system is confirmed by receiving 40.3% of the hydrogen produced by the electrolyzer and being the largest of the three buffers in the system. The total energy lost by converting electricity from the PV panels to ammonia is 34.4%. Resulting in a total energy efficiency of 65.5%. This efficiency is consistent with the value calculated with data from the future of hydrogen report (Birol 2019). This report states an electricity consumption of 35.3 GJ/ton-NH_3 for the whole process of converting electricity to ammonia. This includes the electrolyzer, nitrogen supply and Haber-Bosch plant. Using equation 20 and the energy density of ammonia, 6.25 kWh/kg-NH_3 (Valera-Medina et al. 2018) the result is 63.74%. The efficiency in this report is slightly higher, which is primarily caused by a higher efficiency of the electrolyzer.

$$\eta_{Electricity-NH_3} = \frac{\text{Energy_Density}_{NH_3}}{\text{Electricity_Consumption}_{NH_3}} \tag{20}$$

The short blocks of the feed water and compressor in figure 6.2 justify the assumption made at the beginning of this research to provide these components with electricity from the grid instead of electricity from the PV panels. The height of the blocks shows that they do not consume that much electricity that it would be necessary to connect them with the PV farm. The determination of the height of the compressor was straightforward. By multiplying the compressor's electricity consumption (Com_Ene_H_2) times the amount of hydrogen passing through. However, to determine the value of the feed water in GWh, equation 21 was used. As the feedwater enters the electrolyzer with a temperature of 80 °Celsius, this contains energy which can be calculated by subtracting the ambient temperature of 25 °Celius and multiplying it with the heat capacity of water [kj/(kg· K)] and the total amount of water used in the electrolyzer. Because it is unclear if freshwater is available or if saltwater needs to be desalinated,

the electricity consumed by the reverse osmosis process in a desalination plant is left out of the figure. This would not make a difference since the electricity consumption is relatively small. In a comprehensive overview of the process, 3 kWh/m^3 is used for the electricity consumption (Kim et al. 2019). When multiplying this with the amount of water used, the result is 835.1 MWh. Compared to the result of equation 21 this is 4.7% of that.

$$\text{Electricity consumption Feed Water} = \delta T \cdot \text{Heat_Capacity_}H_2O \cdot H_2O_used \tag{21}$$

The differences in the state of charge of the buffers in figure 6.3 are a result of the location in the system and the differences in the CAPEX and OPEX cost. The SOC of the battery shows that the battery purely acts as temporary storage to bridge the gap between day and night, while the salt cavern clearly shows that it works for long term storage as well. This is observed from the changes in capacity corresponding to irregularities in the PV output. These irregularities in the PV output are caused by clouds blocking the sun rays from hitting the PV panels. In figure 6.3 this phenomenon can be observed around 1800 hours. A gap in the PV Load results in a disturbance in the SOC of the battery. As a result, the salt cavern completely depletes its stored hydrogen showing a decline of 100% in the SOC of the salt cavern. When the sun begins to shine again, the PV load recovers and the salt cavern can build its SOC back up again.

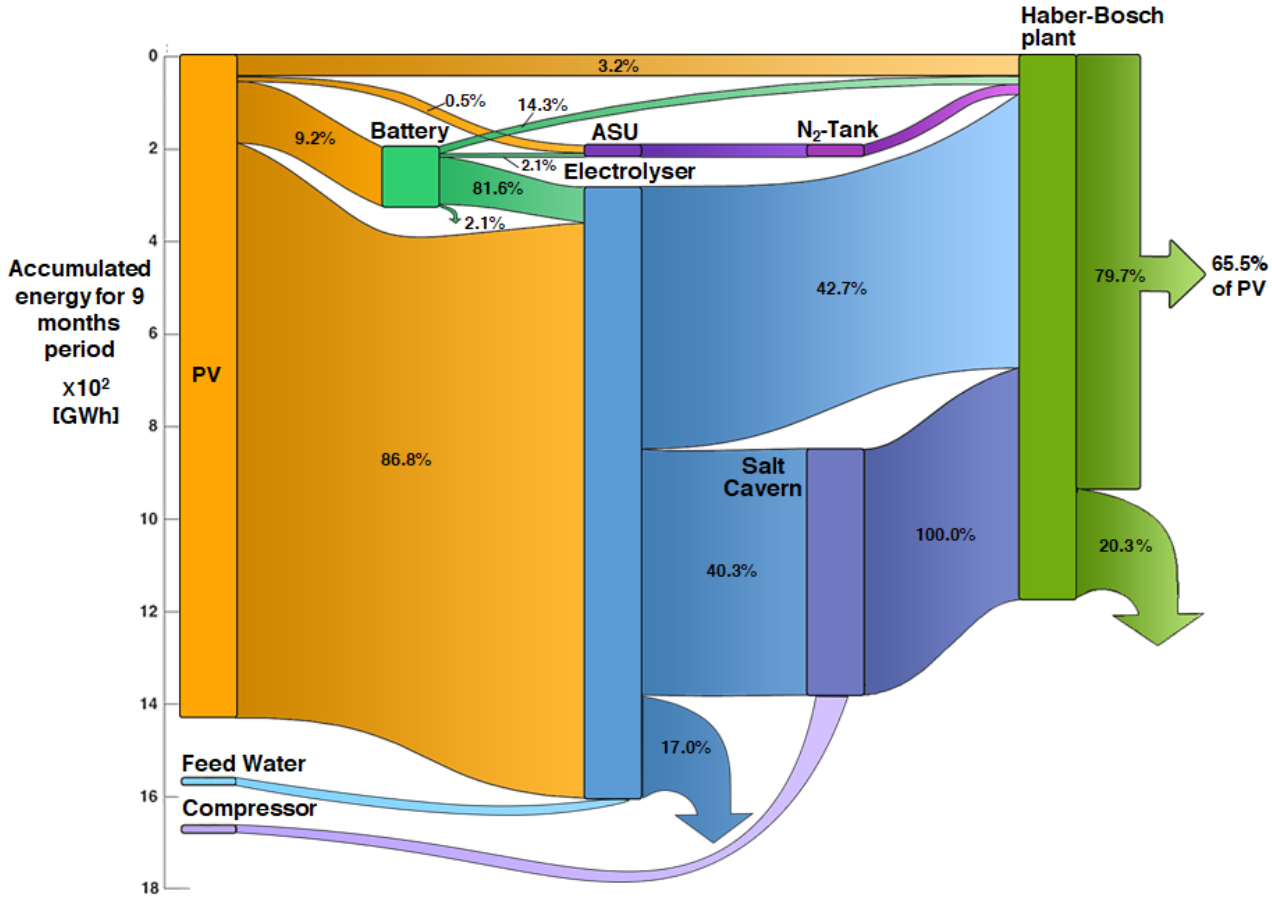


Figure 6.2: Sankey diagram of the allocation of energy carriers. H_2, N_2 and NH_3 values are converted to GWh using energy densities of 39.4 kwh/kg (Harrison et al. 2010), 712 kJ/kg (Rizvi et al. 2021) and 22.5 MJ/kg (Valera-Medina et al. 2018), respectively.

The function of the salt cavern can also be examined by explicitly looking at the summer pe-

riod in figure 6.3. The hours between 3625 - 5833 represent the months June, July and August. In this period, a gradual increase in the SOC of the salt cavern is observed. A more significant increase could be expected as it might be logical to think that the buffers will build up in periods of high irradiation. This is partly true, but the main consequence of the higher irradiance levels in the summer is that the Haber-Bosch plant can run at full capacity observed in figure A.6. This shows that the buffers mainly act to bridge periods of low solar irradiance, quickly increasing their buffers just before the bad weather arrives.

Due to the chosen location close to the desert, as explained in chapter 5, the disturbances by the formation of clouds are relatively small. Therefore, the need for salt cavern capacity is much smaller than if this system were to operate in, for example, the Netherlands or Germany, countries that experience much more cloud opacity throughout the year.

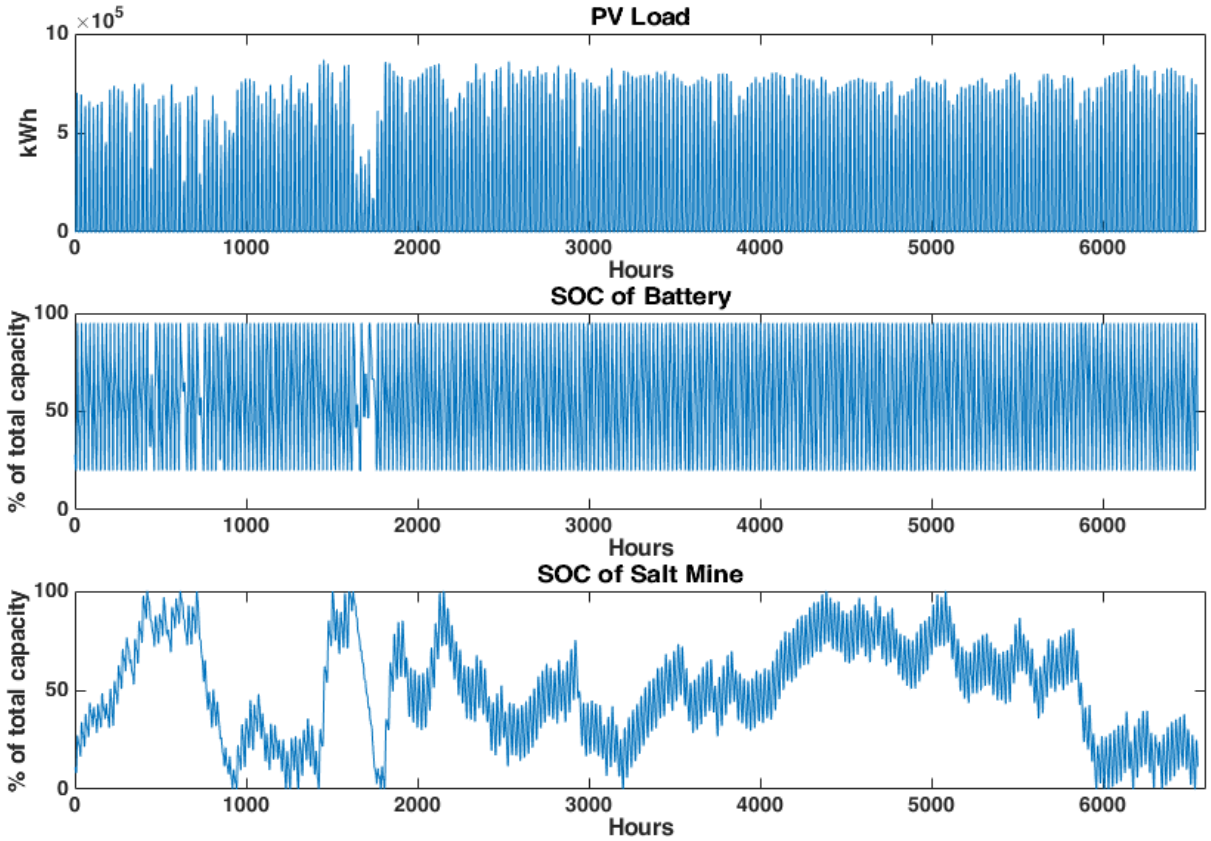


Figure 6.3: In subfigure 1, the electricity output in kWh on an hourly basis of the PV farm is shown. In subfigure 2, the state of charge of the battery is plotted. In the last subfigure, the state of charge of the salt cavern is shown. The clear cut at 20% and 95% in subfigure 2 results from the assumed load range of 20% and 95%. For the salt cavern, the load range is already implemented in the capacity limit calculated in chapter 5.2.2.

To keep the levelized cost to a minimum, the capacity of the most expensive component must be as small as possible. The component must operate as much as possible on its maximum load to achieve this. In this system, the most expensive component is the Haber-Bosch plant, table 2.2. Looking at figure 6.4 which depicts the load distribution of the Haber-Bosch plant, it can be concluded that the model tries to pursue this strategy. After the dip in the solar

farm output around 1800 hours seen in figure 6.3, the Haber-Bosch plant runs on its maximum capacity for around 100 days. The difference with the load distribution can be observed from figure 6.4 as well. Being the cheaper component, the benefit of operating the electrolyzer on its maximum capacity is smaller; therefore, more fluctuations can be observed in the load distribution. The difference between these components shows that the model makes the right design choices.

It has been tried to set the capacity of the Haber-Bosch plant beforehand to reduce the running time of the model. This way, the model could leave one variable out of the equation by taking the average output necessary to reach a total output of 200,00 ton-NH_3 per year and multiplying it with 10%. The assumption was that the capacity of the Haber-Bosch plant would be sufficiently scaled. However, this resulted in an error due to a lack of flexibility.

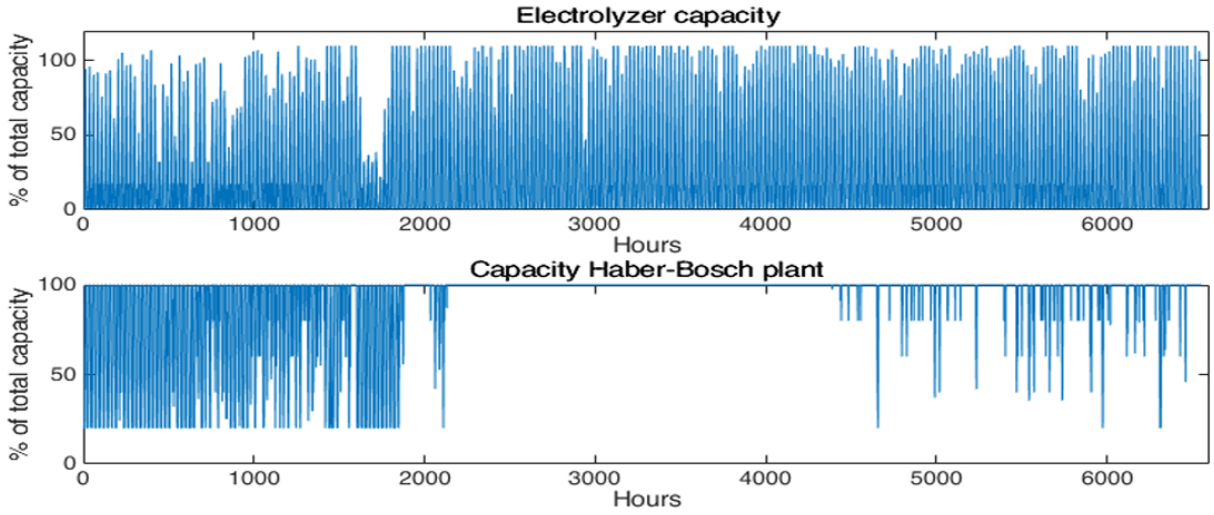


Figure 6.4: The load distributin of the electrolyzer and Haber-Bosch plant during a simulation period of nine months.

6.3 Levelised costs

The levelized costs are vital in making a relevant comparison between different energy carriers. Already stated in chapter 1.1, it ensures that the scale of the project does not influence the comparison. In chapter 6.3.1 the LCOE of the PV power is discussed following an elaboration on the final LCOH and LCOA achieved in this project in chapter 6.3.2

6.3.1 Levelized Cost of Energy

The levelized cost of the electricity produced by the PV panels can also be calculated to evaluate the potential of the PV power as a primary energy source. Dividing the equivalent CAPEX cost for a year plus the OPEX cost with the annual output of electricity produced by the PV panels results in the levelized cost of electricity, equation 22.

$$\mathrm{LCOE_{PV}} = \frac{\left(CRF_{PV} \cdot CAPEX_PV + OPEX_PV\right) * \boldsymbol{Cap_PV}}{Annual\ PV\ Power\ Produced} \tag{22}$$

To compare the $LCOE_{PV}$ achieved in this report with the winning bids in solar energy auctions is difficult because the $LCOE_{PV}$ presented in the bids do not always represent the true LCOE. Antonio Delgado Rigal made a similar statement, the chief executive of energy forecasting service Aleasoft, about the lowest bid ever of 0.01114 €/kWh in a solar energy auction in Portugal (Bellini 2020). To put this bid into perspective, the previous lowest bid was 0.0124 €/kWh (Brinck 2021). However, this was in Abu Dhabi, where the solar irradiance is about 1.2 times higher (Global Solar Atlas 2021). The technological advancement in this period could not explain the difference as there was only a month in between the two auctions. Antonio Delgado Rigal explained that the bidding price is influenced by many more factors than the ones represented in equation 22. In this case, the historically low price was partly caused by a 15-year purchase agreement and the rights for land and grid connection to build solar farms in a certain region in Portugal. These benefits made it possible for the energy company to decrease its bidding price.

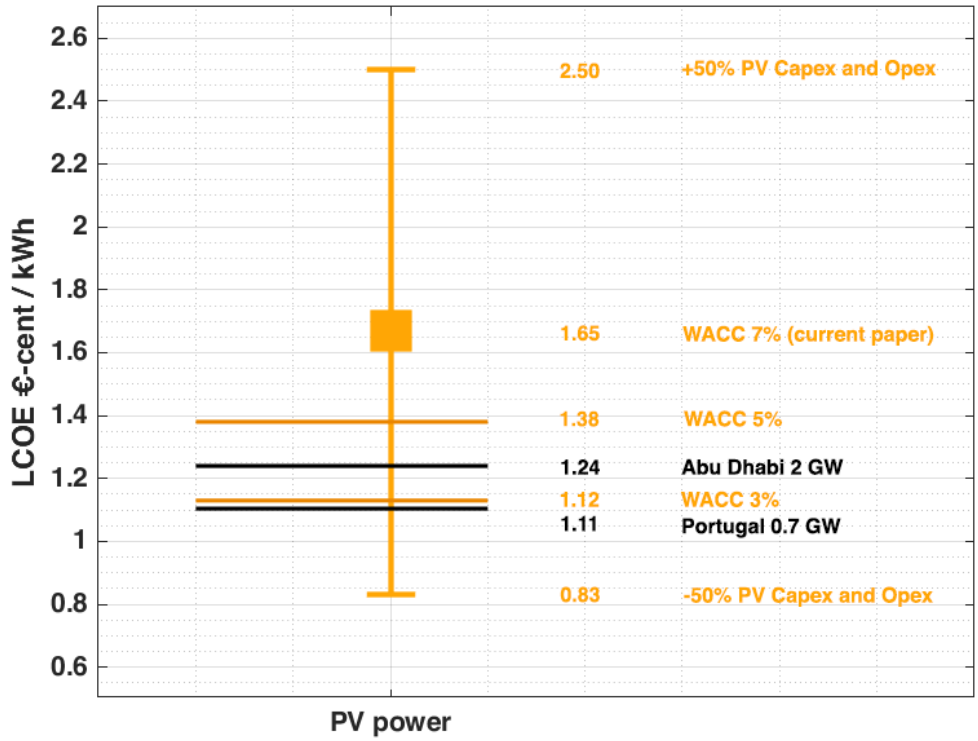


Figure 6.5: The orange numbers are the LCOE of PV power for different variables in this paper and the black numbers represent the lowest bids in solar auctions across the world. Portugal bid (Bellini 2020), Abu Dhabi bid (Global Solar Atlas 2021).

The $LCOE_{PV}$ in this project is calculated to be 0.0165 €/kWh, as can be seen in figure 6.5. The effect of the WACC on the $LCOE_{PV}$ is also clear from the figure. If the WACC would decrease to 5% instead of 7%, the $LCOE_{PV}$ would be 0.0138 €/kWh, and a WACC of 3% would result in a value very close to the lowest bid ever. The effect of the WACC on the levelized cost will be further discussed in chapter 6.4.

6.3.2 LCOH and LCOA

To answer the main research question stated in chapter 1.4 the results displayed in figure 6.6 are essential. The model has determined the lowest possible levelized cost of hydrogen and

ammonia. The costs are split up per component and stacked on top of each other. The graph shows the levelized cost of hydrogen on the left and ammonia on the right. On both sides, the PV and electrolyzer blocks are at the bottom of the graph. This means that the PV farm and the electrolyzer have the biggest influence on the total levelized cost. They contribute to the total LCOH with a combined 78.2%. In table 6.2 all the components are listed with their corresponding contributions to the LCOH and LCOA.

The total LCOH for a simulation time of nine months is 1.63 €/kg-H_2. The total height of the bar on the left in figure 6.6 represents this outcome. In the figure, the grey, blueish area represents the price of hydrogen produced with natural gas. Using a price of 100 €/ton-CO_{2-eq} for the penalty of emitting CO_2 which corresponds to the moderate scenario as discussed in chapter 1.1.2. The minimum levelized cost of blue hydrogen will be 1.41 €/kg-H_2, corresponding with a natural gas price of 2 $/MBTu. Corresponding to the top of the stacked bars is a gas price of 3.16 $/MBTu. This means that the price of natural gas needs to be higher than 3.16 $/MBTu or 12.25 €/MWh for green hydrogen with a LCOH of 1.63 €/kg-H_2 to be cheaper. The positive result for the development of green hydrogen is mainly contributed to the expected rapid decline in electrolyzer and PV costs. The contribution of the carbon price on grey hydrogen is limited. With a price of 100 €/ton-CO_{2-eq} the additional cost to are 0.1 €/kg-$_2$ as shown in table 1.2.

Components and their corresponding contribution to the levelized costs						
LCOH	PV 49.8%	Electrolyzer 28.4%	BOS cost 10.0%	Battery Power 7.1%	Battery Energy 4.5%	Feed Water 0.23%
LCOA	PV 40.0%	Electrolyzer 21.8%	Haber-Bosch 11.2%	BOS cost 10.0%	Battery Power 5.4%	ASU 4.5%
	Bat. Energy 4.11%	Compressor 2.27%	Salt Cavern 0.40%	Feed Water 0.18%	Salt Cavern 0.02%	N_2 Tank 0.01%

Table 6.2: The components are listed from left to right according to their contributions to the levelized cost of hydrogen and ammonia.

The accumulation of the LCOA depicted in figure 6.6 is similar to the LCOH. With the PV and electrolyzer contributing to 61.8% of the total LCOA, their share has fallen because the LCOA is constructed of more components than the LCOH. Next, the second most expensive component, per kWh (Tabel 2.2), is the Haber-Bosch plant with a contribution of 11.2%. The ASU is also only present in the LCOA and fits in after the BOS costs [10%], battery power capacity cost [5.5%] and before the battery energy capacity [4.1%] cost, with a contribution of 4.5%. The other components stated in the last row of the legend in figure 6.6 have a combined contribution of 2.7%. However, this does not mean that they are invaluable in the system. If, for example, the salt cavern would be removed from the system and an alternative form of hydrogen storage would not replace it, the LCOA would be 1.52 €/kg-NH_3, 3.8 times higher. Even though the salt cavern only accounts for 0.42% of the total LCOA. This is because the capacity of the battery energy and nitrogen tank increases by 556% and 1,796%, respectively. To compensate for the absent long term storage of the salt cavern. In total, the LCOA is 0.394 €/kg-NH_3, corresponding to a gas price of 4.49 $/MBTu (17.41 €/MWh). Well-situated to compete with ammonia from fossil fuels that have a predicted minimum levelized cost of 0.29 €/kg-NH_3 when the gas price is 2.0 $/MBTu and a carbon price of 100 €/ton-CO_{2-eq} in 2030.

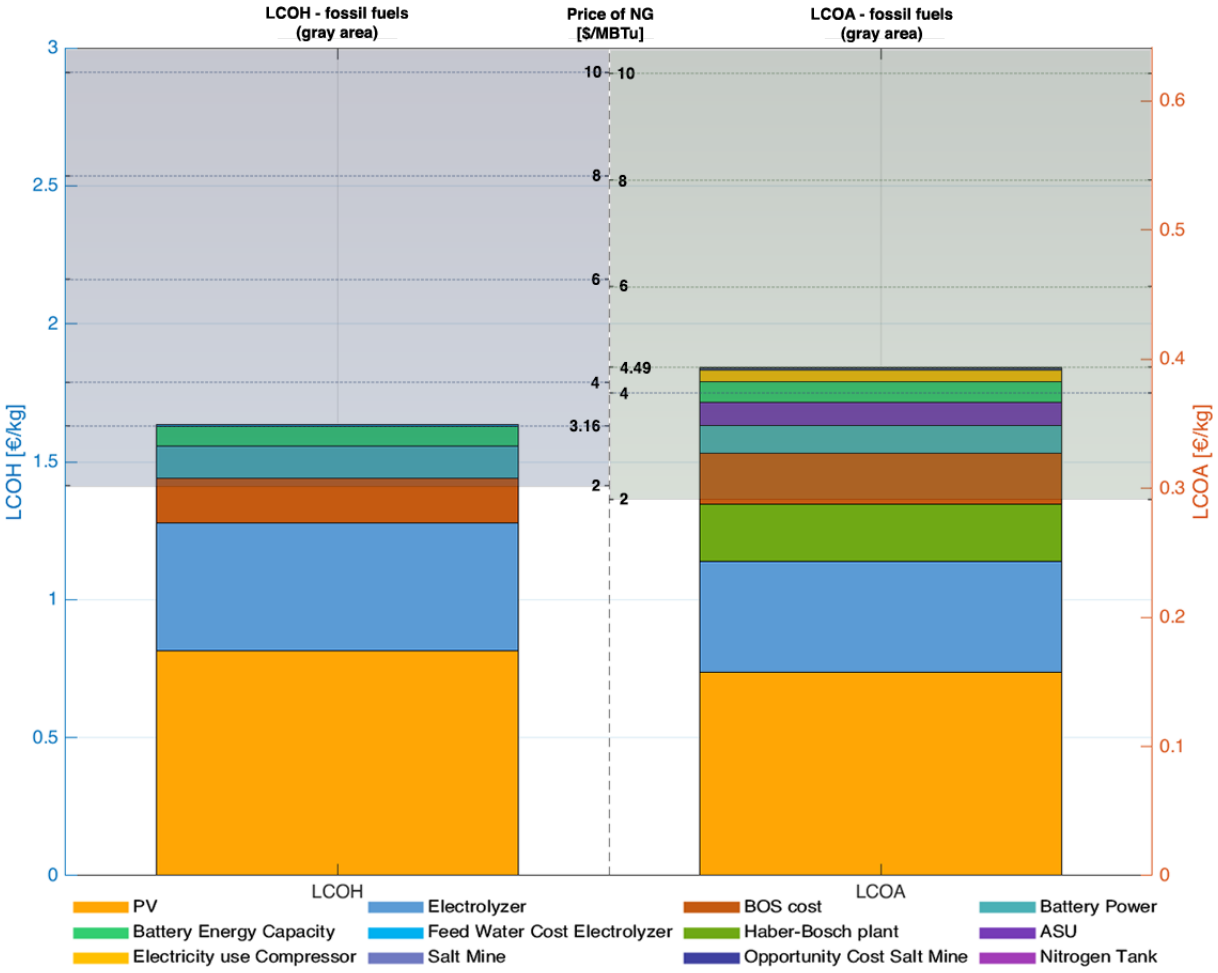


Figure 6.6: The components of the LCOH and LCOA are arranged from their contributions to the levelized cost, with the PV and electrolyzer having the biggest impact on both the LCOH and LCOA. The grey area represents the levelized cost from the method using SMR discussed in chapter 1.1.3. The price of carbon is assumed to be 100 €/ton-CO_2, and the electricity price is 100 $/MWh

6.4 Sensitivity Analysis

The importance of a sensitivity analysis is stated in chapter 6.4.1 together with the results from varying the cost of the components. In chapter 6.4.2 the influence of the levelized cost is also discussed.

6.4.1 Sensitivity to the components

In this paper, the date for the proposed project is set in 2030, as stated in the main research question. The cost assumptions written in table 2.2 have, therefore, quite a lot of uncertainty in their predictions. To develop a broader understanding of the competitiveness of the calculated levelized cost, the CAPEX and OPEX cost uncertainty is elaborated in this chapter through a sensitivity analysis. This analysis has been performed by multiplying the CAPEX and OPEX with 1.5 and 0.5 to simulate an increase and decrease in cost for every component separately. The combined sensitivity of the most contributing components to the levelized cost is also calculated similar manner.

The left-hand side of figure 6.7 represents the sensitivity for the LCOH. As expected, the or-

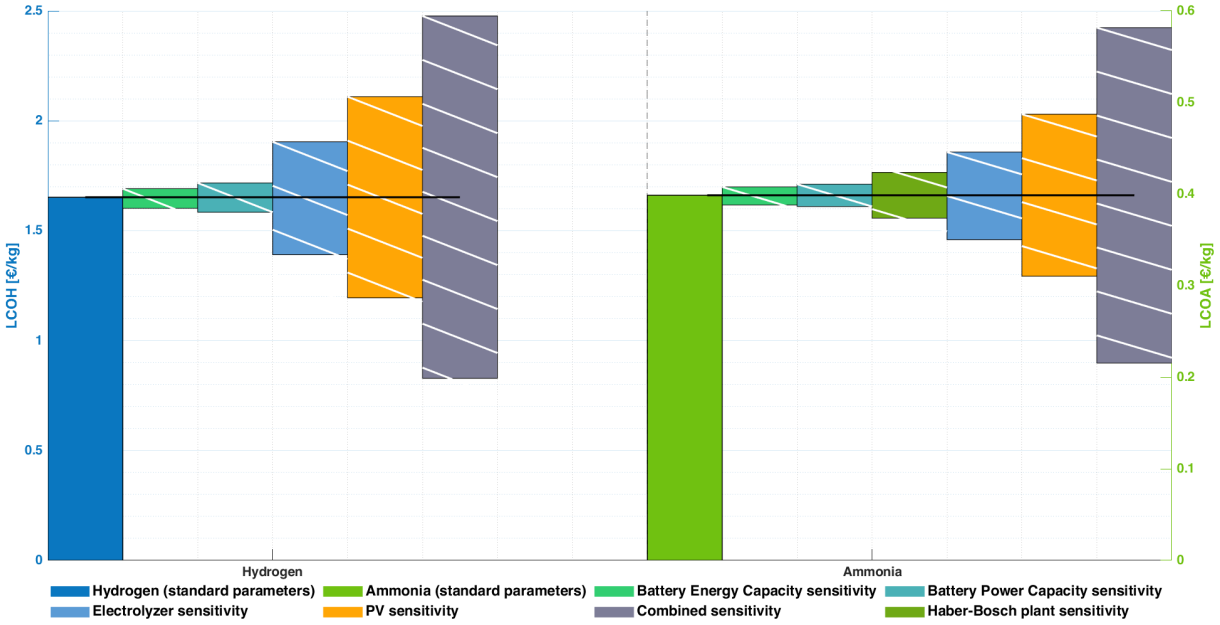


Figure 6.7: Sensitivity analysis of the most contributing components in the production of hydrogen and ammonia. Created by running the model with 50% higher and lower CAPEX and OPEX costs for each component.

der in which the components influence the sensitivity is the same as the order of contributions to the levelized cost. This means that if the costs of batteries would change, whether it is the energy capacity or the power capacity, the levelized cost of the produced hydrogen would only marginally change. An interesting phenomenon observed when closely looking at the bars of the battery energy is that the black line representing the standard LCOH does not divide the bars into two equally large pieces. The upper part is smaller than the lower part. This shows the flexibility of the system. If one component increases in cost, the model will decrease the capacity of this component and increase the capacity of the other components to compensate. This effect is almost absent in the bars representing the sensitivity of the PV power and electrolyzer. For the reason that these components are more difficult to scale down as the PV power is the primary and only energy source of the system.

The sensitivity analysis results in levelized cost prices that can still compete with hydrogen produced from fossil fuels. With a 50% increase in CAPEX and OPEX cost, the total LCOH is 2.48 €/kg-H_2. For ammonia, the levelized cost will be 0.5817 €/kg-NH_3. This compares to a gas price of 7.71 $/MBTu (29.89 €/MWh) and 9.04 $/MBTu (35.05 €/MWh). Due to the low amount of installed electrolyzer power in the world at the moment, figure A.4, the cost for this component is the most uncertain. However, when the cost of the electrolyzer varies by 50%, the LCOH is 1.3911 - 1.9044 €/kg-H_2 (LCOA; 0.3502 - 0.4459 €/kg-NH_3) which will still be under the 2 €/kg-H_2 and therefore well below most alternative production methods in 2030.

6.4.2 Sensitivity to the WACC

The sensitivity of the model to the WACC has also been examined. The WACC, short for Weighted Average Cost of Capital, is the interest that will need to be paid over the loan for the proposed project. A low amount of 5% or even 3% means little risk involved with the

project. The chance that the moneylenders will be paid back is high, and therefore they do not have to charge high interest to make up for this insecurity. Projects that propose a low risk consist of well-proven technologies in stable countries with reliable companies. The impact of the WACC on the levelized cost is substantial figure 6.8. It is, therefore, beneficial to keep it as low as possible. Morocco proposes the lowest risk with a stable government and a proven track record of investments in renewable energy technology from the North-African countries. A WACC of 7% is assumed in this model, resulting in the previous stated LCOH of 1.63 €/kg-H_2 and LCOA of 0.394 €/kg-NH_3. A higher WACC of 9% increases the levelized cost with 16.6% and 15.6% to 1.9267 €/kg-H_2 and 0.4610 €/kg-NH_3, respectively. This amount is already higher than if the electrolyzer would increase with 50% in cost. A WACC of 3% and 5% result in a LCOH of 1.1586 €/kg-H_2 and 1.3989 €/kg-H_2 and LCOA of 0.2863 €/kg-NH_3 and 0.3404 €/kg-NH_3. It can be concluded that a difference in WACC of 2% has about the same effect as a difference in electrolyzer cost of 50%, showing the importance of a safe investment climate to develop the lowest possible value for the WACC.

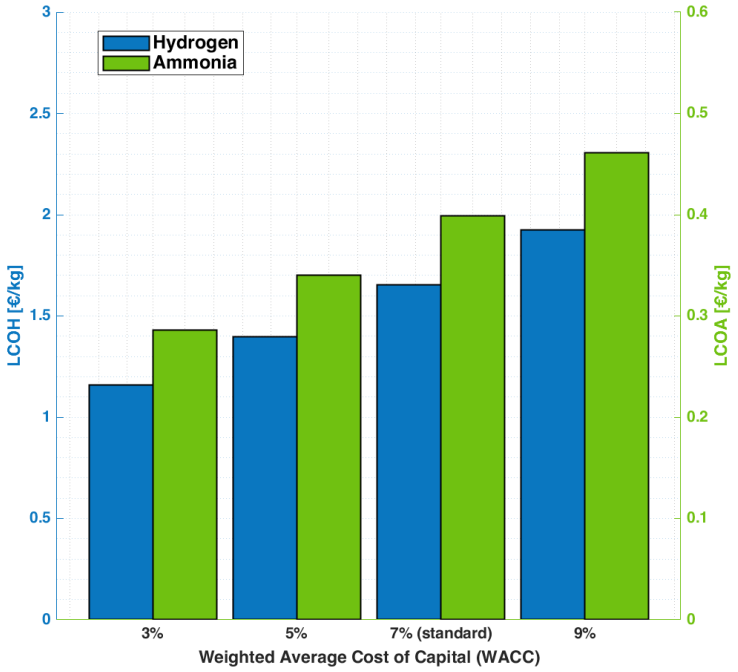


Figure 6.8: Sensitivity analysis of the LCOH and LCOA with a varying WACC.

6.4.3 Sensitivity of the Model

By measuring the effect of large variations in the costs of the components and the WACC the degree of competitiveness can be examined. However, it does not say anything about the resilience of the model. Therefore, smaller variations provide more useful information in determining the model's sensitivity. Unfortunately, a more delicate sensitivity analysis has not been performed in this research. Nonetheless, by examining the model's outcome for different simulation periods, the assumption that a simulation time of nine months is also useful in determining the competitiveness, can be validated.

As previously mentioned, it was not possible to run the model for a longer simulation

period than nine months due to running times longer than seven days. Therefore, the last circle representing the levelized cost stops at nine months. However, it was assumed that the result would get closer to the limit with each increased simulation period. To test how many resources were necessary to run the model it had previously been running for periods of 2, 4, 6 and 7 months. With this information figure 6.4.3 was created, showing an exponential decay and a minimal difference in the levelized cost of nine months compared to twelve months. This suggests that by running the model for only nine months, the outcome can be still be used to compare it against the levelized cost of fossil fuel-based production.

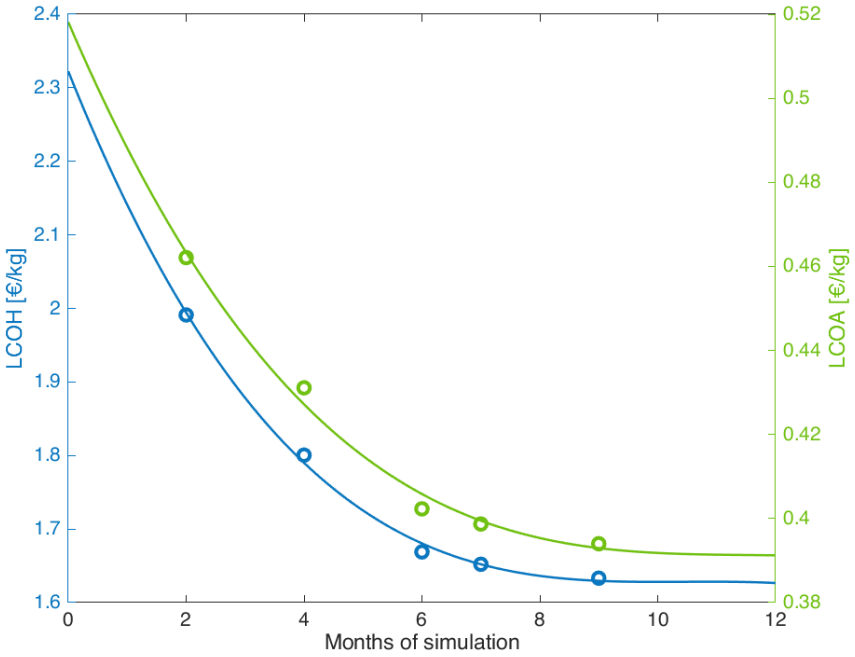


Figure 6.9: Sensitivity of the model to the simulation time. The circles represent the levelized cost corresponding to a certain simulation time.

7 Conclusion

This research aimed to investigate how green hydrogen and ammonia could be competitive with hydrogen and ammonia produced from fossil fuels when comparing the levelized cost for 2030. By designing a flexible system with electricity, hydrogen and nitrogen storage that would produce 200,000-ton of ammonia each year using solar power. The sizes of the components were minimized to produce the lowest possible levelized cost using an optimization model. In this section, the results will be summarized.

The calculated capacity results show that the optimization model has produced credible results. For an output of 200.000 ton-NH_3 per year, the system requires 0.87 GW of PV capacity and 0.68 GW electrolyzer capacity. This can be compared to a recently announced project of a much larger scale. To produce 900.000 ton-NH_3 per year in Oman 3 GW PV capacity and 0.5 GW wind power will be installed (Gupta 2021). When increasing the output of this research to 800.000 ton-NH_3 per year this results in a PV capacity of 3.85 GW which is in the same order of magnitude.

Another interesting finding presented in chapter 6.1 is the calculated required capacity of the salt cavern. If the salt cavern would be used to its maximum potential, it could store 3,300 ton-H_2 with pressures between 59.3 - 197.6 bar. However, only 6.4% of the total available capacity will be necessary for the storage of hydrogen when the system is scaled to an output of 200,000 ton NH_3 a year. If this output were to increase 2 or 4 times, this would result in a salt cavern capacity of 12.7% and 16.8% of the initially assumed capacity. This finding is beneficial for the proposed solar power to ammonia system as more feasible locations can be exploited when the maximum capacity of the salt cavern can be much smaller. However, this will not lead to a better location in Morocco as the other suitable salt basins do not receive more sunlight than in the Essaouira basin. Although, the Souss-Massa basin is located more towards the south, near Agadir. It can be seen in figure A.1 that the levels of solar irradiance are lower than East of Essaouira, where the Tamergat well is located (Lat: 31.41, Lon: -9.55). Secondly, similar projects in the same region will probably use the remaining capacity. Instead of separately developing salt caverns for hydrogen storage, multiple projects can make use of the same cavern. This way, the excavation costs, buffer gas costs, and transport costs through pipelines can be split. Therefore, the assumption that the Essaouira basin is the best location for storing hydrogen in Marocco is justified.

By evaluating the results on the allocation of energy in the different components, it can be concluded that the modelling has been done correctly. Assuming that a small amount of electricity consumption would allow the feed water and hydrogen compressor to be connected to the electricity grid instead of the PV panels turned out to be true. The constraints used to model the components correctly can be validated by observing the Sankey diagram in figure 6.2 and the load distribution curves in figure 6.3 and 6.4. With a total efficiency of 65.5%, which is slightly higher than the calculated efficiency of 63.75% from (Birol 2019). In the load distribution graphs, the consequences of the load range constraints written in figure 4.4 are clearly visible. In the graph depicting the SOC of the battery and the graph depicting the capacity of the Haber-Bosch plant, the blue line is cut-off at 20%, showing that the constraints are taken into account.

The most important result to answer the main question stated in this research, of how green hydrogen and ammonia can compete with fossil fuel-based production, are the levelized cost

results. Having performed an optimization in which every component is minimized in order to keep the levelized cost as low as possible while satisfying all constraints has resulted in a levelized cost of green hydrogen and ammonia of 1.63 €/kg-H_2 and 0.394 €/kg-NH_3 for 2030. This will make green hydrogen competitive when natural gas reaches a price of 3.16 $/MBTu or 12.25 €/MWh, converted using USD/EUR rate of 0.88 and a conversion factor of 0.29308 MWh/MBTU, and taking into account a carbon price of 100 €/ton-CO_{2-eq}. For green ammonia to be cheaper, the gas price must be greater than 4.49 $/MBTu or 17.41 €/MWh. With the recent natural gas prices rising rapidly due to the conflict between Russia and Ukraine, gas prices have already reached multiples of these values. The same conclusion is drawn when including the uncertainty about the development of the CAPEX and OPEX cost for the individual components. Resulting in combined range of 0.8285 - 2.4770 €/kg-H_2 and 0.2155 - 0.5817 €/kg-NH_3 when varying the CAPEX and OPEX cost. The upper margin would compare to a gas price of 7.71 $/MBTu and 9.04 $/MBTu. Lastly, the components with the biggest impact on the levelized cost are the PV farm and the electrolyzer with a contribution of 49.8% and 28.4% to the LCOH and 40.0% and 21.8% to the LCOA. Therefore, these components are the most responsive to changes in the CAPEX and OPEX. This was not assumed as the Haber-Bosch plant was the most expensive component. Nonetheless, this demonstrates the salt cavern's usefulness in keeping the Haber-Bosch plant's capacity to a minimum.

8 Discussion

In this chapter, the relevance of the results is discussed to provide a clear picture of the essence of this research to the existing research of green hydrogen and ammonia systems. This will be achieved by comparing the obtained results with the results of similar research and indicating the limitations of this research.

The results indicate that green ammonia and especially green hydrogen can compete with ammonia and hydrogen produced from fossil fuels in 2030. With a LCOH of 1.63 €/kg-H_2 and a LCOA of 0.394 €/kg-NH_3 for 2030 the natural gas price will have to be higher than 3.16 $/MBTu and 4.49 $/MBTu for green hydrogen and ammonia to be cheaper. In (Birol 2019) the gas price is assumed to vary between 3.5 and 10.7 $/MBTu in 2030, making it very likely for green hydrogen and ammonia to be competitive.

Comparing this to the result of (Nayak-Luke and Bañares-Alcántara 2020) were the median of 534 different locations is a LCOA of 0.457 $/kg-$NH_3$ and 36 locations fall beneath 0.35 $/kg-$NH_3$. Converted to euro's using the exchange rate on the day of the publication (1.1075 EUR-USD (Macrotrends LLC 2021)) this results in a median of 0.42 €/kg-NH_3 and for the best 36 locations a LCOA of 0.32 €/kg-NH_3. In the similar study of (Fasihi et al. 2021) in which battery storage, as well as hydrogen storage, is used, the resulting LCOA for 2030 is a bit lower; 345 - 420 €/ton-NH_3. The LCOA obtained in this research lies well beneath the median of (Nayak-Luke and Bañares-Alcántara 2020). However, the minimum LCOA of both studies is much lower than the result in this study, even though the modelled system is more flexible due to the possibility of nitrogen and battery storage and should therefore produce a lower LCOA. The earlier conclusion can explain that the salt cavern storage is not used to its maximum capacity. Thus the chosen location had to compromise a location with a higher solar irradiance for an unnecessarily large salt cavern.

Similar observations can be made when comparing the LCOH. In (Mallapragada et al. 2020) the calculated LCOH lies between 2.3 \$/kg-H_2 and 11.8 \$kg-H_2, when pressure vessels are used for hydrogen storage. In the same report, the LCOH is calculated using hydrogen storage in a salt cavern instead of pressure vessels. This resulted in a LCOH of 1.9 \$/kg-H_2 - 4.2\$/kg-H_2, the values used for the CAPEX and OPEX of the salt cavern were; 3 \$/kg and 1% (of CAPEX), respectively. Again the exchange rate on the day of the publication is taken to convert the dollars to euros (1.0996 EUR-USD (Macrotrends LLC 2021)). The obtained LCOH is 1.73 - 3.82 \$/kg-H_2. The salt cavern costs must be included in the LCOH to compare the LCOH values of (Mallapragada et al. 2020) with the results produced in this report. In previous stated LCOH this was not included, as was explained in chapter 2.1. Using a higher value for the CAPEX and OPEX cost of the salt cavern (Tabel 2.2), the LCOH with hydrogen storage is 1.64 \$/kg-H_2. This is only a difference of €0.01 with the LCOH without hydrogen storage. This may seem hard to believe, but in chapter 6.3 it was already explained that the salt mine only accounts for 0.42% of the total LCOA. The difference in LCOH between this research and (Mallapragada et al. 2020) is mainly attributed to the lower PV power and electrolyzer CAPEX used in this research. Time will tell what the most accurate predictions of the CAPEX and OPEX costs were as these will converge when more and more green hydrogen and ammonia projects are developed.

A more realistic model could have been developed if it were not for the following limitations. First of all, the efficiency of the different components was now assumed to be constant. In reality, the components will start to perform less when they approach their maximum operational limit. For the electrolyzer stacks, this can be paraphrased in the equation provided in (Morgan et al. 2014). Secondly, the simulation time of the model could be extended from nine to twelve months for a more comprehensive result. The problem is that the run time increases exponentially when the simulation time increases. Running the model on a high-performance computing cluster for nine months already takes two days for the program to complete. Luckily the impact on the levelized cost is minimal. Instead of using hourly data, it has been tried to sum the data in six to twelve-hour resolutions; however, this did not give the desired results.

Comparing the LCOA obtained with a simulation time of 6 months with a simulation of 9 months only results in a 3% decrease, as buffers can be exploited more gradually. Thirdly, the balance of system cost is now represented by 10% of the levelized costs. This quantity can be better defined by investigating the specific costs for the cables, charge controller, and smaller components. Fourthly, the model uses ramping constraints of 20% for the electrolyzer and Haber-Bosch plant while using a time step of one hour. This might over define the system as ramping constraints are meant to restrict the rapid fluctuation in load power, but this might not apply on a longer time scale of one hour. Fifthly, the simulation outcome would be more realistic if maintenance stops for all the components were included. In the current simulation, all the components can run continuously. However, the components will sometimes need to be shut down for maintenance or regular checks. This will increase the necessary buffers in the system, resulting in a higher levelized cost.

During the determination of the location, it is assumed that the solar farm must be located at a close distance to the Tamergat well (Lat: 31.41, Lon: -9.55). As can be seen in figure A.3 the selected salt cavern has a width of 5 km. However, this does not mean that the solar farm must be directly located above this salt cavern. It can also be located more towards the west, bringing it closer to the Sahara desert. Locating the solar farm further away from the sea creates a more stable solar irradiance profile as fewer clouds are present throughout the year. The losses of the electricity transmission using DC cables are relatively low. AC cables can also be

used for transmission as they have a higher efficiency over a distance shorter than 600 – 800 km (Ryndzionek and Sienkiewicz 2020), but then the electricity from the PV panels will need to be converted two times because the electrolyzer runs on DC as well. In summary, the restrictions assumed in the determination process of the location for the PV farm can be loosened as electric cables have low losses, thereby allowing the distance between the electrolyzer and the PV farm to be increased.

9 Recommendations

To further minimize the levelized cost and improve the accuracy of the model. Future research of green hydrogen and ammonia production should focus on; minimizing the optimization variables [1], include maintenance stops [2], take into account degradation of the components [3], variable efficiencies due to variable load [4], connecting the ASU to the grid [5] and finding a more suitable location with less salt cavern capacity, but more solar irradiance [6].

To elaborate on the first point made in the previous paragraph, a model with fewer variables will calculate fewer scenarios and will therefore have a shorter running time. Enabling it to simulate a longer period produces a more realistic outcome of the LCOH and LCOA. To achieve this, the allocation of the energy carriers obtained in this research should be studied to discover when the model decides to allocate the energy to different components. For example, when does the PV farm distribute its electricity to the battery instead of the electrolyzer, Haber-Bosch plant or ASU, and how much does it distribute. This is a complex problem as it depends on the state of charge levels of the buffers and the incident solar irradiance. However, if the system would be operational one day, the best possible way of allocating the energy at any given time should be known to produce green hydrogen and ammonia effectively.

The second, third and fourth recommendations would create a more realistic model. Beginning with the required maintenance stops once in a while for a more realistic simulation. To prevent a full production stop, which would probably result in a penalty for not meeting the production demands. The buffers can be increased to keep the rest of the components running. However, this must be simulated in order to install sufficient capacity. The third point stresses the importance of including the degradation of the components in the model. For the PV panels this can be a considerable amount of 0.2%/yr (National Renewable Energy Laboratory 2019). This would have a big impact on the outcome if the system were to run for 30 years. The last recommendation to create a more realistic model is to vary the efficiency according to the load. Some components perform less when they approach their maximum capacity. Like the electrolyzer explained in chapter 8.

In recommendation five, it is suggested to connect the ASU to the electricity grid. This can be done because, as shown in figure 6.2 the ASU consumes little electricity, and this amount can also be extracted from the electricity grid. Interacting with the electricity network will create a more flexible system and reduce buffer capacities. The system already does not run in a stand-alone mode, so this recommendation does not propose a significant disruption. The last recommendation extends onto one of the main findings of this research. That in order to find a better location for the proposed system, the salt cavern capacity can be 10% of the capacity assumed in this rapport. This reduces the constraints on the geological properties of the salt cavern and allows for a broader range of locations to be feasible locations. As a result,

locations discarded during this research will become available again and might contain higher irradiance levels. Therefore, future research should investigate the geological properties of salt caverns in regions that receive higher irradiance levels and combine this with further research into the transportation of either hydrogen or ammonia.

References

[1] R K Ahluwalia, D D Papadias, J-K Peng, and H S Roh. System Level Analysis of Hydrogen Storage Options. *Argonne National Laboratory*, 2019.

[2] Julien Armijo and Cédric Philibert. Flexible production of green hydrogen and ammonia from variable solar and wind energy: Case study of Chile and Argentina. *International Journal of Hydrogen Energy*, 45(3):1541–1558, 1 2020. ISSN 03603199. doi: 10.1016/j.ijhydene.2019.11.028.

[3] Megan Atkins. Future Hydrogen Town Designing a PV-Hydrogen-Battery-FC system for a typical neighbourhood in the Netherlands. Technical report, Delft University Of Technology, Delft, 8 2020.

[4] Emiliano Bellini. Portuguese government confirms world record solar price of $0.01316/kWh. *pv magazine International*, 8 2020. URL https://www.pv-magazine.com/2020/08/27/portuguese-government-confirms-world-record-solar-price-of-0-01316-kwh/.

[5] Luca Bertuccioli, Alvin Chan, David Hart, Franz Lehner, Ben Madden, and Eleanor Standen. Development of Water Electrolysis in the European Union Final Report Fuel cells and hydrogen Joint undertaking E4tech Sàrl with Element Energy Ltd for the Fuel Cells and Hydrogen Joint Undertaking From To ? Technical report, 2014. URL www.e4tech.com.

[6] Faith Birol. The Future of Hydrogen. Technical report, International Energy Agency, 6 2019.

[7] Mark Bolinger, Joachim Seel, and Dana Robson. Utility-Scale Solar: Empirical Trends in Project Technology, Cost, Performance, and PPA Pricing in the United States –2019 Edition. Technical report, 2019. URL https://escholarship.org/uc/item/336457p8.

[8] Thijs ten Brinck. Zonnestroom onder 1 eurocent per kilowattuur in Saudi Arabië? , 4 2021. URL https://www.wattisduurzaam.nl/5969/energie-opwekken/zonne-energie/zonnestroom-mexico-duikt-4-dollarcent-per-kilowattuur/.

[9] Brown. Trevor. Renewable Energy to Fuels Through Utilization of Energy-Dense Liquids (REFUEL) Program Overview. *ARPA-E, "REFUEL"*, 1 2017. URL http://ageconsearch.umn.edu/bitstream/133410/2/Department-APUC%20Report.pdf;.

[10] U. Bünger, J. Michalski, F. Crotogino, and O. Kruck. Large-scale underground storage of hydrogen for the grid integration of renewable energy and other applications. *Compendium of Hydrogen Energy*, pages 133–163, 1 2016. doi: 10.1016/B978-1-78242-364-5.00007-5.

[11] Molly Burgess. thyssenkrupp to provide over 2GW electrolysis plant for Saudi Arabia's $5bn green hydrogen project, 12 2021. URL https://www.h2-view.com/story/thyssenkrupp-to-provide-over-2gw-electrolysis-plant-for-saudi-arabias-5bn-green-hydrog

[12] Dilara Gulcin Caglayan, Nikolaus Weber, Heidi U. Heinrichs, Jochen Linßen, Martin Robinius, Peter A. Kukla, and Detlef Stolten. Technical potential of salt caverns for hydrogen storage in Europe. *International Journal of Hydrogen Energy*, 45(11):6793–6805, 2 2020. ISSN 0360-3199. doi: 10.1016/J.IJHYDENE.2019.12.161.

[13] Carbon Price Viewer. Carbon Price Viewer, 2022. URL https://sandbag.be/index.php/carbon-price-viewer/.

[14] Izzat Iqbal Cheema and Ulrike Krewer. Operating envelope of Haber–Bosch process design for power-to-ammonia. *RSC Advances*, 8(61):34926–34936, 10 2018. ISSN 2046-2069. doi: 10.1039/C8RA06821F. URL https://pubs.rsc.org/en/content/articlehtml/2018/ra/c8ra06821fhttps://pubs.rsc.org/en/content/articlelanding/2018/ra/c8ra06821f.

[15] Claude Crampes and Stefan Ambec. Europe bets on hydrogen . *Toulouse School of Economics*, 1 2021. URL https://www.tse-fr.eu/europe-bets-hydrogen.

[16] Fritz Crotogino. Larger Scale Hydrogen Storage. *Storing Energy: With Special Reference to Renewable Energy Sources*, pages 411–429, 1 2016. doi: 10.1016/B978-0-12-803440-8.00020-8.

[17] Anna Dumas and Jumana Saleheen. Understanding carbon prices. *CRU group*, 12 2021. URL https://sustainability.crugroup.com/article/understanding-carbon-prices.

[18] European Commission. Proposal for a DIRECTIVE OF THE EUROPEAN PARLIAMENT AND OF THE COUNCIL amending Directive 2003/87/EC establishing a system for greenhouse gas emission allowance trading within the Union, Decision (EU) 2015/1814 concerning the establishment and operation of a market stability reserve for the Union greenhouse gas emission trading scheme and Regulation (EU) 2015/757. Technical report, European Commission, Brussels, 7 2021.

[19] Mahdi Fasihi, Robert Weiss, Jouni Savolainen, and Christian Breyer. Global potential of green ammonia based on hybrid PV-wind power plants. *Applied Energy*, 294:116170, 7 2021. ISSN 0306-2619. doi: 10.1016/J.APENERGY.2020.116170.

[20] Jean Franz. Managing Urban Water Scarcity in Morocco. Technical report, World Bank Group, 11 2017. URL www.worldbank.org.

[21] C. Fúnez Guerra, L. Reyes-Bozo, E. Vyhmeister, M. Jaén Caparrós, José Luis Salazar, and C. Clemente-Jul. Technical-economic analysis for a green ammonia production plant in Chile and its subsequent transport to Japan. *Renewable Energy*, 157:404–414, 9 2020. ISSN 18790682. doi: 10.1016/j.renene.2020.05.041.

[22] Felipe Ignacio Gallardo, Andrea Monforti Ferrario, Mario Lamagna, Enrico Bocci, Davide Astiaso Garcia, and Tomas E. Baeza-Jeria. A Techno-Economic Analysis of solar hydrogen production by electrolysis in the north of Chile and the case of exportation from Atacama Desert to Japan. *International Journal of Hydrogen Energy*, 46(26):13709–13728, 4 2021. ISSN 03603199. doi: 10.1016/j.ijhydene.2020.07.050. URL www.sciencedirect.comhttp://creativecommons.org/licenses/by/4.0/.

[23] Global Solar Atlas. Global Solar Atlas, 2021. URL https://globalsolaratlas.info/support/release-notes.

[24] Google Earth. Google Earth, 11 2021.

[25] Jachin Gorre. Innovative large-scale energy storage tech-nologies and Power-to-Gas concepts after optimisation Report on the optimal time profile and operation of the conversion technology during a repre-sentative year, in the perspective of the available storage capacities. Technical report.

[26] Alexa Grimm, Wouter A. de Jong, and Gert Jan Kramer. Renewable hydrogen production: A techno-economic comparison of photoelectrochemical cells and photovoltaic-electrolysis. *International Journal of Hydrogen Energy*, 45(43):22545–22555, 9 2020. ISSN 03603199. doi: 10.1016/j.ijhydene.2020.06.092.

[27] Uma Gupta. Indian solar developer to build 3.5 GW green hydrogen project in Oman – pv magazine International. *PV Magazine*, 8 2021. URL `https://www.pv-magazine.com/2021/08/24/indian-solar-developer-builds-3-5-gw-green-hydrogen-project-in-oman/`.

[28] LCC Gurobi Optimization. GUROBI OPTIMIZER REFERENCE MANUAL. Version 9.0, 2020.

[29] F. Gutiérrez-Martín, Lidia Amodio, and Maurizio Pagano. Hydrogen production by water electrolysis and off-grid solar PV. *International Journal of Hydrogen Energy*, 2020. ISSN 03603199. doi: 10.1016/j.ijhydene.2020.09.098.

[30] K W Harrison, R Remick, G D Martin, and A Hoskin. Hydrogen Production: Fundamentals and Cas Study Summaries e Preprint. Technical report, 2010. URL `http://www.osti.gov/bridge`.

[31] Gerben Hieminga and Nadège Tillier. High gas prices triple the cost of hydrogen production | Article | ING Think. *ING Economic and Finacial Analysis*, 10 2021. URL `https://think.ing.com/articles/hold-1of4-high-gas-prices-triples-the-cost-of-hydrogen-production`.

[32] M. Hssaisoune, S. Boutaleb, M. Benssaou, B. Bouaakkaz, and L. Bouchaou. Physical geography, geology, and water resource availability of the Souss-Massa River Basin. *Handbook of Environmental Chemistry*, 53:27–56, 2017. doi: 10.1007/698{_}2016{_}68.

[33] IEA. Hydrogen Projects Database. Technical report, 2020. URL `https://www.iea.org/reports/hydrogen-projects-database`.

[34] IEAGHG. Techno-economic evaluation of SMR based standalone (merchant) hydrogen plant with CCS. 2 2017. URL `www.ieaghg.org`.

[35] Jussi Ikäheimo, Juha Kiviluoma, Robert Weiss, and Hannele Holttinen. Power-to-ammonia in future North European 100 % renewable power and heat system. *International Journal of Hydrogen Energy*, 43(36):17295–17308, 9 2018. ISSN 0360-3199. doi: 10.1016/J.IJHYDENE.2018.06.121.

[36] International Finance Corporation. Utility-Scale Solar Photovoltaic Power Plants: a project Developer's guide. Technical report, Wolrd Bank Group, Washington D.C., 2015.

[37] IRENA. Electricity Storage and Renewables: Costs and Markets to 2030. Technical report, International Renewable Energy Agency, Abu Dhabi, 2017. URL `www.irena.org`.

[38] IRENA. Future of Solar Photovoltaic: Deployment, investment, technology, grid integration and socio-economic
}aspects (A Global Energy Transformation: paper). Technical report, International Renewable Energy Agency, Abu Dhabi, 2019.

[39] IRENA. Green hydrogen supply: A guide to policy making,
}International Renewable Energy Agency. Technical report, International Renewable Energy Agency, Abu Dhabi, 2021. URL `www.irena.org`.

[40] Safaa Kasraoui. Morocco's Renewable Energy Capacities Exceed 2020 Forecast, 4 2021. URL https://www.moroccoworldnews.com/2021/04/339140/moroccos-renewable-energy-capacities-exceed-2020-forecast.

[41] A Kavaz, S Hodžić, Tarik Hubana, Semra Curevac, N Đozić, Hamza Merzic, H Tanković, K Dervišević, E Alihodžić, E Sikira, D Rahić, Nihad Kavazovic, Faris Tanković, and B Šestan. Solar Tree Project. 1 2014.

[42] Jungbin Kim, Kiho Park, Dae Ryook Yang, and Seungkwan Hong. A comprehensive review of energy consumption of seawater reverse osmosis desalination plants. *Applied Energy*, 254, 11 2019. ISSN 03062619. doi: 10.1016/J.APENERGY.2019.113652.

[43] David J. Lampert, Hao Cai, and Amgad Elgowainy. Wells to wheels: water consumption for transportation fuels in the United States. *Energy & Environmental Science*, 9(3):787–802, 3 2016. ISSN 1754-5706. doi: 10.1039/C5EE03254G. URL https://pubs.rsc.org/en/content/articlehtml/2016/ee/c5ee03254ghttps://pubs.rsc.org/en/content/articlelanding/2016/ee/c5ee03254g.

[44] Daniel Lincot. The new paradigm of photovoltaics: From powering satellites to powering humanity. *Comptes Rendus Physique*, 18(7-8):381–390, 9 2017. ISSN 1631-0705. doi: 10.1016/J.CRHY.2017.09.003.

[45] Linde AG. Cryogenic Standard Tanks LITS 2. Technical report, The Linde Group, Tachherting, Germany, 2021.

[46] Anna S. Lord, Peter H. Kobos, and David J. Borns. Geologic storage of hydrogen: Scaling up to meet city transportation demands. *International Journal of Hydrogen Energy*, 39(28):15570–15582, 9 2014. ISSN 0360-3199. doi: 10.1016/J.IJHYDENE.2014.07.121.

[47] Macrotrends LLC. Euro Dollar Exchange Rate (EUR USD) - Historical Chart, 2021. URL https://www.macrotrends.net/2548/euro-dollar-exchange-rate-historical-chart.

[48] Sofoklis S Makridis. Hydrogen storage and compression. page 5, 2016.

[49] Dharik S Mallapragada, Diego Diaz Pilas, Pilar Gonzalez Fernandez, and Agustín Delgado Martín. System implications of continued cost declines for wind and solar on driving power sector decarbonization An MIT Energy Initiative Working Paper. Technical report, 2020. URL https://www.eia.gov/todayinenergy/detail.php?id=37392,.

[50] Dharik Sanchan Mallapragada, Emre Gençer, Patrick Insinger, David William Keith, and Francis Martin O'Sullivan. Can Industrial-Scale Solar Hydrogen Supplied from Commodity Technologies Be Cost Competitive by 2030? *Cell Reports Physical Science*, 1(9):100174, 9 2020. ISSN 26663864. doi: 10.1016/j.xcrp.2020.100174. URL https://www.sciencedirect.com/science/article/pii/S2666386420301855#mmc2.

[51] Jan Michalski, Ulrich Bünger, Fritz Crotogino, Sabine Donadei, Gregor Sönke Schneider, Thomas Pregger, Karl Kiên Cao, and Dominik Heide. Hydrogen generation by electrolysis and storage in salt caverns: Potentials, economics and systems aspects with regard to the German energy transition. *International Journal of Hydrogen Energy*, 42(19):13427–13443, 5 2017. ISSN 0360-3199. doi: 10.1016/J.IJHYDENE.2017.02.102.

[52] Eric Morgan, James Manwell, and Jon McGowan. Wind-powered ammonia fuel production for remote islands: A case study. *Renewable Energy*, 72:51–61, 12 2014. ISSN 0960-1481. doi: 10.1016/J.RENENE.2014.06.034.

[53] Fokko Mulder and Hans Geerlings. Electrolysis for hydrogen production 1, 2020.

[54] Narasimhan. Area Required for Solar PV Power Plants. *Suncyclopedia*, 2014. URL http://www.suncyclopedia.com/en/area-required-for-solar-pv-power-plants/.

[55] National Renewable Energy Laboratory. Annual Technology Baseline: Electricity, 2019. URL https://atb.nrel.gov/.

[56] Richard Nayak-Luke, René Bañares-Alcántara, and Ian Wilkinson. "Green" Ammonia: Impact of Renewable Energy Intermittency on Plant Sizing and Levelized Cost of Ammonia. *Industrial & Engineering Chemistry Research*, 57(43):14607–14616, 10 2018. ISSN 15205045. doi: 10.1021/ACS.IECR.8B02447. URL https://pubs.acs.org/doi/full/10.1021/acs.iecr.8b02447.

[57] Richard Michael Nayak-Luke and René Bañares-Alcántara. Techno-economic viability of islanded green ammonia as a carbon-free energy vector and as a substitute for conventional production. *Energy & Environmental Science*, 13 (9):2957–2966, 9 2020. ISSN 17545706. doi: 10.1039/D0EE01707H. URL https://pubs.rsc.org/en/content/articlehtml/2020/ee/d0ee01707hhttps://pubs.rsc.org/en/content/articlelanding/2020/ee/d0ee01707h.

[58] NREL Annual Baseline Technology Report. Utility-Scale Battery Storage . Technical report, National Renewable Energy Laboratory, 2021. URL https://atb.nrel.gov/electricity/2021/utility-scale_battery_storage.

[59] Sean Ong, Clinton Campbell, Paul Denholm, Robert Margolis, and Garvin Heath. Land-Use Requirements for Solar Power Plants in the United States. *National Renewable Energy Laboratory*, 2013. URL www.nrel.gov/publications.

[60] Michael Penev and Chad Hunter. Energy Storage Analysis. Technical report, 2019.

[61] Michael Penev, Neha Rustagi, Chad Hunter, and Josh Eichman. Energy Storage: Days of Service Sensitivity Analysis. Technical report, 2019. URL https://www.energystorageexchange.org/.

[62] Pedro Quintela De Saldanha. Sines í µí°» 2 Hub a cost perspective of the transmission & storage infrastructure of the Sines green hydrogen hub. Technical report, Technical University of Delft, Madrid, 4 2021. URL http://repository.tudelft.nl/.

[63] Bernd Radowitz. Linde to build 'world's largest electrolyser' to produce green hydrogen | Recharge. *RECHARGE*, 1 2021. URL https://www.rechargenews.com/transition/linde-to-build-world-s-largest-electrolyser-to-produce-green-hydrogen/2-1-944080.

[64] Syed Farukh Javaid Rizvi, Sajjad Miran, Mudassar Azam, Waseem Arif, Muhammad Wasif, and Henrique Pacheco Garcia. Numerical Analysis of a Liquid Nitrogen (LN2) Engine for Efficient Energy Conversion. *ACS Omega*, 6(24):15663–15673, 6 2021. doi: 10.1021/ACSOMEGA.1C00582. URL https://pubs.acs.org/doi/full/10.1021/acsomega.1c00582.

[65] Rogier Elmer Roobeek. Shipping Sunshine A techno-economic analysis of a dedicated green hydrogen supply chain from the Port of Sohar to the Port of Rotterdam. Technical report.

[66] Roland Ryndzionek and Łukasz Sienkiewicz. Evolution of the HVDC link connecting offshore wind farms to onshore power systems. *Energies*, 13(8), 4 2020. ISSN 19961073. doi: 10.3390/EN13081914.

[67] Solargis. Solar Radiation Map: Global Horizontal Irradiation Map of Morocco, 2013. URL `https://solargis.com/`.

[68] Solcast. Solar Forecasting & Solar Irradiance Data, 2021. URL `https://solcast.com/`.

[69] J.S Stein, W.F Holmgren, J. Forbess, and C.W Hansen. PVLIB: Open source }photovoltaic performance modeling functions for matlab and python, 2016. URL `https://pvpmc.sandia.gov/`.

[70] G. Tari, B. Novotny, H. Jabour, and M. Hafid. Salt Tectonics Along the Atlantic Margin of NW Africa (Morocco and Mauritania). In *Permo-Triassic Salt Provinces of Europe, North Africa and the Atlantic Margins*, pages 331–351. Elsevier, 2017. doi: 10.1016/b978-0-12-809417-4.00016-1.

[71] Françis Tortochaux. Occurrence and Structure of Evaporites in North Africa. *Special Paper of the Geological Society of America*, 88:107–138, 1968. doi: 10.1130/SPE88-P107.

[72] Alfredo Ursúa, Ernesto L. Barrios, Julio Pascual, Idoia San Martín, and Pablo Sanchis. Integration of commercial alkaline water electrolysers with renewable energies: Limitations and improvements. *International Journal of Hydrogen Energy*, 41(30):12852–12861, 8 2016. ISSN 0360-3199. doi: 10.1016/J.IJHYDENE.2016.06.071.

[73] US Department of Energy. Hydrogen Production: Natural Gas Reforming, 2021. URL `https://www.energy.gov/eere/fuelcells/hydrogen-production-natural-gas-reforming`.

[74] A. Valera-Medina, H. Xiao, M. Owen-Jones, W. I.F. David, and P. J. Bowen. Ammonia for power. *Progress in Energy and Combustion Science*, 69:63–102, 11 2018. ISSN 0360-1285. doi: 10.1016/J.PECS.2018.07.001.

[75] A.J.M. Van Wijk and F. Wouters. Hydrogen, The Bridge between Africa and Europe. (September 2019):31, 2019.

[76] Eero Vartiainen, Gaëtan Masson, Christian Breyer, David Moser, and Eduardo Román Medina. Impact of weighted average cost of capital, capital expenditure, and other parameters on future utility-scale PV levelised cost of electricity. *Progress in Photovoltaics: Research and Applications*, 28(6):439–453, 6 2020. ISSN 1099-159X. doi: 10.1002/PIP.3189. URL `https://onlinelibrary.wiley.com/doi/full/10.1002/pip.3189https://onlinelibrary.wiley.com/doi/abs/10.1002/pip.3189https://onlinelibrary.wiley.com/doi/10.1002/pip.3189`.

[77] World Bank Global Electrification Database. Access to electricity (% of population) - Morocco. Technical report, World Bank, 2019. URL `https://data.worldbank.org/indicator/EG.ELC.ACCS.ZS?locations=MA`.

[78] Worley. Commercial-scale production: turning green hydrogen into ammonia, 2021. URL `https://www.worley.com/sustainability/our-stories/turning-green-hydrogen-into-ammonia`.

A Appendix

A.1 Determined location of the project

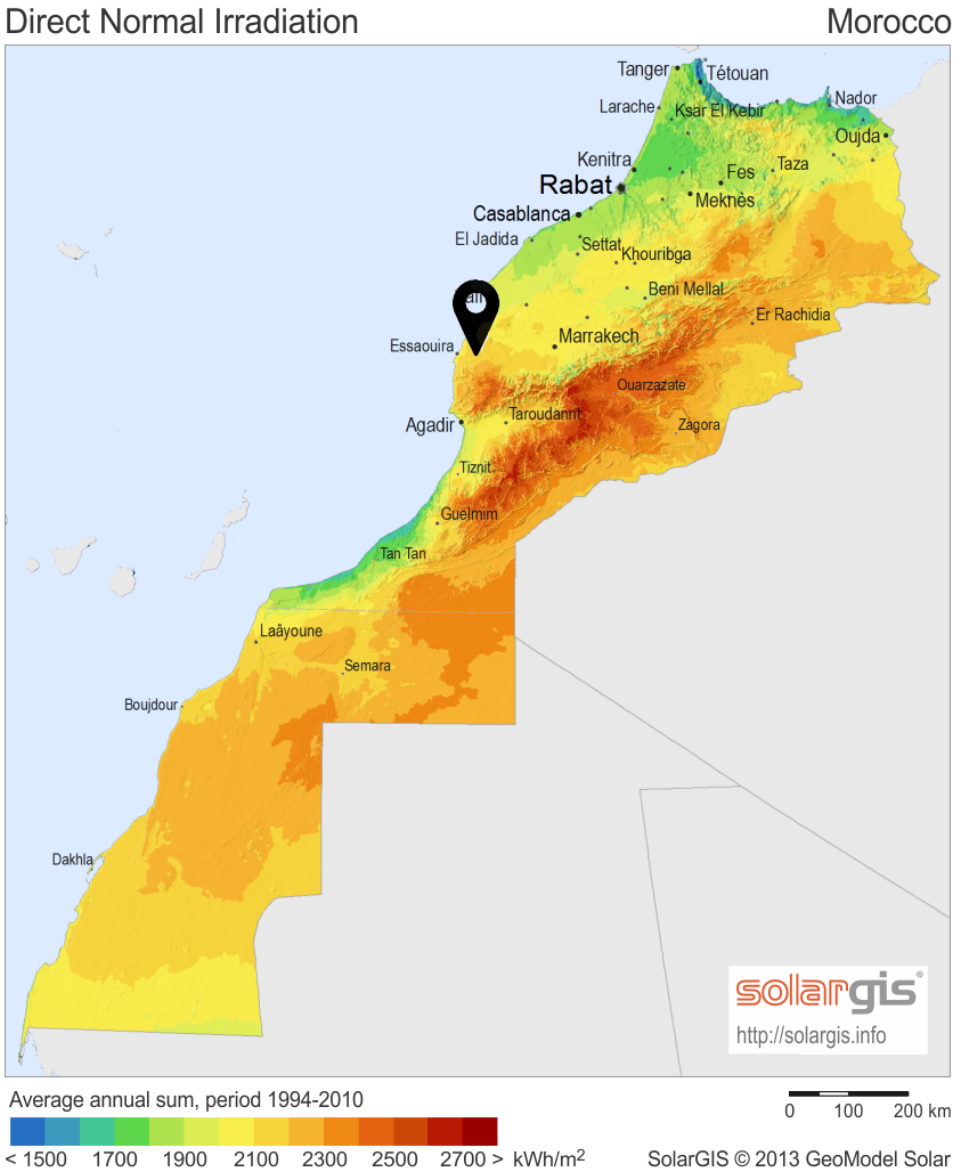


Figure A.1: The location of the proposed project is represented by the pin. One of the conclusions from this research is that the levelized cost could be lower when a smaller salt cavern can be used to find a location with more solar irradiance. Picture taken from (Solargis 2013).

A.2 Temperature influence on PV panels

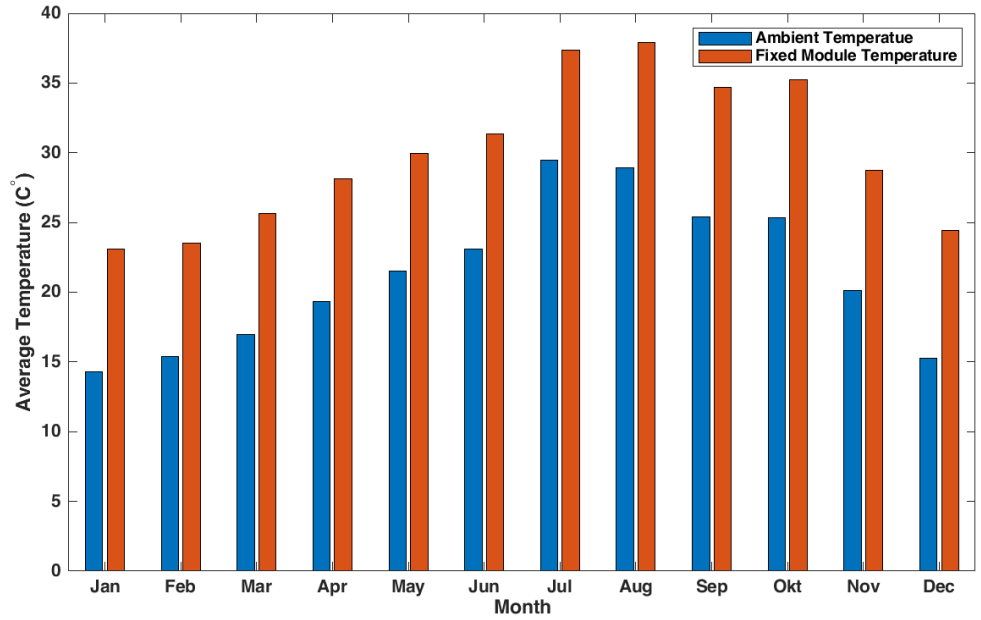


Figure A.2: Comparison between ambient and module temperature during daytime. Created in Matlab using Sandia's National Libraries PV_LIB Toolbox (Stein et al. 2016) and meteorological data from the website Solcast (Solcast 2021)

A.3 Map of the terrain on the proposed location

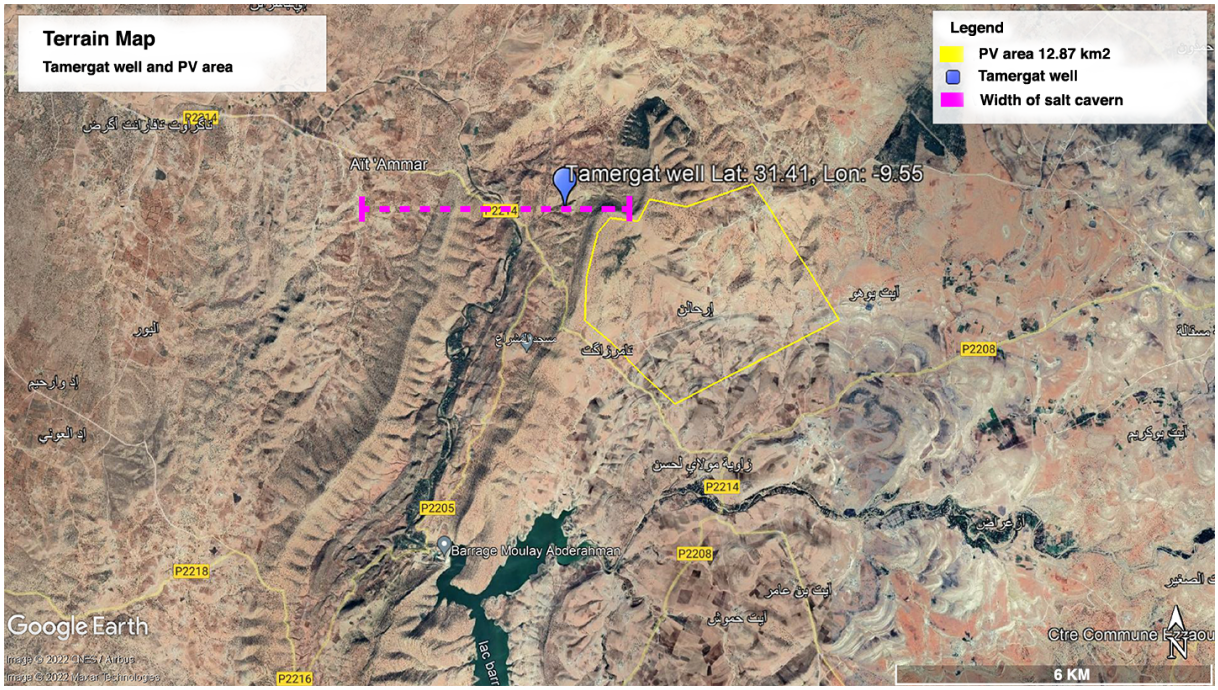


Figure A.3: The area defined by the yellow line represent the PV farm. It is located just South of the Tamergat well discussed in chapter 5.4. (Google Earth 2021) was used to create the image.

A.4 Installed and planned electrolyzer capacity

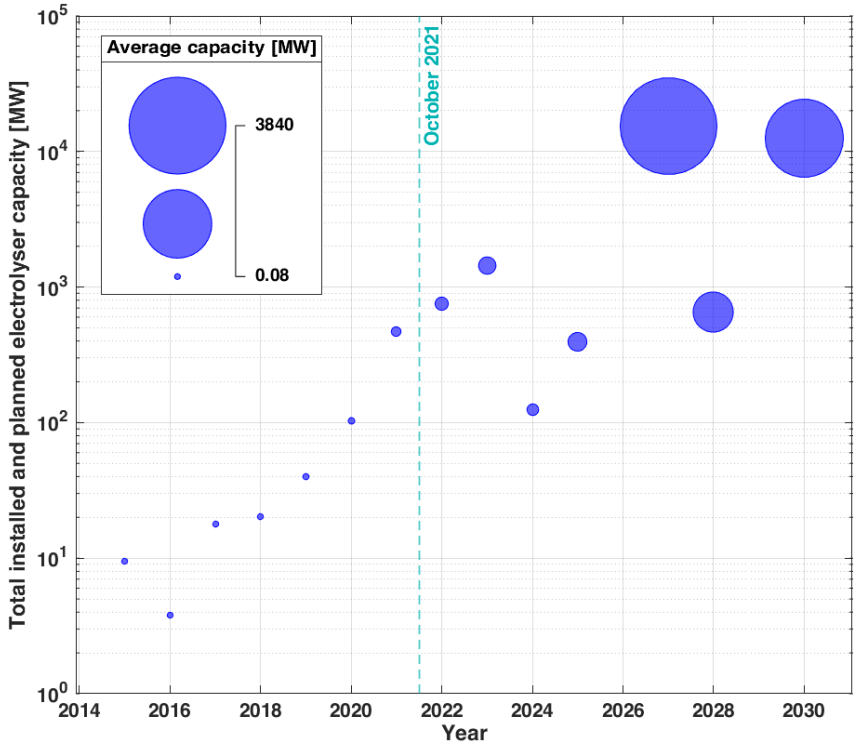


Figure A.4: Installed and planned electrolyzer capacity according to the (IEA 2020) database. The size of the bubbles represents the average electrolyzer capacity, while the vertical axis corresponds to the total sum of installed or planned capacity. The capacity will increase tremendously in the coming years.

A.5 Component load distribution

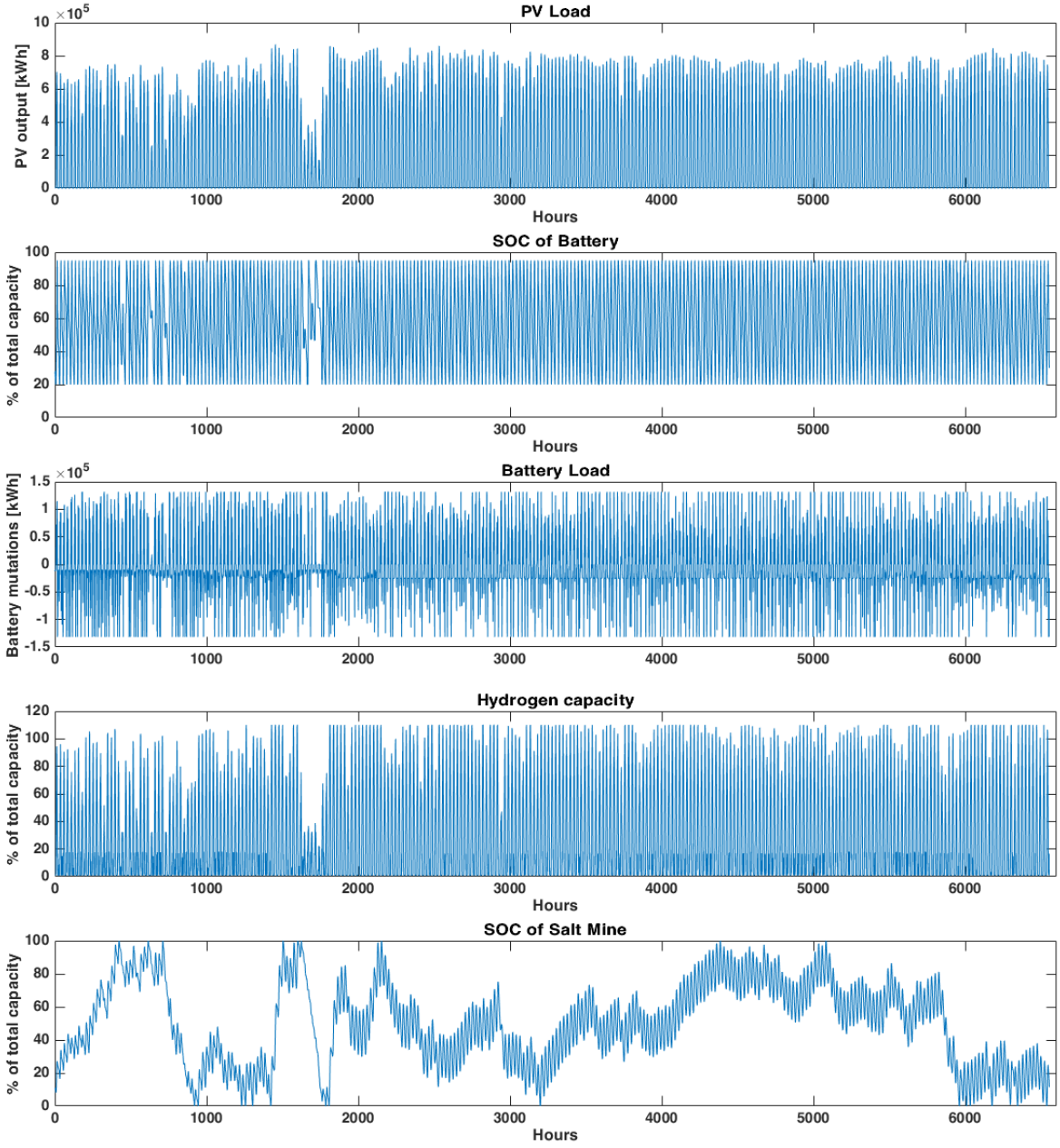


Figure A.5: The load distribution of the PV farm, Battery Electrolyzer and Salt Mine. The load is shown in percentages of certain components to show that they are bounded to a specific load range stated in table 2.2.

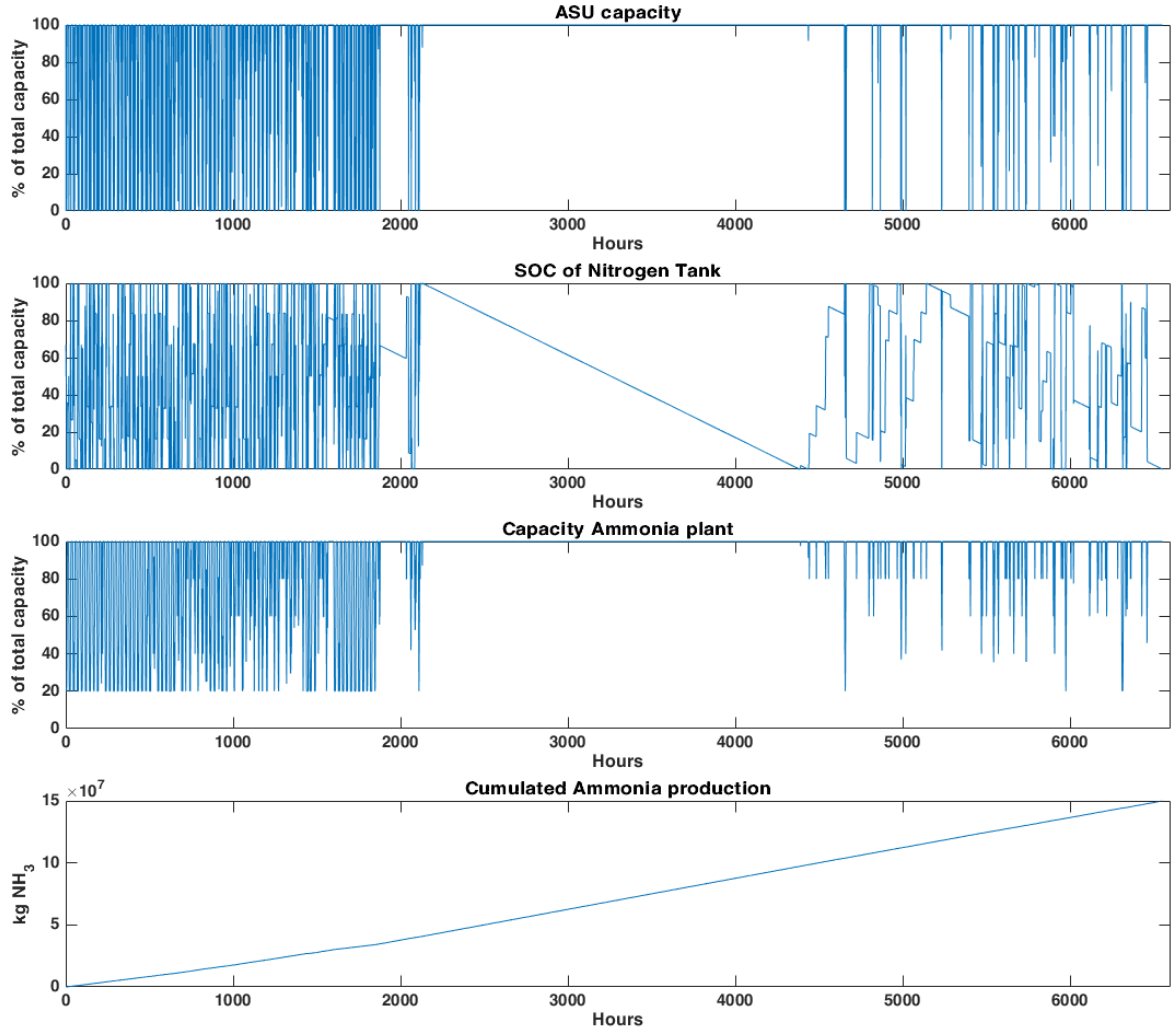


Figure A.6: The load distribution of the PV farm, Battery Electrolyzer and Salt Mine. The load is shown in percentages of certain components to show that they are bounded to a specific load range stated in table 2.2.

A.6 PV distribution

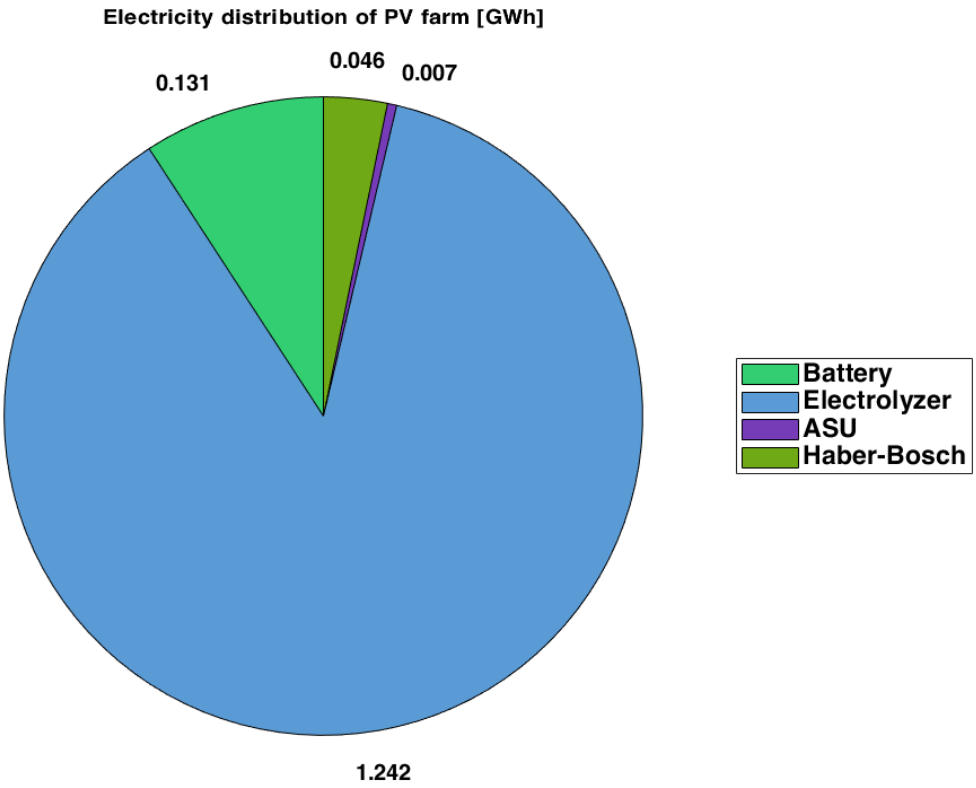


Figure A.7: The total electricity distribution of the PV farm for the entire simulation period of 9 months.

A.7 Wind Capacity Factors

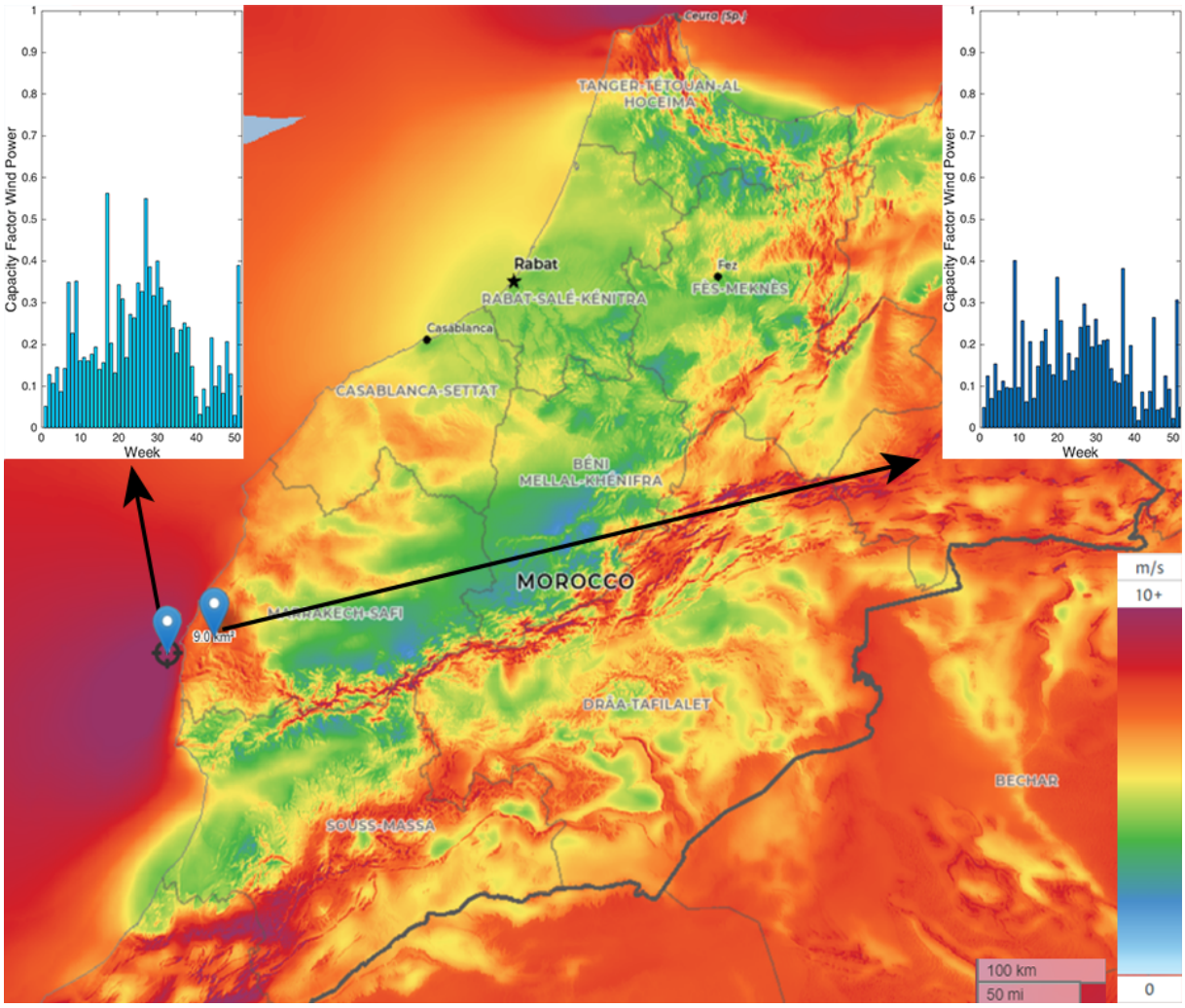


Figure A.8: Retrieved from wind atlas Created with data from (Solcast 2021)

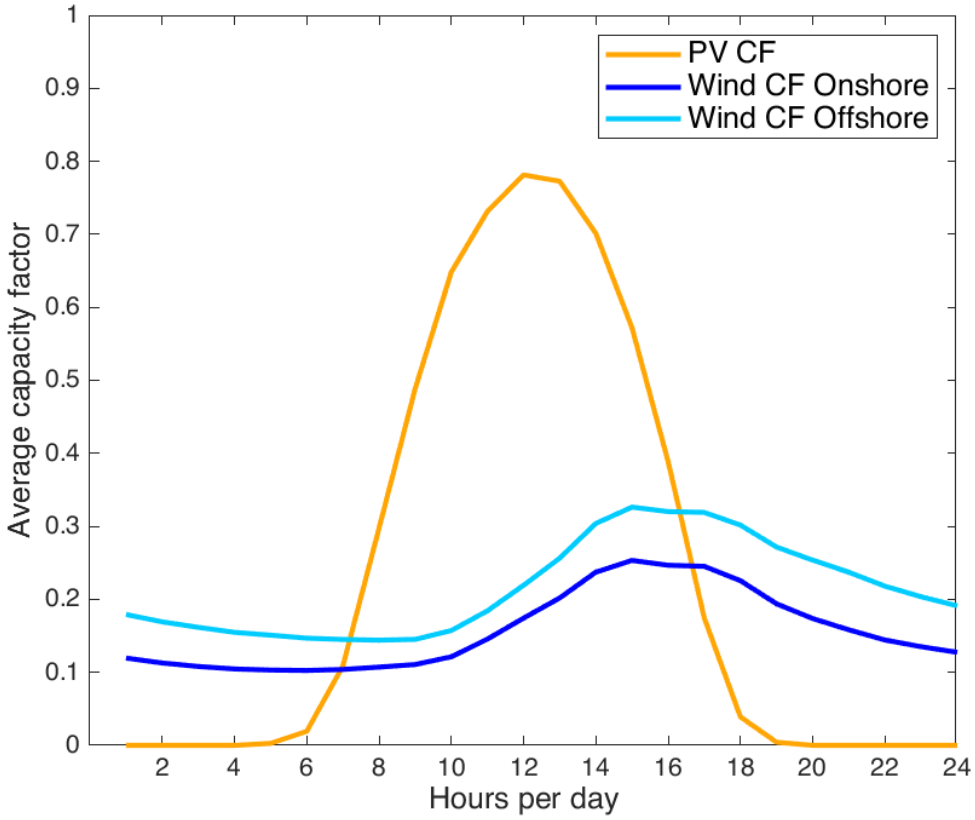


Figure A.9: Created with data from (Solcast 2021)

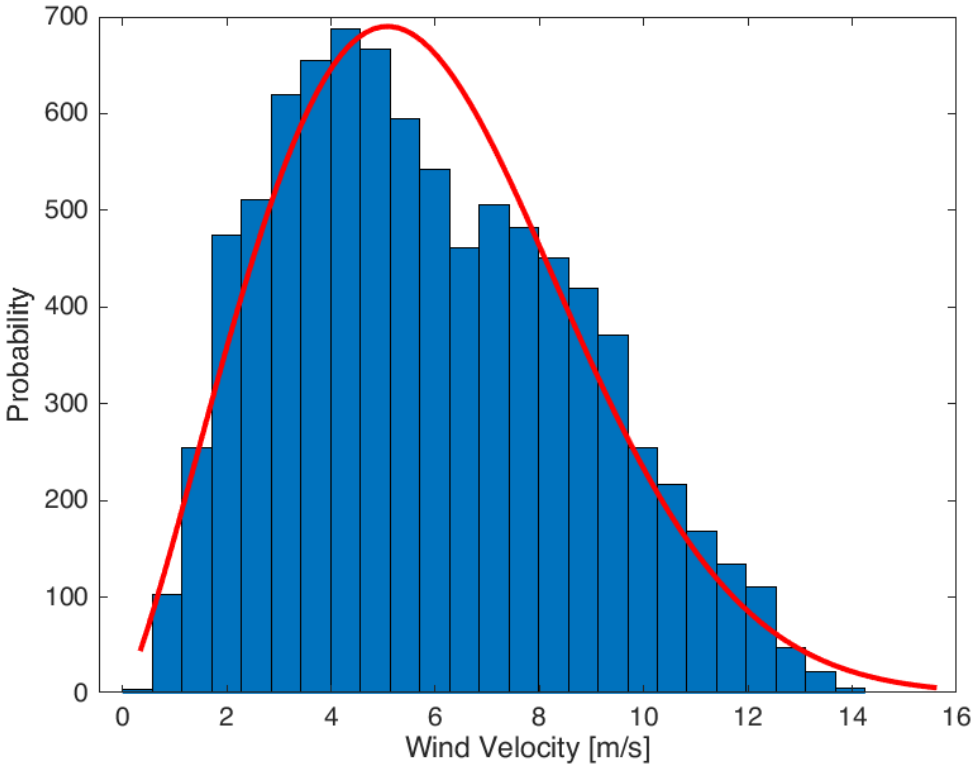


Figure A.10: Created with data from (Solcast 2021)

8.6 Model log output

```
1
2                                                    < M A T L A B (R) >
3                                          Copyright 1984-2020 The MathWorks, Inc.
4                                        R2020b Update 1 (9.9.0.1495850) 64-bit (glnxa64)
5                                                     September 30, 2020
6
7
8   To get started, type doc.
9   For product information, visit www.mathworks.com.
10
11
12  Solving problem using intlinprog.
13  Gurobi Optimizer version 9.1.2 build v9.1.2rc0 (linux64)
14  Thread count: 64 physical cores, 128 logical processors, using up to 32 threads
15  Optimize a model with 176908 rows, 78633 columns and 430166394 nonzeros
16  Model fingerprint: 0xc0065b5a
17  Variable types: 39321 continuous, 39312 integer (0 binary)
18  Coefficient statistics:
19    Matrix range     [6e-06, 5e+05]
20    Objective range  [1e-04, 3e+02]
21    Bounds range     [1e+00, 5e+05]
22    RHS range        [1e+00, 2e+08]
23  Presolve removed 0 rows and 0 columns (presolve time = 17s) ...
24  Presolve removed 4 rows and 0 columns (presolve time = 66s) ...
25  Presolve removed 6556 rows and 6552 columns (presolve time = 105s) ...
                                    •
                                    •
                                    •
115 Presolve removed 36791 rows and 23561 columns (presolve time = 2252s) ...
116 Presolve removed 36791 rows and 23561 columns (presolve time = 2328s) ...
117 Presolve removed 19807 rows and 6577 columns
118 Presolve time: 2328.34s
119 Presolved: 157101 rows, 72056 columns, 334486186 nonzeros
120 Variable types: 45851 continuous, 26205 integer (26205 binary)
121
122 Deterministic concurrent LP optimizer: primal simplex, dual simplex, and barrier
123 Showing barrier log only...
124
125 Root barrier log...
126
127 Elapsed ordering time = 13s
128 Ordering time: 12.84s
129
130 Barrier statistics:
131  AA' NZ     : 2.861e+09
132  Factor NZ  : 7.251e+09 (roughly 60.0 GBytes of memory)
133  Factor Ops : 5.311e+14 (roughly 1000 seconds per iteration)
134  Threads    : 29
135
136                  Objective                Residual
137 Iter       Primal          Dual         Primal    Dual     Compl     Time
138    0   2.84355202e+13 -2.20112591e+12  2.73e+13 2.78e-01  3.43e+11  8694s
```

```
    1   3.06184125e+13 -7.29324332e+12  1.77e+13 3.34e+01  1.83e+11  10338s
    2   1.09899634e+13 -3.86493314e+12  8.05e+12 3.06e+00  7.36e+10  11974s
    3   2.11623384e+12 -2.62595369e+12  6.06e+11 1.28e-01  5.77e+09  13604s
    4   6.57019467e+11 -1.82584511e+12  3.31e+10 1.06e-02  3.40e+08  15230s
    5   4.17441950e+11 -1.41015792e+12  7.18e+08 5.98e-04  1.65e+07  16878s
    6   2.22945600e+11 -7.44683933e+11  1.64e+08 2.19e-04  5.67e+06  18474s
    7   1.34501421e+11 -1.28879446e+11  3.66e+06 5.23e-04  7.31e+05  20050s
    8   1.03822162e+11 -8.52010112e+09  5.38e+04 1.05e-02  5.79e+04  21646s
    9   8.54469885e+10 -1.65514645e+09  1.81e+04 1.30e-02  1.52e+04  23228s
   10   6.24232128e+10 -1.56919402e+08  2.69e+03 1.37e-02  2.70e+03  24815s
   11   4.71967686e+10 -5.79528637e+07  1.14e+03 1.37e-02  1.32e+03  26348s

Barrier performed 11 iterations in 26347.66 seconds
Barrier solve interrupted - model solved by another algorithm

Concurrent spin time: 8956.79s (can be avoided by choosing Method=3)

Solved with dual simplex

Root relaxation: objective 7.091732e+07, 103155 iterations, 23886.01 seconds
Total elapsed time = 26512.02s
Total elapsed time = 26709.47s
Total elapsed time = 26738.77s

     Nodes    |    Current Node    |     Objective Bounds      |     Work
 Expl Unexpl |  Obj  Depth IntInf | Incumbent    BestBd   Gap | It/Node Time

     0     0 7.0917e+07    0 12193          - 7.0917e+07      -     - 41403s
     0     0 7.0917e+07    0 12129          - 7.0917e+07      -     - 114412s
     0     0 7.0917e+07    0 12195          - 7.0917e+07      -     - 115711s
     0     0 7.0917e+07    0 12196          - 7.0917e+07      -     - 117309s
     0     0 7.0917e+07    0 12194          - 7.0917e+07      -     - 117921s
     0     0 7.0917e+07    0 12195          - 7.0917e+07      -     - 118372s
     0     0 7.0917e+07    0 12192          - 7.0917e+07      -     - 118910s
     0     0 7.0917e+07    0 12194          - 7.0917e+07      -     - 119167s
     0     0 7.0917e+07    0 12194          - 7.0917e+07      -     - 119631s
     0     2 7.0917e+07    0 12194          - 7.0917e+07      -     - 138615s
     1     2 infeasible    1               - 7.0917e+07      - 72152 146651s
H    2     2                     7.092894e+07 7.0917e+07  0.02% 36076 148574s

Cutting planes:
  Implied bound: 3405
  Flow cover: 2552
  RLT: 2
  Relax-and-lift: 257

Explored 3 nodes (202175 simplex iterations) in 155139.22 seconds
Thread count was 32 (of 128 available processors)

Solution count 1: 7.09289e+07

Optimal solution found (tolerance 1.00e+00)
Warning: max constraint violation (3.0237e-05) exceeds tolerance
Best objective 7.092894183607e+07, best bound 7.091740047042e+07, gap 0.0163%
```

Figure A.11: The log output of the simulation. Run on the HPC cluster for a period of nine months.

A.8 Model Description

To determine the most cost effective design of the solar to ammonia system a optimization model was made. The optimization was considered as a Mixed Integer Linear Programming problem with the objective function to minimize the costs.

Decision Variables	Unit	Description
Cap_PV	kW	Nominal capacity of PV panels
Cap_Bat_Pow	kW	Power capacity of battery storage (determines speed of charging and discharging)
Cap_Bat_Ene	kWh	Energy capacity of battery storage (determines amount of electricity that can be stored)
Cap_Ele	kW	Capacity of electrolyzer
Cap_Salt_Cavern	kg-H_2	Capacity of Salt cavern used to store hydrogen
Cap_Salt_Cavern_Initial	kg-H_2	Amount of hydrogen present before the whole systems starts running
Cap_ASU	kg-N_2	Capacity of Air Seperation Unit to produce nitrogen
Cap_Nitrogen_Tank	kg-N_2	Capacity of the nitrogen tank
Cap_H_B	kg-NH_3	Capacity of Haber-Bosch plant
H_2O_used	kL	Water used in Hydrogen plant to create H_2
$vElec_Com_used$	kW	Electricity used by compressor in salt cavern
vPV_Load_t	kw	Output of solar farm during hour t
$vBat_{In,t}$	kw	Input of electricity before charging loss during hour t
$vBat_{Out,t}$	kw	Output of battery after discharge loss during hour t
$vElec_In_t$	kW	Electricity use in Electrolyzer during hour t
$vH_B_Elec_t$	kW	Electricity use in Haber-Bosch plant during hour t
$vASU_Elec_t$	kW	Electricity use in ASU during hour t
$vSalt_{In,t}$	kg-H_2	H_2 from electrolyzer to salt cavern storage during hour t
$vSalt_{Out,t}$	kg-H_2	H_2 from salt cavern storage to Haber-Bosch plant plant during hour t
$vN_Tank_{Out,t}$	kg-N_2	Nitrogen leaving the cryogenic tank to the Haber-Bosch plant
vZ_X	0 or 1	Binary variable, 1 when battery is charging
vZ_Y	0 or 1	Binary variable, 1 when battery is discharging
vS_X	0 or 1	Binary variable, 1 when salt cavern is charging
vS_Y	0 or 1	Binary variable, 1 when salt cavern is discharging
vA_X	0 or 1	Binary variable, 1 when N_2 tank is charging
vA_Y	0 or 1	Binary variable, 1 when N_2 tank is discharging

$$vPV_Load_t = CF_{PV} * \boldsymbol{Cap_PV} \tag{23}$$

$$vPV_Load_t + \frac{vBat_{Out,t}}{\eta_{Bat,Discharge}} = vBat_{In,t} * \eta_{Bat,Charge} + vElec_In_t + vH_B_Elec_t + vASU_Elec_t \tag{24}$$

$$SOC_Bat_t = SOC_Bat_{(t-1)} + \frac{vBat_{in,t} * \eta_{Bat,Charge} - \frac{vBat_{Out,t}}{\eta_{Bat,Discharge}}}{\boldsymbol{Cap_Bat_Ene}} \tag{25}$$

$$SOC_Bat_{(t=1)} * 100 = 30\% \tag{26}$$

$$SOC_Bat_{(t=1)} = SOC_Bat_{(t=end)} \tag{27}$$

$$20\% \leq SOC_Bat_t * 100 \leq 95\% \tag{28}$$

$$\mid vBat_{in,t} + \frac{vBat_{Out,t}}{\eta_{Bat,Discharge}} \mid \leq \boldsymbol{Cap_Bat_Pow} \tag{29}$$

$$vSalt_{In,t} \leq M * vZ_X \tag{30}$$

$$vSalt_{Out,t} \geq M * vZ_Y \tag{31}$$

$$vZ_X + vZ_Y \leq 1 \tag{32}$$

$$1\% \leq \left(\frac{vElec_In_t}{\boldsymbol{Cap_Ele}}\right) * 100 \leq 110\% \tag{33}$$

$$SOC_Sal_t = SOC_Sal_{(t-1)} + \frac{vSalt_{In,t} - vSalt_{out,t}}{\boldsymbol{Cap_Sal}} \tag{34}$$

$$SOC_Sal_{(t=1)} = \boldsymbol{Cap_Salt_Cavern_Initial} \tag{35}$$

$$0\% \leq SOC_Sal_t * 100 \leq 100\% \tag{36}$$

$$vBat_{In,t} \leq M * vS_X \tag{37}$$

$$vBat_{Out,t} \geq M * vS_Y \tag{38}$$

$$vS_X + vS_Y \leq 1 \tag{39}$$

$$SOC_Sal_{t=1} = SOC_Sal_{t=end} \tag{40}$$

$$vH_B_Elec_t = \text{Ratio_Elec_NH}_3 * \eta_{H_B} * \text{Ratio_NH}_3\text{_H}_2 * \left(vElec_In_t \right. \tag{41}$$

$$\left. * HHV_H_2 * \eta_{Ele} + vSalt_{Out,t} - vSalt_{In,t}\right) \tag{42}$$

$$20\% \leq \left(\frac{(vSalt_{out,t} + Ele_H_B_t) * \text{Ratio_NH}_3\text{_H}_2}{\boldsymbol{Cap_H_B}}\right) * 100 \leq 100\% \tag{43}$$

$$Amm_{out,t} = \text{Ratio_NH}_3\text{_H}_2 * \eta_{H_B} * \left(vElec_In_t * HHV_H_2 * \eta_{Ele} + vSalt_{Out,t} - vSalt_{In,t}\right) \tag{44}$$

$$\sum_{t=1}^{8760}\left(vAmm_{out,t}\right) = 200{,}000 \text{ [ton-NH}_3\text{]} \tag{45}$$

$$vElec_Com_used = \text{Com_Ene_H}_2 * vSalt_{In,t} \tag{46}$$

$$\tag{47}$$

Constraints:

$$H_2O_used = \text{Ratio_Water_H}_2 * vEle_In_t * \text{HHV_H}_2 \tag{48}$$

$$N_2_Tank_Out_t = \left(vElec_In_t * HHV_H_2 * \eta_{Ele} + vSalt_{Out,t} - vSalt_{In,t} \right) * \text{Ratio_N}_2\text{_H}_2 \tag{49}$$

$$\mid \frac{vASU_Elec_t}{\text{Ratio_Elec_N}_2} \mid - N_2_Tank_Out_t = N_2_Tank_Mut_t \tag{50}$$

$$\frac{vASU_Elec_t}{\text{Ratio_Elec_N}_2} \leq \boldsymbol{Cap_ASU} \tag{51}$$

$$vASU_Elec_t - \boldsymbol{Cap_ASU} * 12.5\% * \text{Ratio_Elec_N}_2 \leq vA_X \tag{52}$$

$$vASU_Elec_t \leq M * (1 - vA_Y) \tag{53}$$

$$vA_X + vA_Y \leq 1 \tag{54}$$

$$0\% \leq \left(\frac{N_2_Tank_Mut_t + N_2_Tank_Mut_{(t-1)}}{\boldsymbol{Cap_Nitrogen_Tank}} \right) * 100 \leq 100\% \tag{55}$$

$$\mid vElec_In_t - vElec_In_{(t-1)} \mid \leq 20\% \tag{56}$$

$$\mid \text{Ratio_NH}_3\text{_H}_2 * \left(\left(vElec_In_t * HHV_H_2 * \eta_{Ele} + vSalt_{Out,t} - vSalt_{In,t} \right) \right. \tag{57}$$

$$\left. - \left(vElec_In_{(t-1)} * HHV_H_2 * \eta_{Ele} + vSalt_{Out,(t-1)} - vSalt_{In,(t-1)} \right) \right) \mid \leq 20\% \tag{58}$$

Model Parameters	Unit	Description
CAPEX_PV	€/kW-DC	Capital cost of photovoltaic plant
CAPEX_Wind	€/kW-AC	Capital cost of wind farm
CAPEX_Rec	€/kW-AC	Capital cost of rectifier (AC to DC)
CAPEX_Bat_Pow	€/kW	Capital cost of battery power
CAPEX_Bat_Ene	€/kWh	Capital cost of battery energy
CAPEX_Elec	€/kW	Capital cost of electrolyzer
CAPEX_Sal	€/kg	Capital cost of H-2 storage in salt cavern
CAPEX_Amm	€/kW	Capital cost of ammonia plant including air fraction unit and ammonia storage
OPEX_PV	€/kW-DC	Operating cost of photovoltaic plant
OPEX_Wind	€/kW-yr	Operating cost of wind farm
OPEX_Rec	€/kW-AC	Operating cost of rectifier
OPEX_Bat_Pow	€/kW-yr	Operating cost of battery power
OPEX_Bat_Ene	€/kWh/a	Operating cost of battery energy
OPEX_Ele	€/kW	Operating cost of electrolyzer
OPEX_Sal	€/kg	Operating cost of H-2 storage in salt cavern
OPEX_Amm	€/kw	Operating cost of ammonia in
Feed_Water_price	€/m^3	Price of water per ton of liter, 4.5MAD per m^3, equal to €0.42/m^3.[20]
Feed_Elec	€/kwh	Estimated price of electricity in 2030 0.07 €/kwh
$\eta_{Bat,Discharge}$	%	Efficiency of battery discharge
$\eta_{Bat,Charge}$	%	Efficiency of battery charging
η_{Rec}	%	Efficiency of rectifier
η_{Ele}	%	Efficiency of electrolyzer
η_{H_B}	%	Efficiency of Haber-Bosch plant
η_{Com}	%	Efficiency of compressor, decreases when SOC of salt cavern increases due to higher required inlet pressure
CF_{PV}	-	Capacity factor of solar farm output per hour
HHV_H_2	kwh/kg	Specific energy of hydrogen at 25 degree. Amount of kWh necessary to produce 1kg of hydrogen
Heat_Capacity_H_2O	kj/(kg· K)	Heat capacity of water, 4.184 kj/(kg· K)
Ratio_NH_3_H_2	kg-NH_3/ kg-H_2	Ratio of Ammonia and Hydrogen that reacts with each other 5.56 kg-NH_3/ kg-H_2
Ratio_N_2_H_2	kg-NH_3/ kg-H_2	6.06 grams of H_2 reacts with 28.02 gram N2 to form 34 gram of NH_3
Com_Ene_H_2	kWh-AC/kg	Electricity needed to compress 1kg of hydrogen
Ratio_Water_H_2	L/kg	Water used in electrolysis per kg of h_2, 10 L/kg[6]
Ratio_Elec_NH_3	MWh/tNH3	Electricity consumption for ammonia production, 0.532 MWh/tNH_3[35]
Ratio_Elec_N_2	MWh/tNH3	Electricity consumption for ammonia production, 0.108 MWh/tNH_3[35]
Lifetime	years	General lifetime of the project, different than the lifetime of the components
M	-	Large number that can not surpass the battery in or output